UNIVERSITÄT PADERBORN
Die Universität der Informationsgesellschaft

FAKULTÄT FÜR ELEKTROTECHNIK, INFORMATIK UND MATHEMATIK

Identification of rubber belts in harsh environments using UHF RFID tags

From the Faculty of Electrical Engineering,
Computer Science and Mathematics
The University of Paderborn

To obtained the academic degree

Doctor of Engineering (Dr.-Ing.)

Approved Dissertation

from

Kelash Kanwar

First Supervisor: Prof. Dr.-Ing. Ulrich Hilleringmann
Second Supervisor: Prof. Dr.rer. nat. Reinhard R. Baumann

Date of examination : 30.04.2015

Paderborn 2015

Diss . EIM - E / 314

Contact:

Kelash Kanwar

Adresse:	Am Rippinger weg 1
	33098 Paderborn
Tel.:	+49 (5251) 93 6678
Mobil.:	+49 (176) 2071 1537
E-Mail:	kelashkanwar@hotmail.com

Abstract

RFID technology is widely used in various industries for labeling, inventory management, sensing the variations e.g. damages and sensor data transfer applications. But its use in rubber products especially for thin and flexible transmission belts having various shapes and sizes is still limited. There is huge potential to bring in benefit of RFID technology using UHF RFID tags for this rubber industry. However, various issues (such as unknown electrical parameters of rubber materials, high flexibility, bending and vulcanization temperature) of the considered rubber belts pose a great challenge to adopt the existing UHF tag antenna design strategies for obtaining an efficient embedded RFID tag. There is a scope to optimize an UHF tag antenna design and the analysis process to obtain an efficient UHF RFID tag for such type of heterogeneous rubber structures.

To develop an efficient tag antenna by optimizing (in terms of transmission coefficient) the UHF RFID tag, a design and analysis process based on the 3D electrical model of a rubber belt is presented. The demonstrated design process can be used to carry out effective investigations and implementations of various RFID applications with efficient UHF RFID tags in such type of heterogeneous complex structures (e.g. rubber transmission belts, rubber tires e.t.c.).

First in this context, to determine the electrical properties of the various rubber materials a simple and fast electrical characterizations setup is developed. This setup is based on the open-ended coaxial probe method and uses the equivalent 3D EM measurement model for extracting the electrical parameters of the rubber materials. The applied extraction process is time consuming, therefore, it is optimized to evaluate the electrical parameters with a simple and faster procedure. In addition, the reliability and accuracy of the presented characterization setup is discussed.

Afterward, a design and analysis process is presented to get an optimized (in terms of transmission coefficient) surface UHF RFID antenna using a 3D model of the belt. With the established process, two different surface UHF RFID tags are designed and then the performance of these tags is inspected in terms of read range. From the results it is found that the read range of the fabricated tags shows a good agreement with the simulated one. In addition, the impact of different kind of variations of the considered belts on the tag characteristics are analyzed. Furthermore, to examine the viability of the surface RFID tags in accurate automated counting of several belts a counting test is performed.

Afterward, using a similar strategy, a design and analysis process of the embedded tag antenna is established. Based on this design process, an embedded UHF RFID tag is designed and few prototype tags are embedded in the real rubber belts. Then, the performance of this tag in terms of read range is examined and results are discussed. From the outcome, it is found that the fabricated tag shows a good coherence with the simulated one. In addition, to acquire a viable and functional UHF RFID tag without damaging the rubber belt structure, in its whole life, preliminary investigations are carried out.

Kurzfassung

RFID ist eine weit verbreitete Technologie in unterschiedlichsten Branchen, wie z.B. der Lager- und Etikettierungindustrie. Zwei exemplarische Anwendungen sind die Übertragung von Sensordaten und Identifikationsnummern. Trotz des großen Potentials der RFID Technologie ist ihr Einsatz in Kautchukprodukten, speziell in dünnen und flexiblen Antriebsriemen, begrenzt. Die Herausforderungen eines optimalen Tag-Entwurfs liegen in den unbekannten elektrischen Parametern, der hohen Flexibilität und der Vulkanisierungstemperatur während des Herstellungsprozesses der Riemen. Daher besteht ein Bedarf, das Entwurfsverfahren von UHF Tag-Antennen für heterogene Gummistrukturen zu optimieren.

Zur Entwicklung einer effizienten UHF RFID Tag-Antenne, bezüglich des Anpassungskoeffizienten, wird ein Analyse und Enktwurfsverfahren, basierend auf elektrischen 3D-Modellen des Gummiriemens, vorgestellt. Dieser Ansatz wird für die effiziente Untersuchung und Realisierung von optimierten UHF-Tags für verschiedene heterogene komplexe Strukturen (z.B. Antriebsriemen, Reifen e.t.c. auf Kautschukbasis) verwendet.

Dazu wird eine einfache und schnelle elektrische Charakterisierungsmethode erarbeitet. Diese basiert auf der Open-Ended Coaxial Probe Methode und nutzt ein äquivalentes 3D-Messmodell zur Extraktion der elektrischen Eigenschaften des Materials. Zusätzlich wird eine weitere Beschleunigung dieses Charakterisierungsverfahrens eingeführt und die Verlässlichkeit und Genauigkeit der präsentierten Ansätze werden diskutiert.

Danach wird ein Analyse- und Entwurfsprozess zur Auslegung eines optimierten UHF-Tags für Oberflächenanwendungen, basierend auf einem 3D-Modell eines Antriebsriemens, dargelegt. Es werden zwei verschiedene UHF RFID Tags für die Oberflächenanwendung entworfen und produziert. Die Leistungsfähigkeit dieser Tags wird bezüglich der Lesereichweite ausgewertet, wobei gemessene und simulierte Lesereichweiten der Tags gut übereinstimmen. Darüber hinaus wird der Einfluss von verschiedenen Streuungen der Antriebsriemenparameter untersucht. Zur Beurteilung der Brauchbarkeit der entworfenen Tags für die automatisierte Anzahlerfassung einer Vielzahl von Antriebsriemen, wird ein entsprechender Test durchgeführt.

Im Anschluss wird die eingeführte Entwurfsmethode für den Entwurf und die Herstellung von eingebetteten Tag-Antennen in Antriebsriemen verwendet. Die Leistungsfähigkeit wird auf Basis der Lesereichweite untersucht und diskutiert. Die Simulation und Messung der hergestellten Antennen zeigen eine gute Übereinstimmung. Zusätzlich werden Voruntersuchungen bezüglich der Lebensdauer der eingebetteten UHF-Tags in Antriebsriemen durchgeführt.

Declaration

This thesis is the result of my own work and includes nothing which is the outcome of work done in collaboration except where specifically indicated. It is not yet published or submitted in whole or in part for a degree at any other university. Some of the work is this thesis has been published in conference proceedings [1–4].

Paderborn, May 11, 2015

Kelash Kanwar

Acknowledgments

First of all, I am thankful to God for providing me the opportunity to study in Germany.

I am sincerely grateful to my supervisor Prof. Dr.-Ing. Ulrich Hilleringmann for his kindness, constant guidance, valuable suggestions and discussions throughout this PhD work. Furthermore, I am thankful for his encouragement and the motivation he gave me during the writing phase of this thesis. Moreover, I am really pleased that he gave me opportunity to work at the Sensor technology Group, University of Paderborn, and provided me opportunity to work in collaboration with Fraunhofer ENAS-ASE, Paderborn, Germany.
I am so grateful to Prof. Dr.rer. nat. Reinhard R. Baumann for his acceptance to become the second supervisor of this thesis.

I would like to give thanks to Dr. Christian Hedayat for providing me the chance to work on an interesting topic and for utilizing the lab facility at the institute of Fraunhofer ENAS-ASE, Paderborn. I am also thankful for his stimulative discussions with me during this work. Furthermore, I am very glad that I worked with many colleagues especially Christian Hangmann, Volker Geniess, Thomas Mager, Maik Julian Büker, Alexander Kokel, Christian Reinhold while completing this thesis. I am very grateful for their support and cooperation to complete this PhD work. Also, I offer my best regards to Elisabeth Mesch and Uwe Gierth for their cooperation.

I would like to thank Arntz Beteiligungs GmbH, Höxter for providing their support and cooperation to complete this thesis. My special thanks go to U. Ballhausen, Stephan Scheele and Alexander Schmidt for their support and cooperation. I am obliged to tagItron GmbH, Salzkotten, Germany for allowing me to utilized their lab facilities, providing me their support and cooperation to complete this work. My special thanks go to Jan Wendisch and Hans-Gerd Ansorge.

I am truly thankful to my parent university QUEST, Nawabshah, Pakistan for providing me the scholarship to pursue the higher study abroad.

Finally I appreciate my family and friends for their encouragement and moral support during my study, especially my mother, father, wife and daughter.

Contents

Abstract / Kurzfassung **iii**

Declaration **v**

Acknowledgments **vi**

1. Introduction **1**
1.1. Motivation 2
1.2. Previous work and state of the art 4
1.3. Focus of this thesis 5

2. RFID technology and tag antenna fundamentals **7**
2.1. Basics related to RFID systems 7
2.2. Passive UHF RFID back-scattered system 9
2.2.1. Frequency bands and power regulations 9
2.2.2. Standards 10
2.2.3. Electronic Product Code (EPC) system 10
2.3. UHF RFID tag 11
2.4. Antenna basics and its various characteristic parameters 13
2.4.1. Antenna patterns 15
2.4.2. Isotropic antenna 17
2.4.3. Antenna gain 18
2.4.4. Directivity 19
2.4.5. Input impedance 19
2.4.6. Radiation efficiency 20
2.5. Antenna radiating field region 21
2.6. Performance evaluation of an UHF RFID tag 22

2.6.1. Estimating the maximum read range by Friis formula 22
2.6.2. Read range estimation via measurement in an anechoic chamber 24

3. Electrical characterization of different rubber sheets 27
3.1. Basics of the electrical characterization of a dielectric material . . . 28
3.2. Basics of electric characterization methods 30
3.2.1. Electrical characterization using a parallel plate dielectric resonator (resonant method) 30
3.2.2. Electrical characterization using an open-end coaxial probe method (non-resonant method) 32
3.3. The measurement system in detail 33
3.4. Extraction of the material properties 36
3.4.1. Extraction of electrical parameters using a 3D EM model . . 37
3.4.2. Modified extraction process in detail 40
3.5. Results of electrical parameters of rubber sheets 43
3.5.1. Electrical parameter of a CR rubber sheet 44
3.5.2. Electrical parameter of the EPDM rubber sheet 47
3.6. Investigating reliability, reproducibility and accuracy of the electrical characterization setup 49
3.6.1. The reliability of the modified extraction code 49
3.6.2. Reproducibility of measurements and the determined electrical parameters 49
3.6.3. Comparing the reliability and accuracy of the determined parameters 50
3.7. Summary of the chapter 52

4. Design process of surface UHF RFID tag for rubber belts 55
4.1. Physical layout of a rubber belt 55
4.2. Representation of a belt with an electrical model 57
4.3. Surface UHF RFID tag design process 59
4.3.1. Basic of designed tag antenna 60
4.3.2. Designed surface UHF RFID tags 64
4.4. Performance analysis of the designed surface tags 64
4.4.1. Estimating the theoretical read range of the surface tags . . 64
4.4.2. Read range estimations of the surface prototype tags via anechoic chamber 68
4.4.3. Checking the model by comparison of the read range for the tags 71
4.4.4. Variation in the read range due to various tolerances 72
4.5. Investigation of the impact of different parameter variations of the belts 73
4.5.1. Impact of the electric parameter variations on the tag characteristics 74

4.5.2. Impact of thickness variations on the tag characteristics . . . 75
4.5.3. Impact of changes in the shape of the rubber belt on the tag characteristics 75
4.5.4. Impact of electrical parameter changes (caused by different chemical recipes) on the tag characteristics 78
4.6. Bulk reading test to investigate logistic application 80
4.7. Summary and outlook of the chapter 81

5. Embedded tag design process for the rubber belt 85
5.1. Determination of a suitable antenna structure and fabrication technique 85
5.2. The embedded UHF RFID tag design process 90
5.3. Mechanical testing of the embedded tag 91
5.3.1. Tag placement inside a physical belt 92
5.3.2. Mechanical test to check damages 93
5.4. High speed test to detect a belt during operation 93
5.5. Performance analysis of the embedded RFID tags 94
5.5.1. Estimating the theoretical read range of the embedded tag based on the simulation 95
5.5.2. Estimating the read range of the embedded tag based on anechoic chamber 96
5.5.3. Variation in the tag performance 97
5.6. Summary of the chapter 98

6. Summary and conclusions 101

A. Appendix 105
A.1. Comparison of the electrical and physical belt model 105
A.2. Impact of the belt on the tag characteristics 106

List of figures 109

List of tables 113

References 115

List of Publications 123

CHAPTER 1

Introduction

Radio frequency identification is a technology that uses wireless signals for data transmission and subsequently to automatically identify objects. This RFID technology has several advantages compared to other automated identification technologies such as bar code and magnetic strip card technologies. The primary advantage is that the tagged objects can be detected without being in contact or in line of sight to a detector system from distances of a few centimeters upto several meters. Other benefits of this technology are the possibility to detect several tags at once, the high data capacity and the insensitivity to dust effects e.t.c.. This technology is considered to be one of the major alternatives to bar codes or universal product codes in the future. Due to all these benefits this technology got a phenomenal growth in various industries. It is being used to identify, track and improve the inventory management of different objects and has resulted in better handling of objects and in reduction of labor costs [5, 6]. In addition, this technology is also used to sense damages or to enable transfer of different sensor data (such as temperature, pressure, stress e.t.c.) [5, 7–9].

A typical block diagram of a general RFID system is shown in figure 1.1. It comprises of mainly two parts, a tag and a reader system. The tag consists of a tag IC (on which different information such as an unique identification code or other data are stored) and a tag antenna. The reader system is combined out of a reader module, an antenna and an application server [10].
With an RFID system the automatic identification process of an object starts when a tag attached to a physical object passes or comes into the detection zone of a reader system. The moment, at which the object enters the detection zone of the reader system, the code information stored in the tag IC is transmitted wirelessly

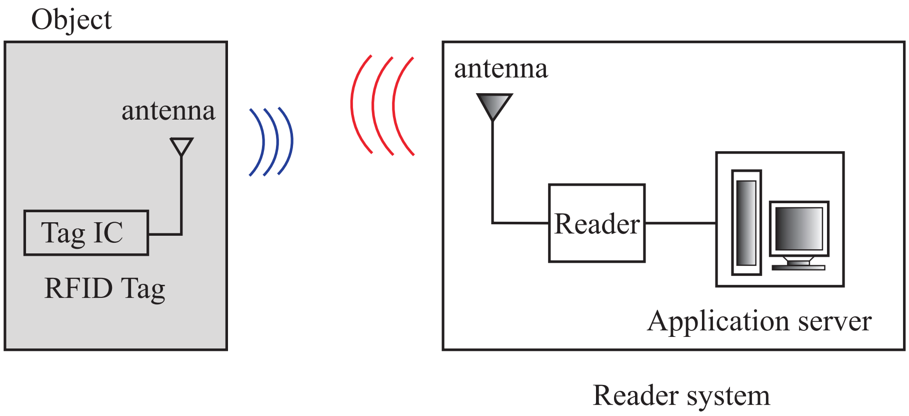

Figure 1.1.: *Block diagram of a typical RFID system*

to the reader module, and the relevant unique code is extracted by passing information to the application software installed on the host system. Additional information (such as authentications, cost, date of manufacturing e.t.c.) related to the detected code can be extracted from the data base accessed via the network [5,6].

There are various fields on which research can be focused. However, in this thesis, a particular focus is given on how to analyze and design high performance ultra high frequency (UHF) RFID tags for different kind of complex objects, especially rubber products (e.g. rubber transmission belts).

1.1. Motivation

As already mentioned, RFID technology is used in various industries but its use in rubber products is still limited especially for rubber transmission belts. These belts are widely used for power transmission applications to produce motion between different parts in various industries such as cement industry, automobile industry, oil industry, civil constructions etc. Due to various applications, these rubber belts have various shapes, sizes and thicknesses. Therefore, the costs of these belts vary considerably and range between ten Euros to around thousand Euro [11]. Few of the scenarios which motivate the usage of RFID technology are mentioned as follows.

At this moment counting and packaging of the rubber belts in a box is carried out manually. It takes a lot of time and causes higher labor costs. Another disadvantage of the manual counting is that sometimes due to human error the counted value is wrong. In some industries it is necessary to minimize the possibility of such mistakes. Especially in the automotive industry such counting mistakes are undesirable because they interrupt the automatic assembling process. Therefore, the manual counting requires some counter verifying mechanism.

Sometimes it is necessary to notify the end user timely about a replacement of the used belt. When the wrapped belt gets older its characteristic is changed. If the belt is not replaced on time then it may cause damage to the machine and result in huge money losses.
When the machines operate continuously for a longer time, the wrapped belts may get heated. This causes some changes in the physical parameter such as the elongations of belt dimensions or the change in stress on the machine e.t.c.. These changes sometimes lead to damages or undesired operation of the machines. Hence, it is necessary to notify the end user promptly about the changes of the physical parameters of the belt to avoid undesired consequences.

In above mentioned application scenarios, improvements can be released with the usage of the UHF RFID tags. Using them, total visibility of the objects at different points during their handling in the supply chain and in inventory management can be realized. In addition, with sensor enabled UHF RFID tags changes in physical parameters can also be monitored [7–9]. Consequently, usage of the UHF RFID tags can provide several benefits such as reduction in the labor costs to the rubber belt manufactures, a way to verify the authenticity and monitor changes of physical parameters of different belts caused by the operations of the rubber belts. However, unknown electrical parameters of rubber materials, various shapes and sizes, and flexible structure pose a great challenge to adopt the existing UHF RFID tag antenna design solutions for achieving efficient embedded tags. Therefore, there is a need to carry out detailed research to improve the design and the analysis of the tag antenna. There are several problems, whereas the major problems are mentioned below. These led to this research work.

When a UHF RFID tag is attached to a belt the tag performance is deteriorated. This is caused by unknown electrical parameters of the materials and the geometrical dimensions of the considered rubber belts. In the intended applications the high performance tags are desired to minimize the overall implementation cost of RFID technology and to develop energy efficient RFID systems. One of the most cost effective way to improve the performance of an UHF RFID tag is to design the UHF tag antenna with the required impedance value to maximize the matching with the attached tag IC. But designing of the tag antenna with the required matching is itself a complex problem for such heterogeneous structures. Hence, an optimized design and analysis process to get an efficient UHF RFID tag needs to be established for such rubber structures.

Another problem is that damages may be caused to a tag or to the belt structure. When a tag is attached or embedded, it may get damaged due to the flexibility, the high speed values during operation and the high vulcanization temperature during the fabrication of the belt. Damages to a belt structure may be caused when a tag, having unappropriated dimensions and fabricated with incompatible materials, is

embedded into it. Hence, it is important to perform tests that the designed tags have no impact on the considered belt structures and survive throughout its full life cycle.
Another problem is to obtain a viable and a cheap tag for the considered structures if RFID is preferred as an alternative to other identification technologies. Tag antennas are structured with different fabrication techniques, but it is not known which technique is suitable, especially for embedding into the belt structure, due to its specific fabrication recipe and layers stack-up. As the cost of embedded tags also depend on the chosen antenna fabrication technique, it is also important to select a suitable fabrication technique to obtain a viable and cheap embedded tag for the considered belt type.

The main problem in the context of establishing the optimized design and analysis process is that electrical parameters of the various rubber sheets are not known. The electrical parameter values of these rubber sheets depend on the specific chemical recipe and fabrication process. Due to this reason no prior information is available. So first it is required to develop an electrical characterization setup via which the electrical parameters of various rubber sheets can be determined.

1.2. Previous work and state of the art

A closely related product is a rubber tire. Here, a similar kind of investigation is carried out to implement different RFID technology applications [12, 13].
In [12] research was carried out on how to design high performance tag antennas for surface applications on rubber materials. The design solutions are obtained by approximating the tire with some approximated models by assuming some average electrical parameter values. For surface tag designing, based on several experimental measurements, these values are obtained by curve fitting with the try and hit approach. This process makes this design strategy time consuming and complicated because it takes a lot of time to approximate the belt model and then to design the high performance UHF RFID tags.
In [13], multiple UHF tag antennas are designed to obtain the required range with a simplified tire model. However, it is not shown how a tag antenna can be designed with the required complex impedance value by considering the complex tire structure. Due to this problem, using this approach it is hard to design and analyze an embedded tag antenna with required complex impedance value for the considered complex structure.
Hence to obtain the desired antenna with required matching and to analyze the impact of rubber material accurately an optimized tag design process needs to be established.

In addition, there are a few commercial UHF RFID tags available for a rubber tire with various shapes and sizes [14–16]. Antennas used in these tags and investigated in numerous other tag applications [17–21] are structured in various forms with different antenna fabrication techniques. But it is not known which antenna structure and technique is suitable especially for embedding in a belt structure due to its specific fabrication recipe and layer stack. Additionally, the cost of an embedded tag depends on the adopted fabrication process for structuring the tag antenna. Therefore, it is also important to find which antenna structure and fabrication technique is suitable to obtain a cheap embedded tag for the thin and flexible rubber belt structures.

In the context of designing a tag antenna, it is necessary to determine the electrical parameters of the rubber sheets used in the considered rubber structures. A closely related application in which similar investigations are carried out is [22]. In [22] a material characterization setup was developed to determine the electrical parameters. However, the extraction process of the electrical parameters is time consuming. Furthermore, this extraction process needs to be repeated for every measurement to determine the electrical properties of dielectric materials. Thus the extraction process needs to be modified to make the overall electrical characterization process simpler and faster.

1.3. Focus of this thesis

The work presented in this thesis focuses on solving some of the above mentioned problems and to investigate the implementation of RFID technology for the complex rubber structures. The details are given as follows:

- An optimized design and analysis process to obtain efficient UHF RFID tags needs to be established for the considered heterogeneous rubber structures. Furthermore, to check the suitability of RFID technology applications for them investigations need to be carried out.

- In context of designing optimized tag antennas it is required to develop an electrical characterization setup to find the electrical parameters of numerous rubber sheets. Furthermore, it is required that the extraction process is simple and fast to evaluate the electrical parameters.

- Various mechanical and adhesion problems need to be investigated for acquiring a viable and cost effective embedded RFID tag design for the considered structures.

CHAPTER 2

RFID technology and tag antenna fundamentals

The main focus of this thesis is the development of a RFID system for transmission belts. There are two major areas, i.e. the rubber material characterization and the design of the tag antennas for rubber transmission belts, on which focus is given. Hence to understand the content and the results of this thesis, the basics are presented separately in two parts. In this chapter, some basics related to RFID technology and antenna characteristics are presented to understand the part of the thesis content especially presented in chapter 4 and chapter 5. Basics related to electrical characterization are presented separately in chapter 3.

2.1. Basics related to RFID systems

RFID systems can be differentiated according to various characteristics such as operating frequency bands, working principles to detect the RFID tag (near field or far field communication), the way they use power to operate a tag (passive, semi-passive or active), and so on [5, 6, 23]. Few of the distinguished features are discussed briefly in the following section.

Features of different RFID system

As already mentioned, RFID technology uses wireless data transmission. Therefore, various RFID systems are developed, which operate at different radio frequencies. Major radio frequency bands of most common RFID systems are depicted in figure 2.1. The common frequency bands are 125/134 kHz (low frequency),

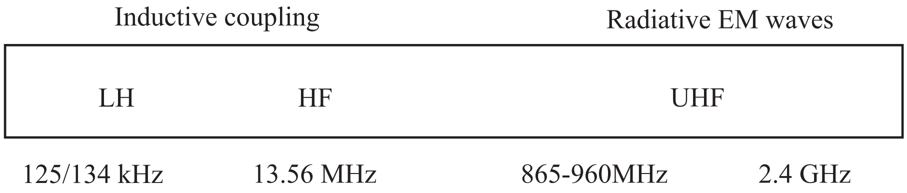

Figure 2.1.: *Common frequency bands in which RFID systems operate*

13.56 MHz (High frequency), 860-960 MHz (Ultra high frequency) and 2.4 GHz (microwave frequency).

The RFID systems operating at 125/134 kHz are most commonly used to track animals, because this frequency band is less insensitive to liquids. The 13.56 MHz systems are used in smart cards, tracking luggage at airports e.t.c. due to their wirelessly communication/authentication capabilities within a short range. The 860-960 MHz RFID systems are used for inventory management in industries and large warehouses due to their ability of tracking bulk objects at several meters. Furthermore, these systems are also used to sense or transmit the various changes such as temperature, pressure e.t.c.. The 2.4 GHz RFID systems are used mostly for sensor applications [5, 6, 23]. Moreover, due to the availability of more bandwidth at higher frequency compared to low RF frequencies, the RFID systems operating at higher bands have higher data rates.

The RFID systems operating at 125/134 kHz and 13.56 kHz are based on the inductive coupling principle. They detect a tag when it enters the near field zone of a reader system. UHF and microwave band RFID systems mainly use the radiative field of the reader system for detecting the presence of a tag [5, 6]. Due to this, earlier types of RFID systems have small read ranges compared to later one (up to one meter vs. several meters). For those who are not familiar with the UHF RFID systems, it is important to mention that UHF tags are still detectable in the near field zone (explained in section 2.5) of the UHF RFID systems.

These RFID systems can be active, semi passive and passive. For active and semi passive RFID systems, batteries need to be attached to the tags to carryout data logging operation of the attached RFID microchips. Whereas, in passive RFID systems, RFID tags use the energy supplied by the reader system to response to its commands. The adding of a battery to the tag makes it bulky and increases the overall cost of the RFID tag [5, 6, 10]. Therefore, final decision to select an appropriate RFID system for a particular application depends on the application requirements and the constrains.

Because of the best compromise in read range, size, cost, higher data rate, detections of several tags at once and sensitivity to environment effect, passive UHF (i.e. working at 868 MHz in European countries) RFID systems are selected in this work for investigation purposes. In the following section, some basics characteristics of a UHF RFID passive system are discussed.

2.2. Passive UHF RFID back-scattered system

A general detection process of a tag with a RFID system was mentioned in chapter 1. In this paragraph, it is discussed how data from an UHF RFID tag are transmitted to a reader module of the passive back-scattered RFID system. A typical layout of such a system is shown in figure 2.2.

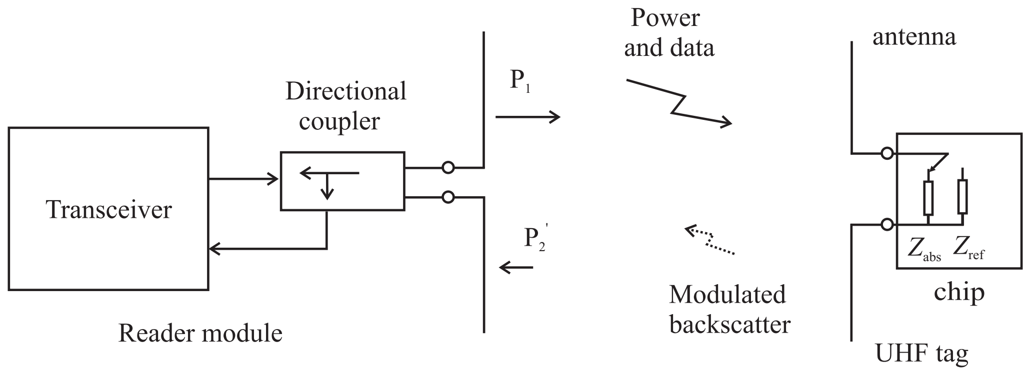

Figure 2.2.: *Passive UHF back scattering RFID system*

In a passive back-scattering RFID system, in forward air link[1] first power plus data are sent to the tag by the reader system. In return, in reverse link[2], once the tag chip's internal circuitry is powered up by the reader antenna emitted fields, the tag sends back the signal to the reader antenna by the antenna's reflective section. The reflected signal is modulated by switching between the two impedance values of the tag chip. The switching between these two impedance values causes either maximum power delivered from the tag antenna to the chip or maximum power reflected back to the antenna. Hence, in this way, the reflected or back scattered signal is modified. The switching between two values is done in dependence on data stored in the tag chip internal memory and is controlled by the modulator circuitry. At the reader system, these changes in the reflected signal are detected and data are decoded [5, 12].

2.2.1. Frequency bands and power regulations

Other RF systems operate near or around the mentioned ISM bands too. Therefore, to avoid interference of the UHF RFID system with other kind of RF systems, different countries across the world have assigned individual frequency bands for the operation of UHF RFID systems. In addition, they also have put different limits on the power to be transmitted by RFID systems to detect the RFID tags in these allocated bands. Table 2.1 shows the frequency band allocation and power

[1]the air link from a reader system to a tag
[2]the air link from a tag to the reader system

transmission limits of UHF RFID systems in various countries around the world [5].

Table 2.1.: *UHF RFID band allocation in different countries around the world*

Country	Frequency Band	Maximum allowed power
EU	865.6-867.6 MHz	2 Watt ERP
USA/Canada/Argentina	902-928 MHz	4 Watt EIRP
China	920.5-928.45 MHz	2 Watt ERP
Australia	920-926 MHz	4 Watt ERP(license required)
Japan	952-956.4 MHz	4 Watt ERP(license required)

2.2.2. Standards

There are several standards drafted by international governing bodies for various types of RFID systems in different countries. The principle purpose of these standards is to specify typical physical and logical operating requirements of the interrogator and tags, so that components manufactured from different companies can fit each other for flawless usage of RFID systems. There are various standardization bodies across the globe, which specify these requirements in their region. The famous standardization bodies for RFID technology are ISO and EPC globe. They have purposed for long range UHF RFID systems ISO 18000-6 and EPC Global Class1Generation2 standard [24]. Based on the desire of end supply users, recently EPCGlass1G2 has been approved by ISO as the ISO 18000-6C standard. After that, the ISO180006C/C1G2 is the dominating communication protocol standard for long range communication in supply chains. The popularity of this standard is caused by the fact that it provides better tracking of objects in the supply chains using the EPC networks. Details about numerous RFID standards can be found in [5, 25, 26].

2.2.3. Electronic Product Code (EPC) system

EPC is a unique code assigning and network system. The concept of EPC was proposed by MIT Auto ID and associated centers [6]. In this system, first a unique EPC ID is assigned to the item via an EPC naming server, and then information of this assigned unique code ID is stored in a central data base. Later on, object authenticity in supply chains can be carried out via internet or network from the central data base by checking the assigned ID with the acquired ID of the object. After the first implementation of this concept, the RFID authenticity concept grew fast in the supply chain management of different objects. Furthermore, due to this the RFID technology also got a distinguished edge to its predecessor technologies

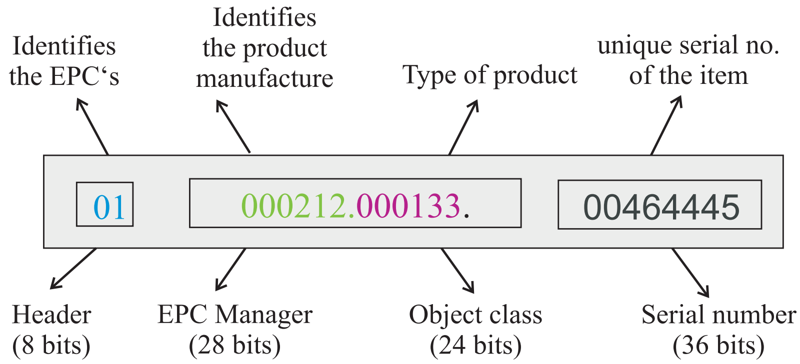

Figure 2.3.: *96 bits EPC data structure*

such as bar codes and magnetic strip cards. In the future, the EPC system is considered to be one of the major alternative to bar code or Universal Product Code [6].

EPC data structure

EPC can be of different bit sizes [5]. A typical 96 bit EPC version is shown in figure 2.3. In this version of the data structure, 32 bits are reserved for the naming of a unique serial number to the item. With these bits around 4.2 billion unique serial numbers can be assigned to each product of a company. 24 bits are dedicated to the naming object classes. Using these bits around 1.6 million of unique code IDs can be assigned to different types of objects of a company. 28 bits are dedicated for naming the EPC manager field. With these bits around 268 million unique IDs could be assigned to different companies. In addition, 8 bits are reserved for the header field which are used to differentiate various versions of the EPC [5, 6].

2.3. UHF RFID tag

As already mentioned, an UHF RFID tag (a few commercials tags are shown in figure 2.4) is a tiny electronic device which is basically comprised of two components; a tag chip and a tag antenna. The electrical function of these individual components can be represented by circuit elements [10]. A simplified circuit representation of a typical tag is shown in figure 2.5. It can be seen that a tag chip and a tag antenna have a certain complex impedance. When a field impinged on the tag antenna from the reader system, a voltage is created across the tag antenna terminal. This causes a current flow in the circuit and hence powers up the internally circuitry of the chip. Once the tag is powered by the external field then it starts to respond to the reader commands. The tag responds to the reader system from several meters if it keeps receiving the minimum power to power up its internal circuitry. The power delivery from the tag antenna to the tag chip and subsequently the UHF tag performance

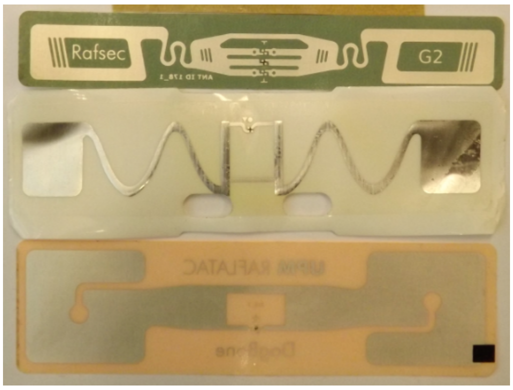

(a) Typical commercial UHF RFID tags

Figure 2.4.: *Typical commercials UHF RFID tags*

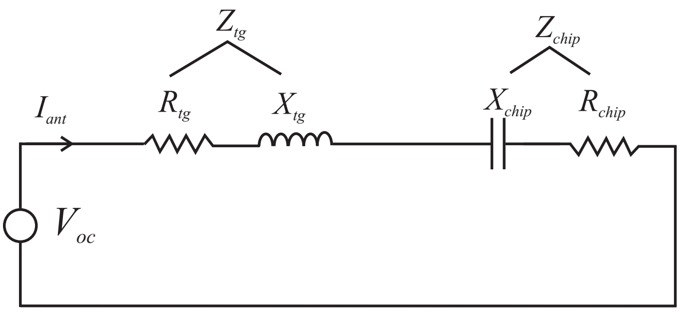

Figure 2.5.: *A UHF tag circuit schematic*

(in term of the maximum detection read range) is quite good when the impedance values of the both components is equal in magnitude but complex conjugate to each other. The parameter which quantifies this impedance match between these two parts is named as the power transmission coefficient (τ). It actually characterizes how much power received by the tag antenna is delivered to the tag chip. It can be calculated with the help of (2.1) [27–29].

$$\tau = 1 - |s|^2 = 1 - \left| \frac{Z_{\text{chip}} - Z_{\text{tg}}^*}{Z_{\text{chip}} + Z_{\text{tg}}} \right|^2 = \frac{4 R_{\text{tg}} R_{\text{chip}}}{|Z_{\text{chip}} + Z_{\text{tg}}|^2} \tag{2.1}$$

with s representing the power reflection coefficient, $Z_{\text{tg}} = R_{\text{tg}} + jX_{\text{tg}}$ and $Z_{\text{chip}} = R_{\text{chip}} + jX_{\text{chip}}$

For the maximum power transformation, it is required that the power transmission coefficient factor should have the value 1.

When an UHF tag optimized for ambient air (by matching the complex conjugates with each other) is attached on the surface of a belt or embedded in them, the complex impedance value of the tag antenna alters, which in turn results in a mismatch between the tag IC and the tag antenna complex impedance values. Due to this mismatch, the power received by the tag antenna is not completely transferred to a tag IC, and it results in a decrease in read range of an UHF RFID tag. This mismatch can be improved either by changing the tag IC parameters by redesigning a new IC or by changing the tag antenna parameters. Since designing costs of a new tag IC are huge, the UHF tag antennas are redesigned with required parameters [2, 27].

In the design of efficient passive UHF tags, most commonly selected tag antennas are of the dipole type having the overall $\frac{\lambda}{2}$ size or length [30]. For several tag applications the required size of the dipole antennas at UHF frequency is too big or need to be shrunk in certain areas due to application constrains (e.g. available space, the flexibility and the environment around the tagged object). Therefore the tag antennas are wrapped in the meander form and in arbitrary shapes to reduce their overall size, so that these can be fixed or attached suitably on the tagged objects. As antenna characteristics depend on these various constrains it is quite hard to determine special characteristic parameters of a tag antenna and design the tag antennas by analytical method [17]. Therefore mostly tag antennas are designed with the help of numerical EM solvers by modeling the specific application scenario. Then those models are counter verified by the measurements [30–33].

2.4. Antenna basics and its various characteristic parameters

In chapter 4 and 5, it is shown how the tag antennas are designed for the considered complex heterogeneous rubber structures using a numerical EM simulation model. However, to understand general antenna characteristics and the special tag antenna characteristics presented in those chapters, in the following section some basics of various antenna characteristic parameters are discussed.

The application of antennas is so diverse that they are designed in various shapes and sizes [6, 30]. Generally, the basic purpose of an antenna in all these applications is to transmit or receive electromagnetic (EM) waves. It transmits an EM wave when an alternative source is attached to it, and it receives the signals when the changing field is impinge on it. Due to reciprocity characteristics and cost effectiveness generally a single antenna is used to perform both options. To give a general idea of the EM field transmission or reception, the mechanism of field transmission from the simplest form of an antenna structure is explained below.
The simplest form of an antenna is a linear dipole antenna (as shown in figure 2.6)

[34]. The mechanism of field transmission from this simplest antenna structure can

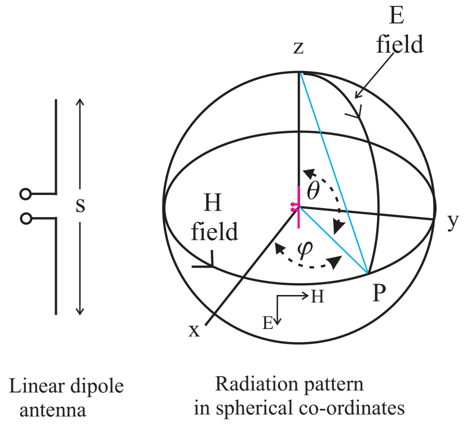

Figure 2.6.: *Linear dipole antenna and its typical orientation in spherical coordinate system*

be explained with the help of two port transmission line theory [35]. The circuit schematic of the two transmission lines is shown in figure 2.7. When an alternating field source is applied from one end, i.e. from the source end, and is opened at the other end, i.e. the load side, a sinusoidal standing wave pattern is created on them due to back and forth motion of the current. A typical standing wave pattern is

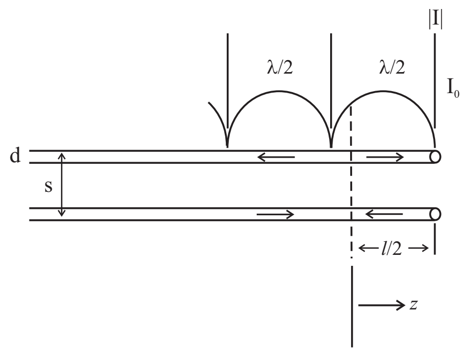

Figure 2.7.: *Two port transmission line*

shown in figure 2.7. Such a type of transmission line has a minimum current at the open ends, and exhibits a maximum at a distance of $\frac{\lambda}{4}$ and a zero again at a distance of $\frac{\lambda}{2}$ from the open ends. Similarly on the transmission line this pattern is repeated for multiple of these distances with increase of the distance from the open ends. Furthermore due to back and forth motion of currents after every 180 degrees a phase shift occurs, which is represented on the transmission line by a change in the direction of the arrows (depicted in figure 2.7).
This type of transmission line generally transmits very little amount of the electromagnetic fields in the air due to closeness of each wire to each other. However, if both wires from each transmission line are either bended, curved or mismatched

e.t.c. then the electromagnetic field is transmitted from the changed sections to the air. A vice-versa phenomena is observed when field impinges on such segments or structures [35].
If both wires from each transmission line are bended by $\frac{\lambda}{4}$ length and making the overall size of the bended portion $\frac{\lambda}{2}$, a simple form of dipole structure is created. On such a structure a similar type of sinusoidal radiation pattern, associated with the current density, is observed than that seen in $\frac{\lambda}{2}$ length on the transmission line. The typical one is shown in figure 2.8. The reason of creation of similar patterns

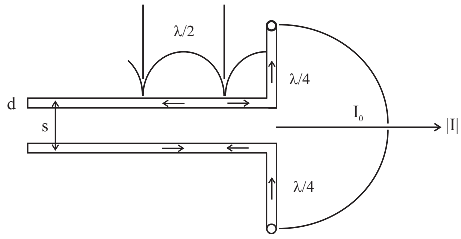

Figure 2.8.: *A simple form of linear dipole structure on the two port transmission line*

across its bended segment is that due to the bending, in each quart length portion, the currents in both sections of the lines have opposite directions, which add up in a constructive way.
If the length of the bended segment is greater than half and less than 3 quarter of the wavelength, then the behavior in the pattern as shown in figure 2.9 is observed due to spatial change. Hence depending on the overall length of the bended section,

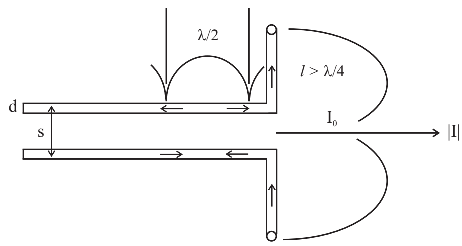

Figure 2.9.: *Changes in radiation pattern due to different bended lengths*

zero and different kinds of patterns are observed. At $\frac{\lambda}{2}$ length the dipole has maximum transmission and reception characteristics [34, 35]. Due to this characteristic behavior, mostly in designing the high performance UHF tags, tag antennas with overall $\frac{\lambda}{2}$ length are obtained.

2.4.1. Antenna patterns

The antenna radiation patterns give information on how electromagnetic fields are oriented around it as a function of direction [36]. Generally there are various antenna characteristic parameters which can be displayed and analyzed to study the behavior and performance of an antenna. These patterns can be studied with the help of 2D or 3D dimension plots. As an example, a linear dipole antenna gain (described later) pattern in 3D dimension is shown in figure 2.10, whereas, 2D (E plane and H plane [35]) is shown in figure 2.11. Generally 2D field patterns

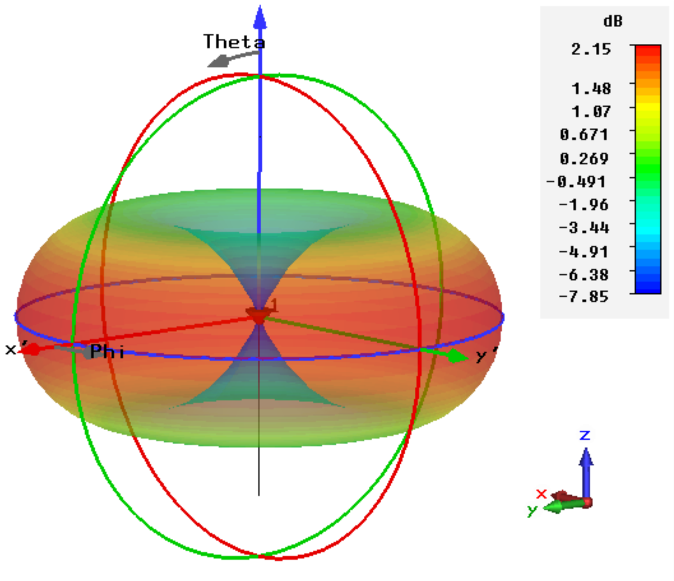

Figure 2.10.: *3D far field Radiation pattern of a resonant dipole wire antenna*

provide actual values of different antenna parameters as a function of angle around the antenna. Whereas, 3D field patterns are good for visualizing the fields around the antenna structure and provide a few information [35]. Often, various antenna characteristic parameters are plotted in terms of decibel (dB). Due to this, these are normalized to their maximum value or referenced to a fixed value. For example, the gain of a reader antenna is usually expressed in dBi, which means the gain is referenced to the isotopic antenna.

Power or intensity pattern

The radiation pattern can be specified either in terms of power or intensity. The power pattern specifies how much power density is passing through a sphere of a certain radius. The typical average value of power density around an antenna structure is related to the electrical and the magnetic field intensity [35, 36]. Its value at a point can be obtained with the help of a pointing vector relation given as

$$P = \frac{1}{2}\left(E_0.H_0\right) \tag{2.2}$$

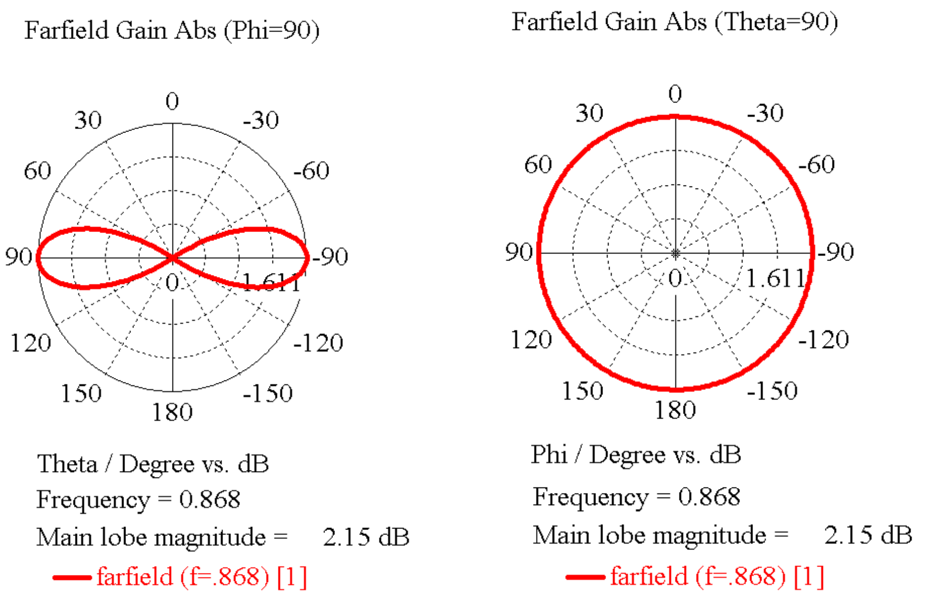

(a) 2D far far field pattern in E plane

(b) 2D far field pattern in H plane(across dipole)

Figure 2.11.: *Radiation pattern of a resonant dipole wire antenna in E and H plane*

where E_0 represents the electrical field with the unit V/m, whereas H_0 represents the magnetic field and its unit is A/m, P represents the power and its unit is Watt/m^2.
These E and H fields are related to each other. In air, the relationship between these quantities is given by

$$H = \frac{E}{377\,\Omega} \tag{2.3}$$

Therefore specifying one of these quantities directly gives the other value.

2.4.2. Isotropic antenna

An isotropic antenna is an ideal antenna (practically does not exist) whose radiation pattern is often used for reference purpose to compare the radiation pattern of other antenna with it. In theory, an isotropic antenna is assumed to be a point source which radiates power equally in all directions. Often the directive gain or the gain of a tag or a reader antenna is referenced to it, and the results are given in dB or dBi [34, 35].

2.4.3. Antenna gain

In antenna design, the power gain is of great importance. Thus when the term gain is used, it implies the power gain of the antenna. Generally it describes how well the power received by the antenna is radiated in EM waves compared to a loss-less isotropic antenna or a reference antenna. Due to this the gain (G) is defined in terms of an absolute or a relative value.
The absolute gain of an antenna can be defined as the ratio of transmitted power (P) in the direction of the main radiated beam of an antenna to the power which would have been transmitted by the antenna isotropically [35]. The power transmitted by an isotropic antenna is equal to the power accepted by the antenna divided by 4π. In mathematical form it can be written as

$$G = \frac{P}{P_{\text{iso}}} = \frac{P(\theta, \phi)}{\frac{P_{\text{in}}}{4\pi}} \tag{2.4}$$

where $P\left(\theta, \phi\right)$ represents the radiated power per unit solid angle in the direction of (θ, ϕ).
In terms of relative gain it is defined or calculated by determining the power gain in a given direction to the power gain of a reference antenna in that direction. To calculate or determine the relative gain mostly horn, dipole, isotropic or any other antennas are considered whose antenna gain value is known or can be measured.

If the reference antenna is an isotropic antenna then the relative gain and absolute gain are the same. Typically the $\frac{\lambda}{2}$ loss-less linear dipole antenna has the maximum gain value of 2.15 dB or 2.15 dBi to emphasize that it is referenced to the isotropic antenna [34, 35]. When it is referenced to the dipole antenna then it has the typical gain of 1.64 dBd. An illustration comparison between the gain pattern of an isotropic and a dipole antenna is shown in figure 2.12.

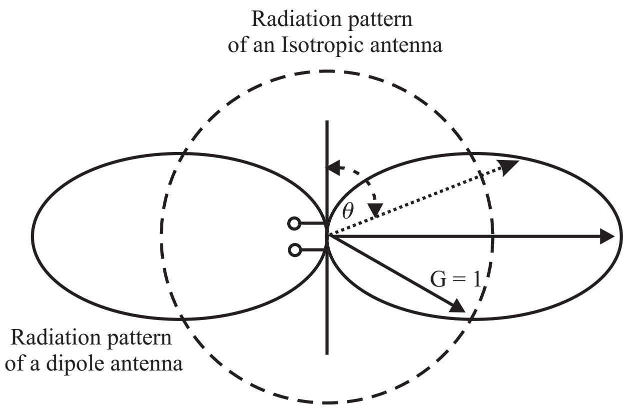

Figure 2.12.: *Comparison of a typical isotropic vs dipole antenna radiation pattern*

2.4.4. Directivity

Generally, directivity (D) of an antenna describes how much power is concentrated in a given direction compared to the reference antenna. It can be described as the ratio of maximum power transmitted in the direction of the main radiated beam peak point of an antenna to the average radiated power (P_{ave}) in an isotropic antenna [35]. Mathematically it can be mentioned as

$$D = \frac{P}{P_{\text{ave}}} = \frac{P(\theta, \phi)}{\frac{P_{\text{rad}}}{4\pi}} \tag{2.5}$$

where P_{rad} is the total radiated power by the antenna and $P(\theta, \phi)$ represents the radiated power per unit solid angle in the direction of (θ, ϕ).
The difference between the gain and the directive gain of an antenna is discussed in section 2.4.6.

2.4.5. Input impedance

As already mentioned, functional behavior of an antenna could be described using circuit elements. A more accurate model of a typical antenna structure is shown in figure 2.13. In this circuit, X_{ant} represents the total antenna reactance, and it

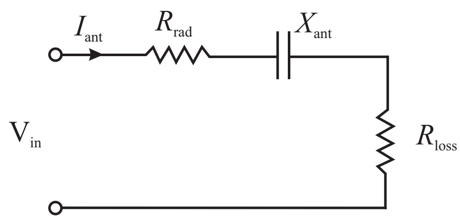

Figure 2.13.: *Antenna circuit schematic*

characterizes how much the antenna stores energy in the field near the antenna. R_{rad} represents the radiation resistance and it takes into account the energy transfer in the propagated fields. The R_{loss} models the losses of the surrounding material to which an antenna is attached [35].
In that case, the total complex impedance value of an antenna structure can be described as

$$Z_{\text{ant}} = X_{\text{ant}} + R_{\text{ant}} = X_{\text{ant}} + R_{\text{rad}} + R_{\text{loss}} \tag{2.6}$$

In general, the total impedance value of an antenna depends on various parameters, such as size, shape, surrounding material, frequency e.t.c.. As an example, the dependence of the impedance value on the frequency of a linear dipole antenna is shown in figure 2.14.

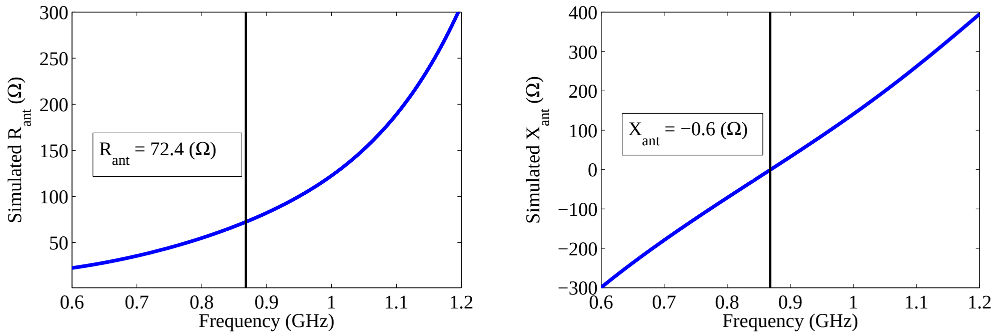

(a) Frequency vs. R_{ant} (b) Frequency vs. X_{ant}

Figure 2.14.: *Dependance of the impedance value versus frequency of a linear dipole antenna*

2.4.6. Radiation efficiency

As mentioned above, the useful power from an antenna structure is the power that is radiated, not the power loss that is lost in terms of heat. The power dissipating elements in the antenna structure are shown in figure 2.15. It can be seen that the

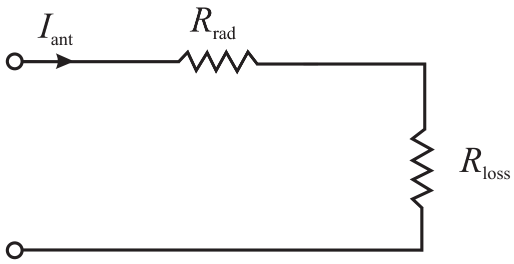

Figure 2.15.: *Power dissipated by different component of a antenna*

X_{ant} element is not considered because it just stores the energy. Hence, the total amount of power dissipated in the antenna structure based on circuit analysis can be given as

$$P_{\mathrm{ant}} = P_{\mathrm{rad}} + P_{\mathrm{diss}} = I_{\mathrm{ant}}^2 \left(R_{\mathrm{rad}} + R_{\mathrm{loss}}\right) \tag{2.7}$$

and the amount of radiated power is given by

$$P_{\mathrm{rad}} = I_{\mathrm{ant}}^2 . R_{\mathrm{rad}} \tag{2.8}$$

Then the power radiating efficiency (η) of the antenna can be defined by

$$\eta = \frac{P_{\mathrm{rad}}}{P_{\mathrm{ant}}} = \frac{R_{\mathrm{rad}}}{R_{\mathrm{rad}} + R_{\mathrm{diss}}} \tag{2.9}$$

In terms of radiation efficiency of the antenna the directivity and the gain of an antenna are related to each other [35]. The relationship among these quantities can be mentioned as

$$\eta = \frac{G}{D} \tag{2.10}$$

η represents the radiation efficiency of the antenna.
In brief, the major difference between G and D is that the gain takes into account the effects of losses in the antenna and surrounding structures, whereas the directivity is solely determined by the radiation pattern shape of the antenna. In lossy environment, the value of G is less than D because some power is consumed in terms of heat [35].

2.5. Antenna radiating field region

The field radiated around an antenna can be divided into different field regions. The major field regions are near field region, transition or radiation near field region and far/Fraunhofer field region. These are discussed one by one as follows:
In the near field region (r), reactive fields are predominating. This field region is of great interest for RFID systems which operate using the near coupling principle i.e. RFID systems which operate in 125 kHz and 13.5 MHz bands. In this region, the radiated field around the antenna decay quite fast with distance r. Approximately fields decay with a factor of $\frac{1}{r^3}$ [35]. Due to this, the detection range is quite small [10, 34]. An approximately maximum range limit of this region can be determined using

$$r < 0.62\sqrt{\frac{L^3}{\lambda}}, \tag{2.11}$$

where L is the largest dimension of the antenna and λ represents the wavelength of the operating frequency.
In the Fraunhofer or far field region, the radiated field predominates. In this region, angular field distribution almost stretches from angular to straight form and therefore the radiated field is independent of the angular distance from the antenna. Mostly, back-scatter passive long range UHF RFID systems use this field region for operation. Approximately, the beginning of this region can be obtained by [10,34,35]

$$r > \frac{2L^2}{\lambda} \tag{2.12}$$

The transition or radiation near field lays in between these above mentioned two field regions and approximately can be given by

$$0.62\sqrt{\frac{L^3}{\lambda}} < r > \frac{2L^2}{\lambda} \tag{2.13}$$

In this region the fields are in transit phase and the radiation fields depend on the angular direction.

2.6. Performance evaluation of an UHF RFID tag

One way to analyze the performance of a tag design is to determine the maximum detection read range. It is the distance at which an RFID tag attached to an object can be detected in free space by an RFID reader, when the maximum allowed power is transmitted. By comparing the read range of designed and fabricated prototype tag with each other performance of tag can be evaluated. Furthermore using this indirect way it is possible to determine the usefulness of an electrical model of a structure [2]. Using that procedure basically the simulated and the measured maximum read range of the designed tag are compared with each other. Using that strategy, the developed electrical model of belt suitability is checked and results are presented in chapter 4. However, in the following section some basics related to estimate the simulated and the measured maximum read range of a tag are discussed.

2.6.1. Estimating the maximum read range by Friis formula

The read range of a tagged objected can be estimated using the Friis formula [5, 27]. Details about how to derive the general expression and how to evaluate the maximum read range of an UHF tag are discussed below.
Schematically a passive UHF RFID system can be represented by figure 2.16. A

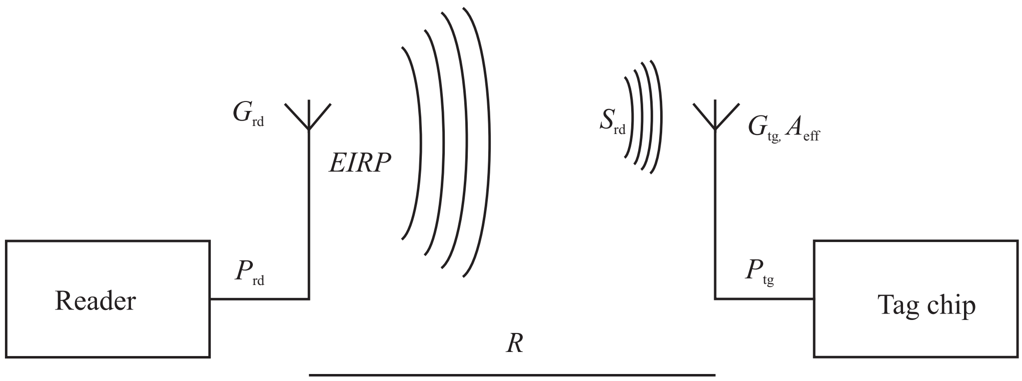

Figure 2.16.: *A passive UHF RFID system schematic redraw*

typical value of the received power by the tag antenna P_{tg} from the reader module can be given as

$$P_{\text{tg}} = S_{\text{rd}}.A_{\text{eff}} \tag{2.14}$$

where S_{rd} is the radiated power density at the tag antenna and A_{eff} is the effective aperture of the tag antenna.
If the tag antenna is placed at a distance R from the reader antenna, sufficient apart from the near field region, then the value of S_{rd} can be specified by

$$S_{\mathrm{rd}} = \frac{P_{\mathrm{rd}} G_{\mathrm{rd}}}{4\pi R^2} \tag{2.15}$$

Generally, A_{eff} depends on the wavelength (λ) of the operating frequency and the gain of the tag antenna G_{tg}. Its value can be calculated as

$$A_{\mathrm{eff}} = \frac{\lambda^2}{4\pi} G_{\mathrm{tg}} \tag{2.16}$$

If the value of (2.15) and (2.16) are put into (2.14) then the power received at the tag antenna can be determined by

$$P_{\mathrm{tg}} = G_{\mathrm{tg}} G_{\mathrm{rd}} P_{\mathrm{rd}} \left(\frac{\lambda}{4\pi R} \right)^2 \tag{2.17}$$

The relation given in (2.17) is known as Friis formula. Now it will be shown how (2.17) is modified to determine the read range of an UHF RFID tag.
The amount of power the tag antenna receives is not delivered optimally to the tag chip if the impedance of the tag antenna and the tag IC do not match. The parameter which defines this mismatch is known as, already defined by (2.1), τ. By Incorporating that parameter in (2.17), the power delivered to the tag chip (P_{chip}) can be calculated as

$$P_{\mathrm{chip}} = P_{\mathrm{tg}} \tau = G_{\mathrm{tg}} G_{\mathrm{rd}} P_{\mathrm{rd}} \tau \left(\frac{\lambda}{4\pi R} \right)^2 \tag{2.18}$$

If (2.18) is rearranged in terms of R then the maximum read range can be calculated as

$$R = \left(\frac{\lambda}{4\pi} \right) \sqrt{\frac{G_{\mathrm{tg}} G_{\mathrm{rd}} P_{\mathrm{rd}} \tau}{P_{\mathrm{chip}}}} \tag{2.19}$$

The equation (2.19) may be simplified as (2.20) because the maximum power to be transmitted from the reader system is controlled from regulating authorities.

$$R = \left(\frac{\lambda}{4\pi} \right) \sqrt{\frac{G_{\mathrm{tg}} \tau EIRP}{P_{\mathrm{chip}}}} \tag{2.20}$$

where $EIRP$ represents the effective isotropic radiated power and is equal to the product of G_{rd} and P_{rd}. The maximum of 3.28 Watt $EIRP$ is allowed to be transmitted by UHF reader systems in the European ISM band [6]. P_{chip} represents the typical minimum power at which the tag chip starts giving response to the reader system.

Basically to determine the maximum read distance using (2.20), information about the three parameters are required. Those parameters are the chip sensitivity, the gain and the power transmission coefficient.
In general, the minimum power value P_{chip} is usually given by the RFID tag chip manufacturer in their data sheets. For example the Impinj GmbH and the NXP GmbH [37, 38] mention this value in their Tag IC data sheets. Additionally, the impedance value of a tag chip is also given by the chip manufactures too. Hence, to estimate the read range via (2.20) information regarding the tag antenna impedance Z_{tg} and the tag gain G_{tg} are required. These can be determined either by measurement or with the help of numerical EM simulations [17, 29, 39, 40]. In this thesis, these parameters are obtained using the later approach i.e via the numerical electromagnetic simulation results. Therefore the theoretical read range is named as R_{sim}, and the modified equation to determine the theoretical read range is given as

$$R_{\text{sim}} = \frac{\lambda}{4\pi}\sqrt{\frac{G_{\text{tg}} EIRP \tau}{P_{\text{th}}}} \tag{2.21}$$

2.6.2. Read range estimation via measurement in an anechoic chamber

The read range of an UHF RFID tag depends on many factors [41, 42]. Typically, it is upto 10 to 14 m for maximum allowed transmitted power [42]. Generally it is hard to measure the maximum read range in the open air space condition due to multiple path effects. Therefore, the read range of a tag is mostly estimated based on measurement performed in an anechoic chamber [42–44]. An anechoic chamber is a 3D box/room inside which, on their walls, field absorber materials are stacked to absorb the impinged electrical fields. Due to field absorbers, minimum reflection occurs with minimum impact on the measurement results. Therefore, such a chamber is suitable for measuring the different antenna parameters.
Usually the size of an anechoic chamber is small compared to the maximum read range of tagged objects in air, therefore the maximum read range can only be estimated indirectly by measurements. The read range (R_{mea}) of a prototype tag in air for maximum allowed EIRP can be calculated as [27, 42, 45]

$$R_{\text{meas}} = \mathrm{d}_{\text{rt}}\sqrt{\frac{EIRP}{G_{\text{rd}} L_{\text{loss}} P_{\text{min}}}} \tag{2.22}$$

where d_{rt} is the distance between the reader antenna and the tag, L_{loss} are the total losses of coaxial cables connected between the reader module and the reader antenna, and P_{min} is the minimum power required to be transmitted via an RFID reader to detect the presence of the tag.

A typical setup used to carryout the measurement is shown in figure 2.17. Principally, to estimate the maximum read range of a tag with this method, only

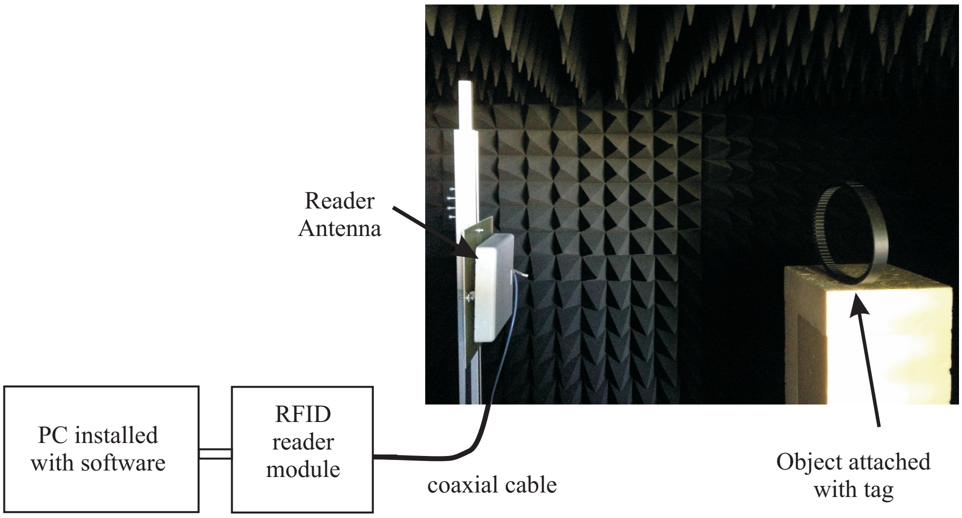

Figure 2.17.: *The layout of the setup used to measure read range of a tag*

one parameter, i.e. the $P_{\min}$ value, needs to be determined. To find this value, in an anechoic chamber, a tag or a tagged object is placed at a fixed distance in front of the reader antenna. Then, the power from the reader module is stepped up gradually at the desired frequency by changing the attenuator factor until the tag presence is detected by it. The minimum power at which the tag is detected, by the reader, corresponds to $P_{\min}$ [2, 3].

CHAPTER **3**

Electrical characterization of different rubber sheets

Generally, a raw rubber (obtained from trees or synthetic) is blended with various chemical compounds in different percentages to obtain the requested flexibility and hardness. Usually the materials are available in block or sheet forms. Depending on the desired physical characteristic and shape in the end rubber product, various rubber materials of a given thickness with some additional cords (if required) are manufactured in the desired layer-stack. Then this layer-stack is shaped into different forms to get the end rubber product [46–48]. As rubber applications are so diverse the used recipes are not unique. Due to this reason various kind of rubber sheets have different electrical parameter values, and usually information regarding them is not known or given in any data sheet. At least these are not available for the considered rubber belts.

As mentioned in chapter 1, it is intended to establish and optimize the design and analysis process of UHF RFID tag antennas for the rubber belts. First, for that, it is required to study the electrical characteristics of the various rubber sheets, and then to take account their impact on the tag antenna performance. Furthermore, it is desired to cover a wide range of different structures of belts with a minimum number of different tags. To explore that, it is required to find the typical range of the electrical parameters for different rubber sheets[1], the electrical parameters of the specific rubber sheets used in the rubber belt and the variation in the parameters.

In this regard, an electrical characterization setup is developed to determine the electric parameter values of different rubber materials [1]. The detail of it is pre-

[1]used in the considered variety of rubber belts

sented in this chapter. In addition, the reliability and accuracy of the setup is examined and its results are discussed. Furthermore, by utilizing this setup the electrical properties of two important materials (i.e. EPDM and CR) used in the considered rubber belts are evaluated, and results are discussed.

3.1. Basics of the electrical characterization of a dielectric material

Every material basically consists of atoms and molecules which are arranged in either random or symmetrical order. The basic form of each atom and molecule is composed of negative and positive charged particles. These charged particles change their positions and directions when an EM field is applied to them. This results in creation of either electric or magnetic dipoles or both in the material [49]. These generated dipoles create an extra field and exert an opposite force to the applied field. If the number of created and aligned dipoles is sufficient, then these dipoles create a measurable change in the applied field. Based on these phenomena, a material is characterized either as dielectric or as magnetic material. As the focus of this chapter is to investigate the electrical properties of rubber material, the electrical properties can be examined by considering it as a lossy dielectric material [12]. Therefore, some fundamentals are presented below to study the electrical properties of such materials.

When a sinusoidal electrical field is applied to a linear isotropic material then the relationship between the applied field $\vec{\boldsymbol{E}}$ and the generated electrical dipoles, in phasor form, can be described as follows [50]

$$\vec{\boldsymbol{D}} = \epsilon_0 \left(1 + \boldsymbol{\chi}\right) \vec{\boldsymbol{E}} = \epsilon_0 \vec{\boldsymbol{E}} + \boldsymbol{P} = \boldsymbol{\epsilon} \vec{\boldsymbol{E}} \tag{3.1}$$

where $\vec{\boldsymbol{D}}$ is the displacement field vector, ϵ_0 denotes the permittivity value of free space, $\boldsymbol{\chi}$ is a complex constant of proportionality called the electric susceptibility, $\boldsymbol{P} = \epsilon_0 \chi \vec{\boldsymbol{E}}$ corresponds to the electric polarization of the material and takes into account average dipole moments created in unit volume, and $\boldsymbol{\epsilon}$ represents the complex permittivity of the material [50, 51].
The complex permittivity consists of the real part $\epsilon^{'}$ and the imaginary part $\epsilon^{''}$. This can be described as

$$\boldsymbol{\epsilon} = \epsilon^{'} - j\epsilon^{''} = \epsilon_0 \left(1 + \boldsymbol{\chi}\right) \tag{3.2}$$

where $\epsilon^{'}$ corresponds to the total energy stored in the material, $\epsilon^{''}$ takes into account the energy consumed in the material due to frequency dependent effects (i.e. the fractional force which exist while moving the generated charge in a frequency cycle) [12, 51].

Generally energy loss in the dielectric material may occur due to some ionic conductivity σ and due to frequency dependent mechanism. It is hard to differentiate this loss mechanism from the loss mechanism caused by the attenuating effect as far as external causes related to power dissipation are concerned [51]. The significance of such type of losses to our investigations may also be described as follows: Generally, in a conductive dielectric material, the relationship between the ionic conductivity (σ) and the resultant conduction's current density $\vec{\boldsymbol{J}}$ can be described as [49]

$$\vec{\boldsymbol{J}} = \sigma \vec{\boldsymbol{E}} \tag{3.3}$$

When the field with the angular frequency ω is applied to a material, then, using one of the Maxwell equations[2] [51], the relation between the conductive current and the displacement current in the material can be given as

$$\vec{\nabla} \times \vec{\boldsymbol{H}} = j\omega\vec{\boldsymbol{D}} + \vec{\boldsymbol{J}} = j\omega\vec{\boldsymbol{D}} + \sigma\vec{\boldsymbol{E}} \tag{3.4}$$

where $\vec{\nabla}\times$ represents the curl operator.
If the value of (3.1) and (3.2) is substituted in (3.4) then

$$\vec{\nabla} \times \vec{\boldsymbol{H}} = j\omega\left(\epsilon^{'} - j\epsilon^{''}\right)\vec{\boldsymbol{E}} + \sigma\vec{\boldsymbol{E}} \tag{3.5}$$

is given.
If real and imaginary parts are rearranged then (3.5) can be modified as follows

$$\vec{\nabla} \times \vec{\boldsymbol{H}} = j\omega\epsilon^{'}\vec{\boldsymbol{E}} + \left(\sigma + \omega\epsilon^{''}\right)\vec{\boldsymbol{E}} = j\omega\left(\epsilon^{'} - j\left(\epsilon^{''} + \frac{\sigma}{\omega}\right)\right)\vec{\boldsymbol{E}} \tag{3.6}$$

Equation (3.6) shows that the total effective conductivity of the material is $\left(\sigma + \omega\epsilon^{''}\right)$.

With the help of (3.6) the loss of a dielectric material can be defined by

$$\tan\delta = \frac{\left(\sigma + \omega\epsilon^{''}\right)}{\omega\epsilon^{'}} \tag{3.7}$$

It means that tangent loss measurements include the conductive loss of a material too. At higher frequency bands in low conductive dielectric materials, the value of σ is much smaller than $\omega\epsilon^{''}$ [51]. Therefore the contribution of losses due to σ can be neglected. Hence (3.7) can be modified as

$$\tan\delta = \frac{\epsilon^{''}}{\epsilon^{'}} \tag{3.8}$$

[2] through which the wave propagation and interaction of EM waves with the material can be studied in detail

Practically, the real part of the permittivity value of a material is defined relative to the permittivity value of air. The relative permittivity value of any material can be defined as

$$\epsilon_{\mathrm{r}} = \frac{\epsilon^{'}}{\epsilon_0} \tag{3.9}$$

where ϵ_{r} is relative permittivity of a material. It characterizes the amount of energy stored in the material relative to air.

If the value of (3.8) and (3.9) is substituted in (3.2) then the complex permittivity ϵ can also be defined as

$$\epsilon = \epsilon^{'} - j\epsilon^{''} = \epsilon^{'}\left(1 - j\tan\delta\right) = \epsilon_{\mathrm{r}}\epsilon_0\left(1 - j\tan\delta\right) \tag{3.10}$$

In the tag design process, the ϵ_{r} value of a material mainly influences the size of the tag antenna. The $\tan\delta$ value mainly affects the impedance, the gain (typically its radiation efficiency) and impedance bandwidth of an UHF RFID tag antenna.

3.2. Basics of electric characterization methods

The operation of radio frequency (RF) and microwave frequency electronic devices is influenced by the dielectric properties of the materials [52]. Therefore, the knowledge of dielectric parameters of the materials is quite important for RF and microwave engineering. Applications of electronic devices are so diverse that numerous materials are utilized in such devices. These devices are widely used in common people daily life, military, space, telecommunication communication e.t.c. Thus to determine the electric properties of diverse materials numbers of electric characterization setups have been developed. Broadly working principles of these setups is either based on resonant or non resonant methods [52]. To investigate and to evaluate the electric properties of the various rubber materials used in a rubber transmission belt, based on each method, the electrical characterization is carried out. Basics of these methods are discussed in the following section, and later the results will be presented.

3.2.1. Electrical characterization using a parallel plate dielectric resonator (resonant method)

Based on a resonance method, a parallel plate dielectric resonator (as shown in figure 3.1) is constructed to determine the electrical parameters of the rubber materials [52,53]. It is a typical application of a rectangular waveguide [52,54,55]. Using this method, the electrical parameters of a sample sheet, placed between the plates, are calculated at the excited transverse electrical (TE_{mn}) resonance mode frequencies using the approximated analytical expressions [1]. These modes are excited between the plates when energy is provided via an external source such as a Vector network analyzer (VNA). As the rectangular waveguide is not closed from all sides,

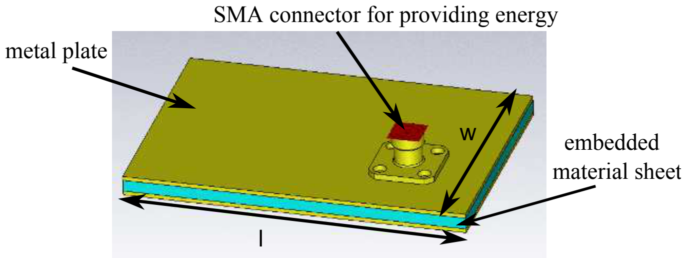

Figure 3.1.: *A parallel plate dielectric resonator*

an analytical formula can be used to approximate the ϵ_r value of a material based on the excited TE_{mn} resonance mode frequencies and the dimension of the parallel plates:

$$\epsilon_r = \left[\frac{1}{2f_{mn}\pi\sqrt{\mu_r\mu_0\epsilon_0}}\sqrt{\left(\frac{m\pi}{w}\right)^2 + \left(\frac{n\pi}{l}\right)^2}\right]^2 \tag{3.11}$$

w is the width of the plate, l describes the length of the plate, f_{mn} defines the resonance mode frequency, and m and n represent the excited mode number.

The approximated tanδ value at the excited resonance mode can be calculated by [1, 52]

$$\tan\delta = \frac{2\left(\Delta f_r\right)_{-3\mathrm{dB}}}{f_r} \tag{3.12}$$

where, $(\Delta f_r)_{-3\mathrm{dB}}$ is the value of the frequency point around the resonant mode where the magnitude of the mode changes by -3 dB.

The advantage of this method is that it uses analytical expressions to calculate the electrical parameter values of a material. Hence the reliability of the determined results is quite accurate. The major disadvantage of this method is that to determine the unknown electrical parameters of a sample sheet at the frequency of interest, the resonance mode (especially TE_{01}) should be excited with the proper chosen dimensions of the parallel plates. Experimentally, the selection of proper dimensions of the parallel plate is an iterative approach, as excitation of the principle TE_{01} resonance mode at a particular frequency depends on ϵ_r. Therefore, it is required to construct a separate fixture using an iterative approach to determine the electrical parameters of every rubber sheet. Hence the evaluation of the electrical parameters is quite time consuming. In addition, practically it is observed that excitations of resonance mode frequencies and its magnitudes are also slightly varying due to

difficulty in pressing the parallel plate resonator fixture with homogenous force. This adds some inaccuracies in the results [1].
To avoid these problems, this method is not used to determine the electrical properties of all rubber sheets which are used in the considered rubber belt. However, to compare the accuracy of measurements taken from the open ended coaxial method (described in the next section), this method is implemented once and results of the comparison are presented in table 3.5 on page 52.

3.2.2. Electrical characterization using an open-end coaxial probe method (non-resonant method)

An open-ended coaxial probe method is a type on non-resonant method. It is applied to determine the electrical properties of various high loss materials [1, 22, 52, 56–58]. Basically using this method, electrical parameters of an unknown dielectric material are determined in two steps.

First Step: In the first step, changes on the impinged signal caused by a material under test (MUT) are measured. Figure 3.2 shows a typical layout of a measurement system used to detect such changes [22, 56, 57]. To measure the

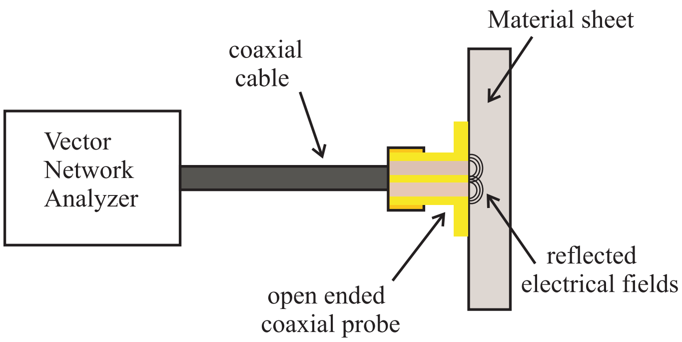

Figure 3.2.: *Measurement setup to measure changes in the applied signal*

changes, first an open-ended coaxial probe is placed on a material under test. Then, EM fields are launched through this probe via a vector network analyzer (VNA) and are impinged on the MUT. Due to the applied field the MUT gets polarized and causes variations in the applied field at the probe and MUT interface as discussed in the section 3.1. These are measured via the VNA, usually in terms of the complex reflection coefficient (S_{11}) or impedance/admittance value.

Second step: In the second step, these measured value is compared to the calculated value, obtained based on various techniques (such as complex mathematics computation [59], modeling techniques[3] [60], numerical electromagnetic

[3]such as capacitive model, antenna model, virtual line model, rational functional model

computation using full wave solver [1, 22] e.t.c.) to extract the electrical parameter values.
Broadly in all such extraction approaches, the measured and the estimated value are compared with each other and the error between these two values is reduced to determine the electrical parameter values [61].

There are several advantages of this method. The major benefit is that only a single fixture is required to determine the electrical parameters of various material sheets. Furthermore, using the simple implementation process the electrical parameters can be determined at any desired frequency [1, 22, 56, 57]. Due to these benefits this method is preferred over the parallel plate resonant method to determine the electrical properties of the different rubber materials. The details of the developed setup, based on the open-ended coaxial method, are presented in the following section [1].

3.3. The measurement system in detail

As just discussed, the electrical characterization using the open-ended coaxial probe method is carried out in two steps. In the first step the changes caused by the MUT is measured. In the second step the electrical properties with some extraction technique are evaluated. In this section, details of the system used to measure the changes are given. Afterward, in the next section the details of the applied extraction technique will be discussed.

Figure 3.3 shows the complete measurement system built up in the laboratory, utilized to sense the changes of the numerous rubber material sheets [1]. This setup consists of the following major components:

- An open-ended coaxial probe
- Spring fixture
- Robot arm
- Vector network analyzer (VNA)

The function of these parts in the setup is discussed one by one as follows.

An open-ended coaxial probe
Basically, an open-ended coaxial probe is a typical type of a coaxial line. It usually consists of an inner conductor, an outer conductor and a dielectric material which is filled between them. The dimensions of these conductors and the electrical parameter values of the dielectric material affect the total impedance value of the coaxial

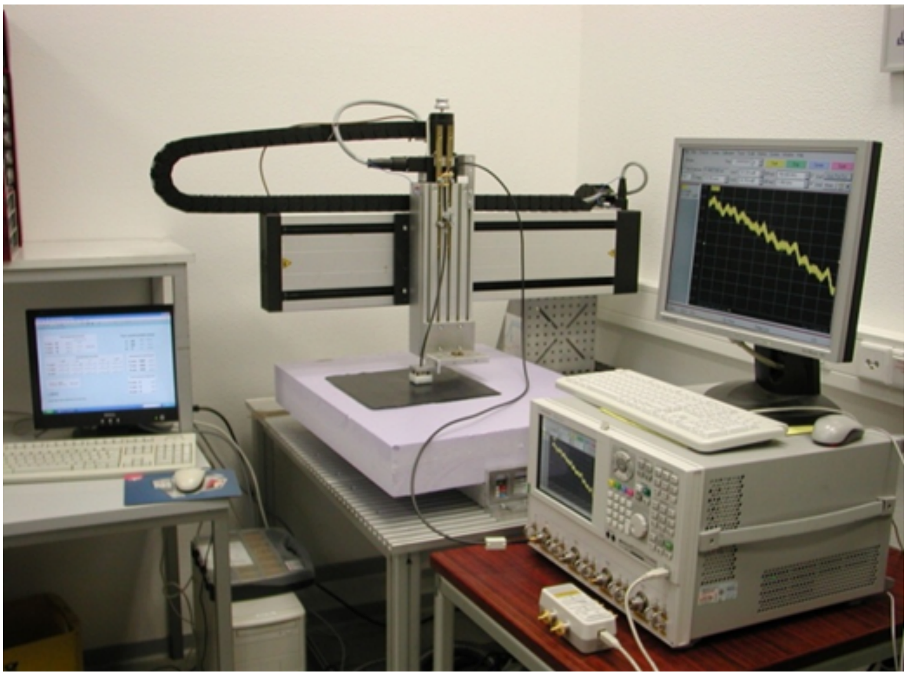

Figure 3.3.: *Picture of the complete measurement system built up in the lab utilized to detect the changes in terms of the reflection coefficient*

probe [51]. A general expression showing the relation between these parameters and the impedance is given by (3.13).

$$Z_{\mathrm{c}} = \frac{1}{2\pi}\sqrt{\frac{\mu}{\epsilon}}\ln\left(\frac{b}{a}\right) \tag{3.13}$$

where a denotes the diameter of the inner conductor, b represents the diameter of the outer conductor and Z_{c} is the total impedance value of the coaxial model.
To built the measurement setup, an open-ended coaxial probe, having 50 Ω impedance, from the HUBER and SUHNER (HUBER and SUHNER 23 SMA 50 01 [62]) is selected. The considered probe is shown in figure 3.4. The inner conductor has a diameter of 1.2 mm, whereas, the outer conductor has a diameter of 4.1 mm. A Teflon material exists between these connectors. Typical electrical parameter values of the Teflon dielectric material are $\epsilon_{\mathrm{r}} = 4.3$ and tanδ=0.003. To measure the changes in the reflection coefficient accurately, it is attached to a spring fixture [1].

Spring fixture
To ensure a proper contact of an open-ended coaxial probe with the sheets, a spring fixture is designed and fabricated. The fabricated one is shown in figure 3.5(a).

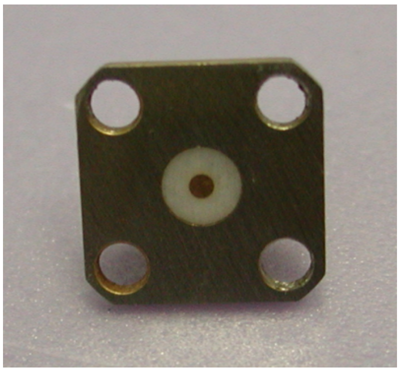

Figure 3.4.: *An open-ended coaxial probe*

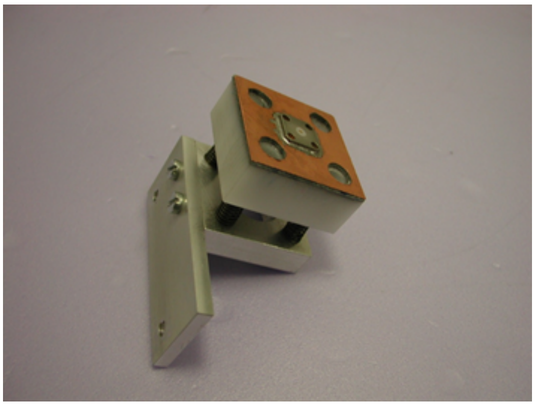

(a) A spring fixture

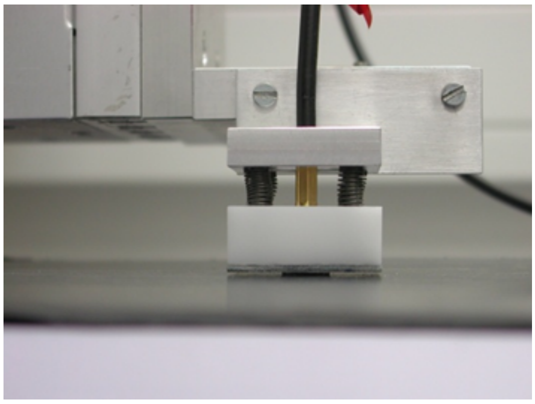

(b) An open-ended probe placed over a material sheet

Figure 3.5.: *Spring fixture and its contact to a rubber sheet*

A pressing mechanism in this spring fixture helps to reduce the air gap between the open-ended probe and the sample (as shown in figure 3.5(b)). Additionally, it also helps to apply a proper force between the open-ended probe and the sample. In absence of the fixture, it would have been quite hard to hold and press the probe over a sample sheet with a constant force for a longer time to measure the correct changes [1].

A robot arm

A robot arm is used to control the position of the probe over the sample sheet. With the help of the robot arm, it becomes easy to perform reproducible measurements [1]. To show that the developed setup can reproduce the results, a reproducibility test is carried out, and results are presented in subsection 3.6.2.

Vector Network Analyzer (VNA)
The vector network analyzer is an important device that is used at radio or microwave frequency to determine or analyze various materials, components and analog circuit's electrical characteristics. Basically it measures the reflection coefficient, magnitude and phases of transmission and reflection of a material or an analog circuit. Then it utilizes them to reveal all the electrical characteristics [52]. The basic how to perform the measurements using a VNA can be found in [63].
A MUT can not be put directly on the detector of the VNA, therefore, a coaxial cable is attached to the device to extend it's measurement plane. Before detecting the actual changes caused by a MUT, a calibration of the device needs to be performed. Basically by using the calibration process, the impact of the attached coaxial cable on the actual measurements is removed and the measurement plane is extended to the end of an attached coaxial cable [64]. Calibration can be performed via the user built fixtures or the electronic kit provided by the device manufacturer such as Agilent [1, 64].
To carry out the measurements via the considered VNA, one port calibration is performed using the electronic calibration kit. The following settings of the device are set: frequency range from 600 MHz to 1150 MHz with 20000 points, device output power of 0 dBm and filter bandwidth of 7 kHz. Once the calibration process is carried out the open-end probe fixture is attached to the coaxial cable and then changes are measured using the VNA.

Precaution while taking measurements

The following points need to be taken care of while taking the measurements using the system [1]:

- A coaxial cable attached to a VNA should not move while carrying out the measurement because movement of the cable affects the detected reflected value.

- To measure the changes accurately it is required that the surface of the material sheet and the plat-form on which the sheet is placed must be flat.

3.4. Extraction of the material properties

In the above section, the details of the measurement system are presented. Now in this section, it is discussed how the electrical parameters are extracted from the corresponding measured changes [1]. Afterward, it will be shown how the complete electrical characterization setup is used to find the electrical parameters of the various rubber materials.

3.4.1. Extraction of electrical parameters using a 3D EM model

In this thesis, the electrical properties of a material are extracted by an equivalent 3D model of the measurement setup (as shown in figure 3.6) using numerical electromagnetic computation. The equivalent model consists of an open-ended

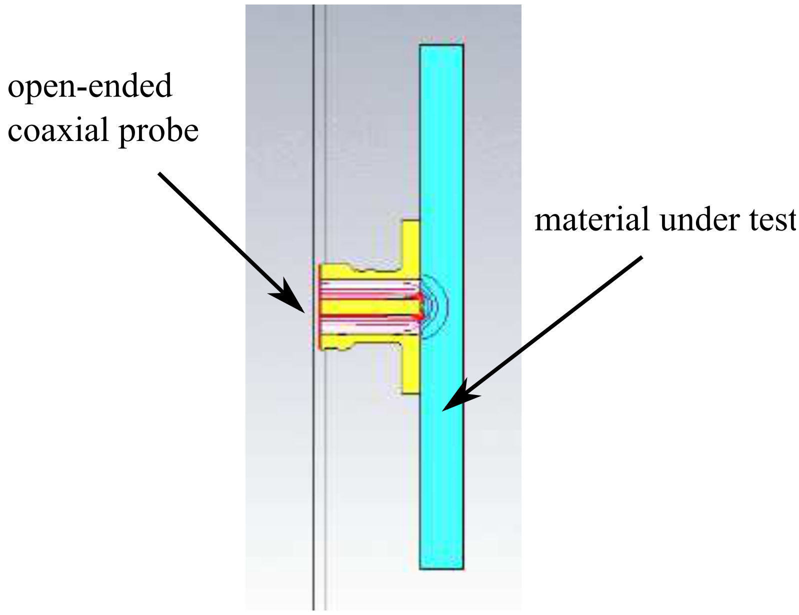

Figure 3.6.: An equivalent model of the measurement setup to extract electrical parameters from the measured reflection coefficient

probe and a sample sheet model (further detail of the model is presented later in this subsection). Starting from default values the electrical parameters of a material model during the simulation are varied as long as the simulation result fits to the measured result. These final model parameters are assumed to be the characteristic material parameters of the measured material. Furthermore, to make the process of finding the electrical parameters simple, fast and independent of parametrized simulations, a look-up table is created. The table is defined, based on the simulation results with predefined electrical parameter values, by writing a Matlab script [1]. Then the electrical parameters are extracted from it similar to an inverse like problem [65]. The detail about this extended extraction process will be given in subsection 3.4.2.

The major benefit of the numerical electromagnetic computation technique is that without solving tedious mathematics or using reference materials, electrical parameters of unknown materials can be determined quite easily [59, 66].

A similar numerical electromagnetic computation technique has been applied in [22] with some differences. In [22] every time sequences of simulations need to be performed to extract the material parameters. In this thesis, with the help of the modified numerical algorithm or based on the defined look-up table, the material parameters are determined instantly without performing repetitive parametrized simulations. Hence the proposed extraction strategy is more time efficient once the loop-up table is constructed [1].

The thickness of a sample sheet is the main parameter on which the obtained simulated reflection coefficient and the accuracy of this method depends. One of the simplest ways to determine the required minimum thickness of a sample sheet for the considered coaxial probe is to use parametrized numerical EM simulations. In this thesis, the required minimum thickness of a sample sheet is determined by a 3D numerical EM solver program (using CST Design Studio). To find this value, a parametrized sweep of thickness parameters is carried out with the simulation model. To accomplish this parametrized sweep, typical electrical parameter values are supposed in the simulation model ($\epsilon_r = 7.3$ and $\tan\delta = 0.10$). These are the typical values which are expected for a rubber sheet. The results of this thickness parametrized sweeps are shown in figure 3.7. It can be observed that the change

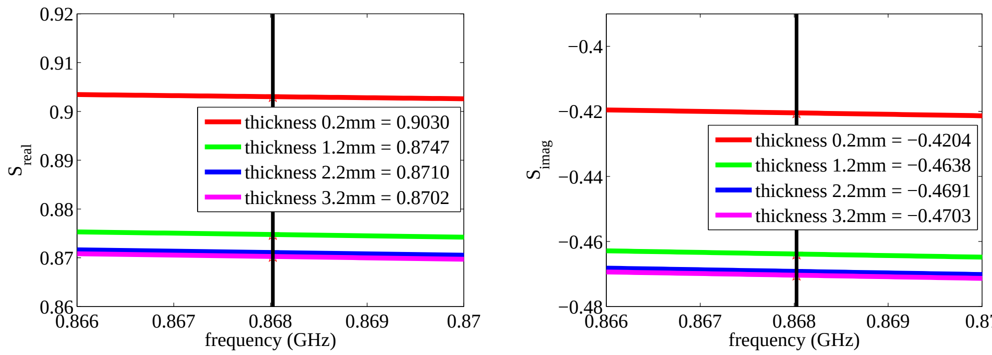

(a) Real part of the reflection coefficient (b) Imaginary part of the reflection coefficient

Figure 3.7.: *Relationship between thickness of a sample and corresponding simulated reflection coefficient values*

in the reflection coefficient value is not significant once the sample thickness becomes more than 2.2 mm. To be sure that sufficient thickness of the sample sheet is included in the model, the final thickness of 3.2 mm is considered for the sample sheet [1].

Detail of the 3D virtual measurement model

As just described above, the 3D virtual measurement model is used to extract the electrical parameters. The detail of the virtual model (depicted in figure 3.8), used in CST studio, is mentioned as follows. It consists of an open-ended probe and a

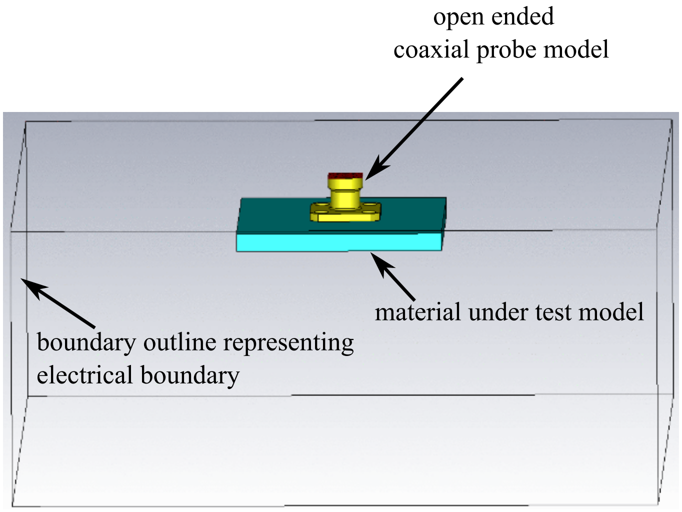

Figure 3.8.: *3D numerical EM model of measurement setup*

sample sheet model. The 3D model of the coaxial probe is constructed from the CAD file provided from the manufacturer [62], whereas a material sheet 3D model, having a thickness of 3.2 mm, is constructed using drawing tools provided by the field solver.

After the construction of the 3D model, the next stage is to set a proper simulation setting to acquire the simulated reflection coefficient. For that, the appropriate port to launch the energy on the sample sheet, the boundary condition, a proper field solver and the meshing of the both components are need to be chosen. The selection of these various settings impact the amount of accuracy and the simulation time. Therefore a compromise needs to be made between time and accuracy. For the constructed model, the following settings for the various parameters are set/selected.

- A wave guide port is selected to launch the EM fields.
- A frequency solver with tetrahedral mesh is selected as field solver.
- Frequency range between 600 MHz to 1050 MHz with 20000 points is set.
- Add open space option is selected and a distance of 40 mm is set in all direction except the wave guide port side to minimize the reflection of energy.
- Tetra meshing of the sample sheet, the inner conductor, the Teflon dielectric material and outer flange conductor body is set locally. The considered maximum step width of meshing for these parts is 1.99, 0.69, 0.70 and 0.70 respectively.

3.4.2. Modified extraction process in detail

As explained in the above subsection, the measured reflection coefficient is compared with the simulated reflection coefficient to extract the electrical parameters. To obtain the required comparable simulation reflection coefficient value, the electrical parameters of the sheet which represent the equivalent MUT in the 3D model, are varied as long as the simulation result fits to the measured result. At the point, where both coefficient values matches with each other, these final electrical parameters of the simulated sheet model are assumed to be the electrical parameters of the MUT. This extraction technique gets time consuming and has to be repeated to find electrical parameters corresponding to each measurement. To avoid this, a modified extraction method is applied based on an inverse modeling principle to determine the electrical parameters [1]. In the following paragraph, the detail about the extraction process is given.

First, several discrete simulations of the measurement model are performed, within the prior predictable range of ϵ_{r} and $\tan\delta$, in the numerical electromagnetic field solver, to obtain the corresponding simulated complex reflection coefficients. The relationship between these electrical parameters and the simulated reflection coefficients can be described mathematically as

$$S_{11}^{\mathrm{sim}} = g(\epsilon_{\mathrm{r}}, \tan\delta) \tag{3.14}$$

where $S_{11}^{\mathrm{sim}} = S_{\mathrm{real}}^{\mathrm{sim}} - jS_{\mathrm{imag}}^{\mathrm{sim}}$, represents the simulated complex reflection coefficient. Then these data points are imported from the field solver program, and a look-up table is created by writing a Matlab script. In this manuscript, basically first a relationship between the simulated reflection coefficient and the electrical parameters is stored using two mathematical functions (separately defined for each electrical parameter as shown in (3.15) and (3.16)).

$$F1 = \mathrm{TriScatteredInterp}(S_{\mathrm{real}}^{\mathrm{sim}}, S_{\mathrm{imag}}^{\mathrm{sim}}, \epsilon_{\mathrm{r}}) \tag{3.15}$$

$$F2 = \mathrm{TriScatteredInterp}(S_{\mathrm{real}}^{\mathrm{sim}}, S_{\mathrm{imag}}^{\mathrm{sim}}, \tan\delta) \tag{3.16}$$

The TriScatteredInterp function is selected to create the relationship. Basically this function creates a relationship between the simulated reflection data points and the corresponding defined electrical parameter value and cover the intermediate space using interpolation [67]. Then based on the measured reflection coefficient, electrical parameters are evaluated from the look-up table, like inverse problem [65]. The syntax of the used command to determine the electrical parameter is given below.

$$\epsilon_{\mathrm{r}} = F1(S_{\mathrm{real}}^{\mathrm{meas}}, S_{\mathrm{imag}}^{\mathrm{meas}}) \tag{3.17}$$

$$\tan\delta = F2(S_{\mathrm{real}}^{\mathrm{meas}}, S_{\mathrm{imag}}^{\mathrm{meas}}) \tag{3.18}$$

where $S_{\text{real}}^{\text{meas}} - jS_{\text{imag}}^{\text{meas}}$ denotes the measured real and imaginary part of the reflection coefficient.
Basically, these functions first individually locate the position of the measured reflection coefficient within the 3 nearest points in which the measured reflections lay and then use, triangle interpolation, to find the approximated value of the electrical parameter value [67]. The concept of evaluating, the electrical parameter value is shown in figure 3.9.

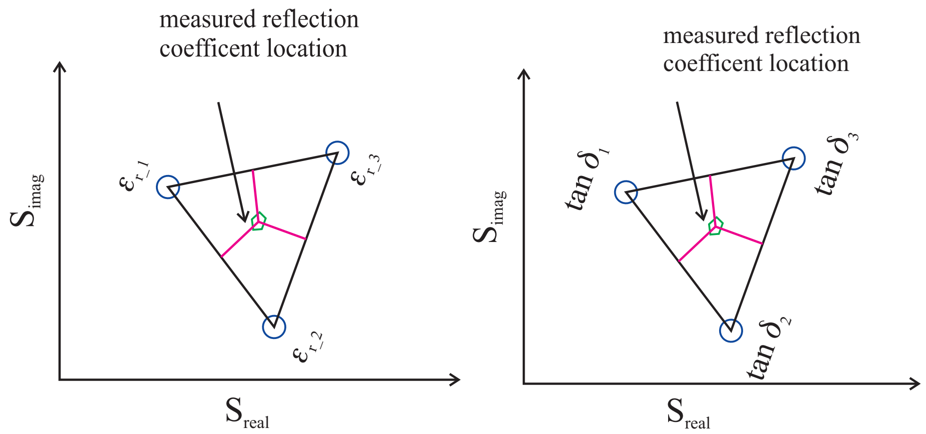

(a) Extractions of ϵ_{r} (b) Extractions of tanδ

Figure 3.9.: *Concept of extraction of electric parameters from the measured point*

From electrical characterization experience it is noticed that the electrical properties of the investigated rubber sheets vary within a certain range. Hence the prior relationship between the electrical parameters and corresponding simulated reflection coefficients are established within that certain range only (i.e. ϵ_{r} between 3 to 18 and $tan\delta$ between 0.01 to 0.7). However, this range can be extended by performing additional simulations and including those results in the defined mathematical model [1]. Figure 3.10 shows a relationship created between the simulated reflection coefficient and the corresponding electrical parameter values. Furthermore, as the relationship is frequency dependent [61], the relationship in the interpolated functions is defined only at the frequency of interest, i.e. at the 868 MHz, to determine the electrical parameters accurately. However by following a similar procedure, the relationship can be defined at any frequency of interest, and then the electrical parameters can be evaluated accurately.
Another approach[4] can be applied to determine the electrical parameters at other frequencies of interest if the electrical parameters are known at a frequency point. In this approach, a material model (such as Debye model which assume frequency dependence behavior [68]) used in a full wave solver can be utilized to evaluate

[4] which may not be as accurate as described above

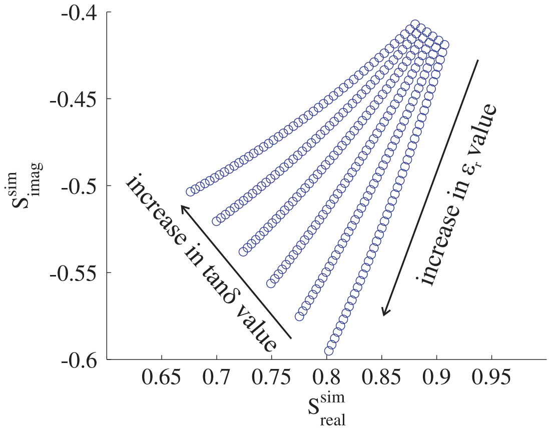

(a) Relationship between the simulated coefficient and the electrical parameters in 2D

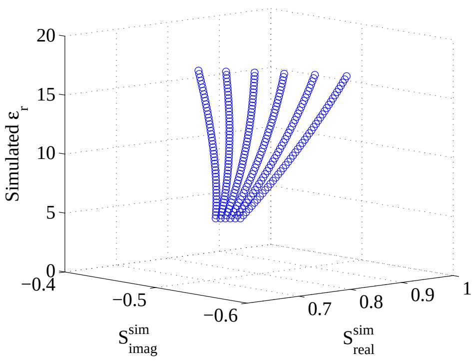

(b) Relationship between the simulated reflection and ϵ_r in 3D

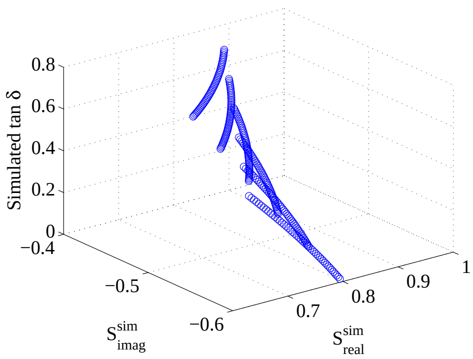

(c) Relationship between the simulated reflection and tanδ in 3D

Figure 3.10.: *Look-up data showing the relationship between the simulated reflection coefficient and the electrical parameters*

electrical parameters at other frequency points [53]. For example, if the electrical parameter values are defined at a frequency point in the material model then at any desired broad frequencies range, with the help of the material models (utilized in the CST studio), the approximated electrical parameters can be evaluated. In the CST studio, usually such type of a material model is applied to consider the approximated electrical parameter values at various frequency points during the simulation of 3D electrical models.

3.5. Results of electrical parameters of rubber sheets

The developed electrical characterization setup, based on the open-ended coaxial method, can be applied to determine the electrical parameters of various materials [1]. In this thesis, this setup is applied to determine the electric properties of various rubber sheets used in the rubber transmission belt. Before presenting and discussing the results, the basic about the investigated rubber materials is given below.
Generally, the recipes of these two major rubber sheets, used in the investigated transmission belts, are changed, and various rubber belts with numerous physical characteristics are manufactured from them. Typical chemical names of two of the rubber sheets are:

- Chloroprene rubber (CR)
- Ethylene Propylene Diene Monomer (EPDM)

A brief information about these rubber materials is given below.

Chloroprene rubber (CR)
The typical chemical name of a chloroprene rubber sheet is 2-chlorobuta-1,3 diene. Its annual world wide consumption in various applications is thousand of tons. Typical characteristics of such a considered rubber type are: good mechanical strength, weather resistant, good aging resistant, adhesion to many substrates e.t.c. It is widely used in various applications such as goods, transmission belts, cables, conveyor belts e.t.c. [46, 47].

Ethylene Propylene Diene Monomer (EPDM)
Terpolymer, ethylene propylene diene (EPDM) rubber, due to economic costs and various physical characteristics is used in huge quantity in various products. Its typical characteristics are: it has high resistance to environment hazards and moisture, and it is therefore mostly used on the exterior side of tires, walls and roofs e.t.c. to protect them from these effects. In addition, it has several other characteristics, such as it depicts high resistance to oil or polar fluids and has a high resilience [46, 47].

Typically considered rubber sheets are thinner in thickness in the raw form than the minimum required thickness for various applications. Therefore number of raw sheets are combined together to get the desired thickness. For investigation purposes, rubber sheets with required thickness are obtained by vulcanizing a few of these sheets together in the lab. Furthermore, the recipe of these selected rubber sheets is also company specific, and no detail information is given due to the company policy. Subsequently the determined parameters will be specific, too. However, using the setup based on the open-ended coaxial probe method, electrical parameters of various kinds of materials, especially rubber sheets can be determined quite fast [1].

By determining the electric parameters of these two sheets the typical range of the electrical parameters can be determined. Results of these sheets will be discussed and presented in section 3.5.1 and 3.5.2. The evaluated electrical parameters of both sheets using the electrical characterization setup can be presented directly without showing the step results in between. However, for analyzing the results in a better way the measurements results of one of the selected sheet (CR) are discussed in detail. Afterwards the results of the other remaining rubber sheets are presented directly.

3.5.1. Electrical parameter of a CR rubber sheet

First, using the measurement setup, the reflection caused by the considered rubber sheet is measured at several locations by moving the rubber sheet under the probe fixture. The measured reflection coefficients are shown in figure 3.11. The reason for

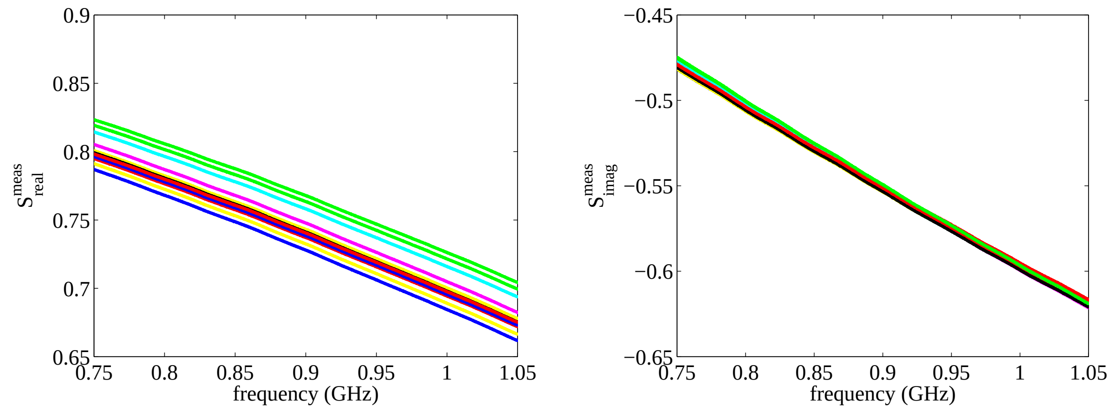

(a) Measured $S_{\mathrm{real}}^{\mathrm{meas}}$ value over a broad frequency

(b) Measured $S_{\mathrm{imag}}^{\mathrm{meas}}$ value over a broad frequency

Figure 3.11.: *S_{11}^{meas} values measured at various positions on the CR sheet*

taking several measurements is to determine the average and variations of electrical parameters over the sheet. At the desire frequency point i.e. 868MHz, the S_{11}^{meas} values from these measurements are shown in figure 3.12. It can be seen that the measured complex reflection coefficients have some different discrete values. Then, corresponding to each measured reflection coefficient value, electrical parameters are determined with the help of the defined mathematical functions. Afterward, these determined parameters are further processed, using statistic principles, to obtain an average, a minimum and a maximum value of each parameter. The summary of the determined electrical parameters is shown in table 3.1.

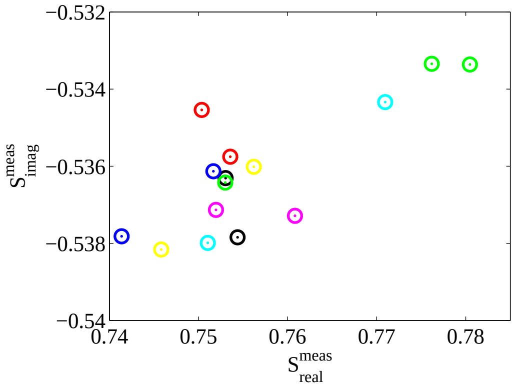

Figure 3.12.: *Measured complex S_{11} in complex form of CR rubber sheet at 868 MHz at different positions*

Table 3.1.: *Electrical parameters of the CR rubber sheet*

	CR sheet	
	ϵ_r	tanδ
minimum	15.1	0.27
Average	16.3	0.34
Maximum	17.1	0.37

Note: Once the reflection coefficients are measured, then it takes approximately a couple of minutes to load the measurement data files, determine these electrical parameters and display them from the developed modified extraction look-up table.

Examining reasons for the electrical parameters variations

To show that the variations in the determined parameters are caused by variations in the sheet, not by the numerical approximations, first, the one to one relationship between the measured reflection coefficient and the corresponding determined electrical parameter is plotted and shown in figure 3.13. Then measured reflections are plotted in the parameter space of the look-up table, shown in figure 3.14. If in these figures the location of these points is closely examined, then it can be observed that the difference in the evaluated electrical parameter values is mainly due to possible material variations, not due to any interpolation approximation.
Furthermore, from this one to one investigation experience, it is observed that, the minimum and the maximum of two evaluated electrical parameters may not correspond to each other for the same measured reflection value, i.e. if tanδ has its maximum value at that measurement point, the ϵ_r may not have the maximum value. Similarly, when tanδ has minimum value at that measurement

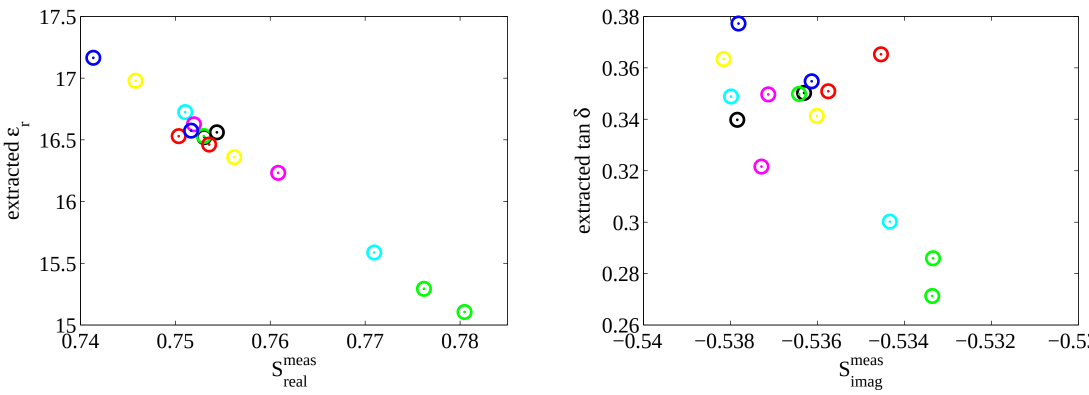

(a) Relationship between ϵ_r vs $S_{\text{real}}^{\text{meas}}$

(b) Relationship between tanδ vs $S_{\text{imag}}^{\text{meas}}$

Figure 3.13.: *One to one relationship between the measured S_{11}^{meas} and determined electrical parameters*

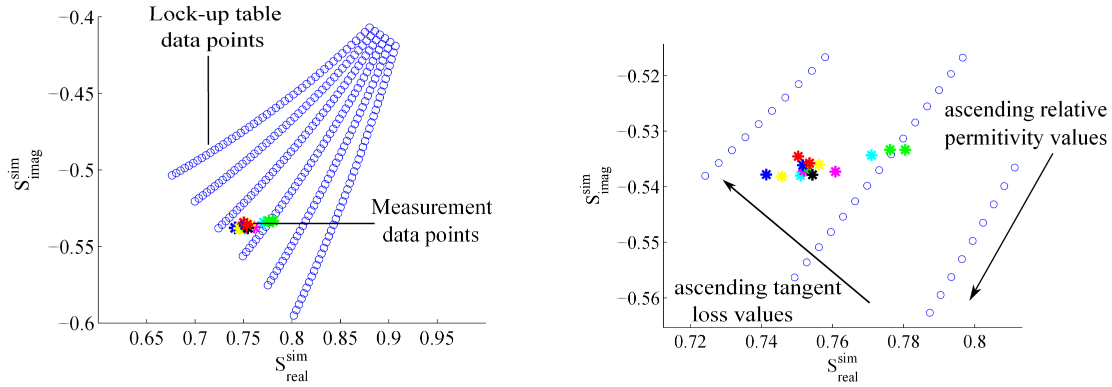

(a) Placement of measured S_{11}^{meas} in the simulated parameter space

(b) Placement of measured S_{11}^{meas} in the simulated parameter space by zooming

Figure 3.14.: *Placement of measured S_{11}^{meas} in the simulated parameter space of the look-up table*

point, the ϵ_r may not have the minimum value. Due to this phenomena, there could be principally four minimum and maximum pairs which could indicate the range of the evaluated electrical parameter values. However, to simplify the investigation cases using statistic principles, simply the minimum and the maximum value of each parameter are paired together and are tabulated in table 3.1.

Difference in the electrical parameter values due to rubbed and non rubbed surface of a sheet (CR)

From the measurement experience, it is observed that when these sheets are fabricated in the lab, a different chemical layer of approximately a few hundred μm is formed over the fabricated sheets. This layer has some impact on the determined electrical parameters. Therefore, to find more accurate parameter values for the sheet under observation, this layer should be removed from the top surface. A scraper tool can be used to remove such a layer. To show the difference, electrical parameters of a CR sheet with and without rubbed surface are determined and shown in table 3.2. It can be seen that up to 10 percent variations in the electrical

Table 3.2.: *Electrical parameters of rubber and not rubbed CR rubber sheet*

	CR rubbed		CR not rubbed	
	ϵ_r	tanδ	ϵ_r	tanδ
minimum	13.7	0.28	15.1	0.27
Average	15	0.31	16.3	0.34
Maximum	15.9	0.34	17.1	0.37

parameters are noticed due to the chemical layer created over the sheet. However, if the overall range of variation in the electrical parameters of both, rubbed and non rubbed sheet, are compared, then it can be noticed that non rubbed sheet have comparatively more variations. Hence, to evaluate the more accurate electrical parameters it is required to scratch the surface of the rubber sheets. The electrical parameters of the different rubber sheets, presented on wards (if not mentioned), are determined by rubbing their surfaces.

3.5.2. Electrical parameter of the EPDM rubber sheet

The electrical parameters of the EPDM sheet are also determined by following similar steps to find the electrical parameters of the CR sheet.

First, several measurements are taken at various positions on the EPDM sheet, and the results are shown in figure 3.15.
After that, measured reflection coefficient values for 868 MHz frequency point are noted. The measured reflection values are shown in figure 3.16.
Then using the defined Matlab script (i.e. loop-up table) the electrical parameters are determined. The evaluated average, minimum and maximum electrical parameter values of the EPDM sheet are shown in table 3.3.

If the determined electrical parameters of the EPDM material rubber sheet are compared with the CR material rubber sheet then it can be observed that EPDM

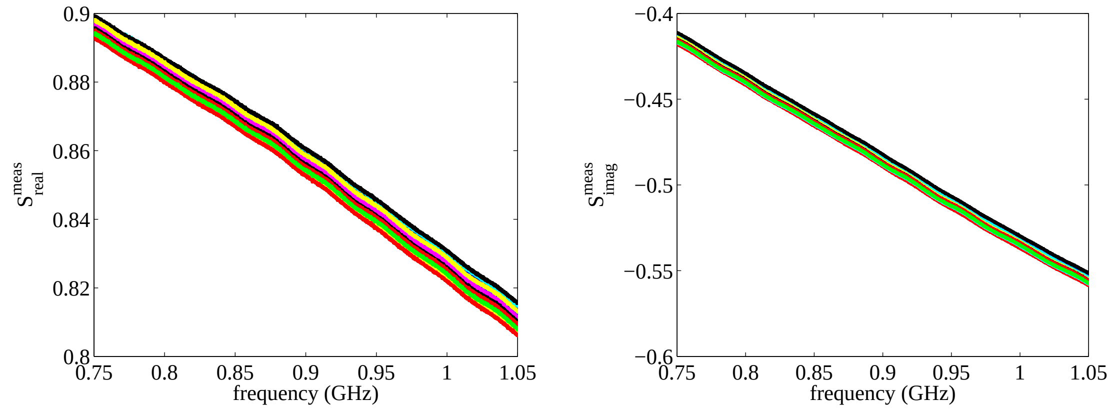

(a) S_{real}^{meas} (b) S_{imag}^{meas}

Figure 3.15.: *Measured complex S_{11} at various positions on the EPDM*

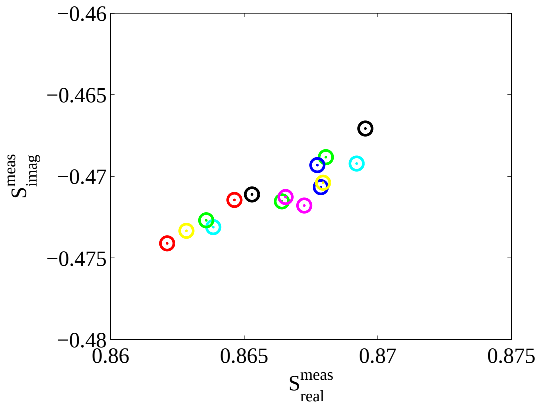

Figure 3.16.: *EPDM measured S_{11}^{meas} values at 868 MHz at different positions*

Table 3.3.: *Electrical parameters of the EPDM rubber sheet*

	EPDM sheet	
	ϵ_r	$\tan\delta$
minimum	7.3	0.11
Average	7.68	0.12
Maximum	8.0	0.14

based rubber have smaller electrical parameter values compared to the CR rubber sheet.

3.6. Investigating reliability, reproducibility and accuracy of the electrical characterization setup

3.6.1. The reliability of the modified extraction code

To show the reliability of the defined extracting strategy[5] one of the measurement curves is compared with the simulated curve. The comparison results are shown in figure 3.17. The simulated curve is obtained by performing simulations of the virtual

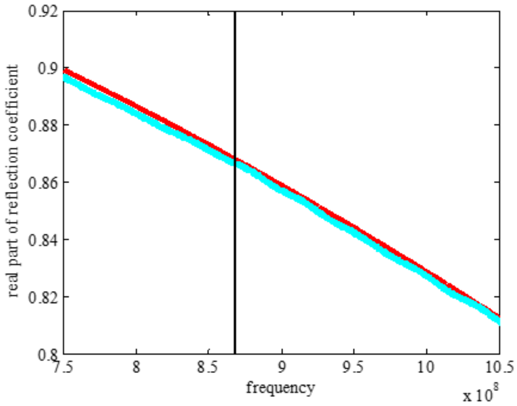

(a) real part of the reflection coefficients

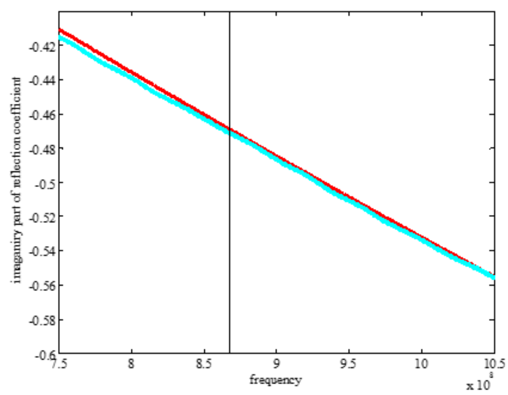

(b) imaginary part of the reflection coefficients

Figure 3.17.: *Comparison of measured and simulated curves to show effectiveness of the numerical code (red color curve shows the simulated curve and the cyan color shows the measured curve)*

measurement model. In the virtual model, the evaluated electrical parameters are set by determining it using the defined look-up table. If we look at both reflection coefficient curves i.e. the simulated and the measured one, then, it can be seen that both curves fit quite good with each other. This shows that the defined code can be utilized to find the electric parameters of unknown materials without performing repetitive simulations. Furthermore by doing so, simulation such as CST studio license resources and simulation time can be saved.

3.6.2. Reproducibility of measurements and the determined electrical parameters

To determine that the characterization setup can reproduce the results, a reproducibility test is carried out. The reproducibility of the results can be checked by

[5] i.e. the electrical parameters can be determined by the defined Matlab script with good accuracy without the need of parametrized simulations

comparing the reflection coefficient value of a material sheet measured at the same position after some time gap[6] and by comparing the corresponding extracted electric parameter values with each other. To show the setup reproducibility, several rubber sheet's reflection coefficient values are measured. Then corresponding to the measured reflection values, the electrical parameter values are extracted using the defined Matlab script. These determined values are tabulated in table 3.4. From

Table 3.4.: *Reproducibility test results*

	Measured S_{11}	ϵ_r	tanδ
sheet 1	$0.7612 - j0.5320$	15.87	0.3432
sheet 1 repeat	$0.7591 - j0.5329$	16.01	0.3455
sheet 2	$0.7743 - j0.5282$	15.03	0.3149
sheet 2 repeat	$0.7729 - j0.5286$	15.13	0.3180
sheet 3	$0.8615 - j0.4738$	8.03	0.15
sheet 3 repeat	$0.8606 - j0.4743$	8.09	0.1502

these results, it can be seen clearly that the developed setup shows a quite good reproducibility.

3.6.3. Comparing the reliability and accuracy of the determined parameters

To show that the developed setup can determine electrical parameters with good reliability and accuracy, electrical parameters of one of the considered rubber sheets (in this case the EPDM sheet) are determined based on the rectangular waveguide resonance method as explained in subsection 3.2.1. Then these are compared with each other [1]. The details about the built fixture, experimental procedure and obtained results are given in the following section.

Determining electrical parameters of the EPDM sheet using the parallel plate method for comparision

As already mentioned, to excite the TE_{01} mode at the desired 868 MHz frequency, first it is required to determine the parallel plate dimensions. For that, based on the evaluated[7] ϵ_r average value of the EPDM sheet, suitable plate dimensions are determined using (3.11). The following dimensions i.e. w = 45 mm and l = 66 mm of each parallel plate are selected. Using these dimensions, it is expected that the TE_{01} mode is excited at the desired frequency, and the higher resonant modes

[6] around couple of minutes

[7] using the open-ended characterization method

are excited at sufficient separable distances from each other, so that these can be differentiated easily. Then an EPDM sample sheet is inserted between the plates. Then the resonator fixture is constructed as shown in figure 3.18. After that, energy

Figure 3.18.: *Prototype of fabricated parallel plate dielectric resonator*

is launched in the fixture to excite several modes, which are then measured using the VNA. The measured response is shown in figure 3.19. It can be seen that the

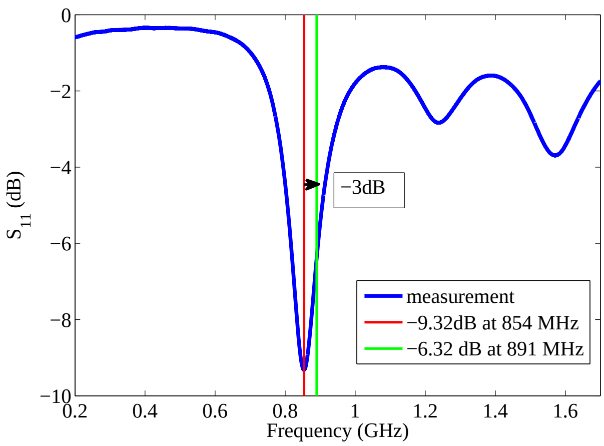

Figure 3.19.: *Resonance modes excited in the fabricated parallel plate dielectric resonator*

TE_{01} mode is not excited at the intended resonance frequency. It means that the electrical parameters of the EPDM sheet determined via the open-ended coaxial method are slightly different from the parallel plate method. However, the ϵ_{r} value, at the excited frequency point i.e. 854 MHz, for the considered dimensions can be recalculated using (3.11). The calculated value of the sheet is $\epsilon_{\mathrm{r}} = 7.1$ [1].
Then based on the measured results, as shown in figure 3.19, the tanδ value is calculated using (3.12). The calculated value is tan$\delta = 0.09$ [1].

Once the electrical parameters are determined using the parallel plate resonant method, the electrical parameters determined using both methods are summarized

Table 3.5.: *Comparison between the measurement results of two characterization methods*

	Open-ended probe method		Parallel plate method	
	ϵ_r	$\tan\delta$	ϵ_r	$\tan\delta$
Average	7.68	0.12	7.1	0.09

in table 3.5. By ignoring the variations in the electrical parameters caused by frequency shifts, it can be observed that the determined electrical parameters match quite well. This shows that, based on the open-ended coaxial method, electrical parameters of a material can be determined with good reliability and accuracy [1].

3.7. Summary of the chapter

A measurement setup for the electrical characterization of different materials (especially for rubber mixture sheets) is developed. The measurement setup is based on the open-ended coaxial probe method and uses the 3D electromagnetic simulation model for determining the electrical parameters of materials. To simplify the measurement process, a numerical algorithm is defined based on the 3D EM simulation results. A summary of the steps to determine the electrical parameters using the developed characterization setup is shown in figure 3.20.

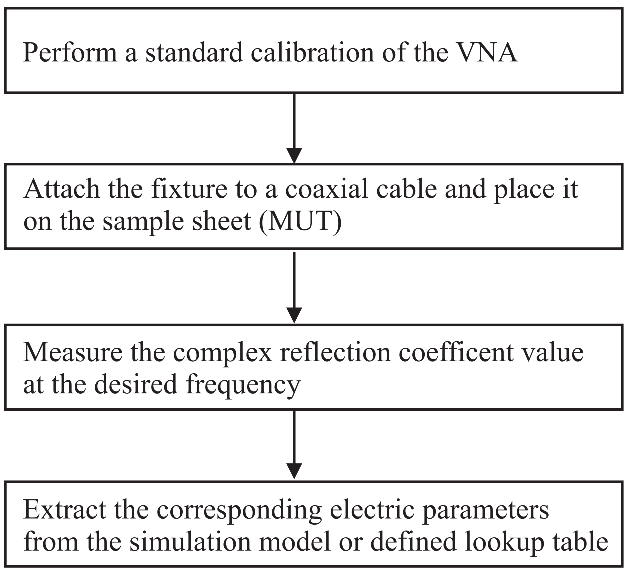

Figure 3.20.: *Summary of the steps to find the electrical parameters of an unknown rubber material*

For typical 15 measurements, the corresponding electrical parameters from the developed look-up are determined within a few seconds. Whereas, it takes approximately a couple of minutes to load the measurement data files, determine these electrical parameters and display them using the defined Matlab script. Using the proposed method, the electrical properties of the selected rubber sheets are evaluated and presented in this thesis. In addition, the reliability and accuracy of the measurement result are discussed. Values are compared with the parallel plate waveguide resonance method.

CHAPTER 4

Design process of surface UHF RFID tag for rubber belts

As already mentioned in chapter 1, the major aim of this thesis is to optimize the design and analysis process for developing high performance and cost effective UHF RFID tags in flexible and heterogeneous rubber belts. However unknown electrical parameters of rubber materials, various shapes, different sizes and the higher flexibility of structures requests for great challenges to adopt the existing UHF RFID tag solutions.
For that, in this chapter as a first step preliminary investigations are explained. First, a design and analysis process for surface UHF RFID tags based on a 3D model for the physical rubber belts is established and its details are presented [2]. To show the effectiveness of the established design process for UHF tags on rubber belts, a set of surface UHF RFID tags are designed and fabricated. Then their performance in terms of read range is analyzed. The details about the whole process are discussed, too. Furthermore, to determine the impact of different variations[1] of the considered rubber belts on the tag characteristics, various investigations are carried out and results are presented [2, 4].

4.1. Physical layout of a rubber belt

There are numerous kinds of rubber belts for which it is interesting to implement an UHF RFID tag. These belts are widely used for power transmission applications to produce motion or revolution between different parts, like in industries such as the

[1] such as different shapes, various thicknesses and distinct electrical parameters

cement industry, the automobile industry, the oil industry, the civil constructions etc. Due to various applications, these rubber belts have numerous shapes and sizes. A few types of the rubber transmission belts are shown in figure 4.1. The cost of these belts vary considerably and range between tens of Euros up to a thousand Euros [11]. For investigation purposes a rubber belt, as shown in figure 4.2, is selected. The

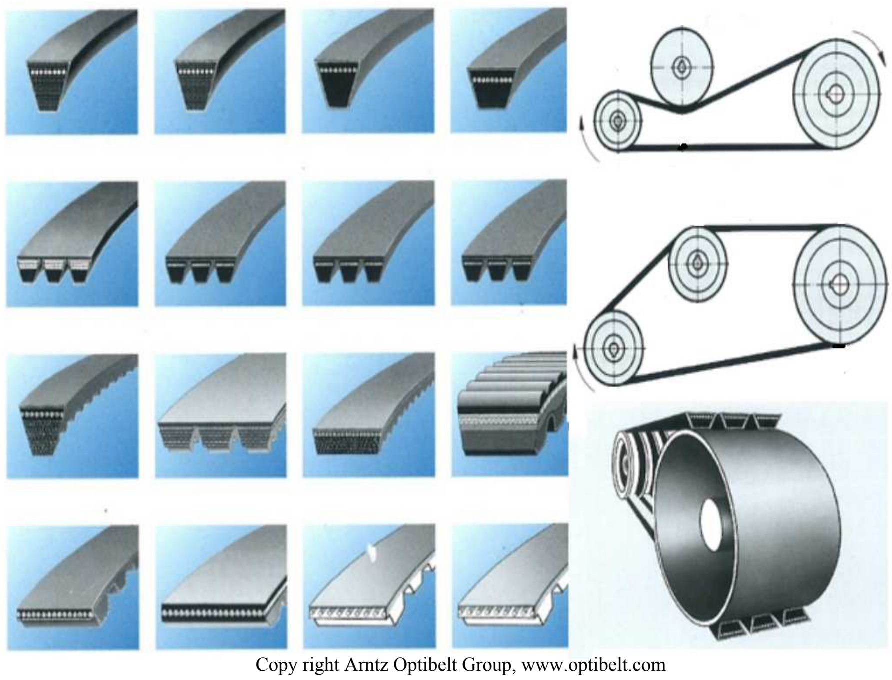

Figure 4.1.: *Different configurations of rubber transmission belts*

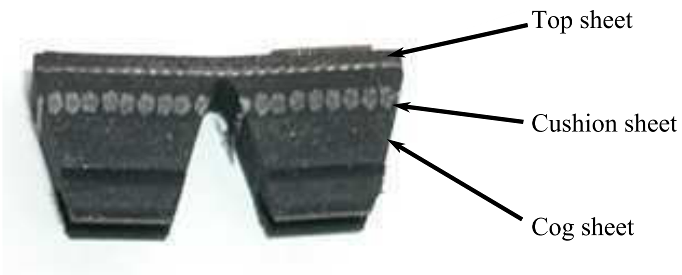

Figure 4.2.: *Physical layout of the chosen rubber belt*

selected rubber belt is fabricated in various shapes and sizes (width and length) with a similar rubber sheet layer stack. Few of them are shown in figure 4.3. As already mentioned in section 2.3, it is quite hard to determine various characteristic parameters of a tag antenna, and to design the tag antennas by analytical methods. Therefore mostly tag antennas for complex applications are designed with the help of numerical EM solvers by modeling [2,17]. Hence, to obtain the high performance

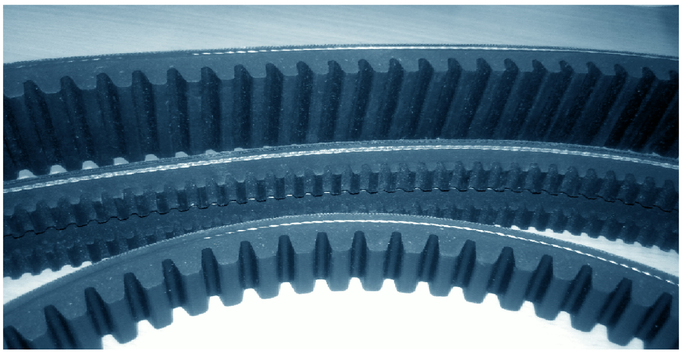

Figure 4.3.: *Various rubber belts having a similar layer stack up*

tag for the belt, the tag antennas with their desired parameters are designed using numerical electromagnetic simulations. However, it is required to represent the belt with a 3D electrical model. First, details on the electrical modeling process of the belt are presented in the following section. Later, it will be shown how to use this model to design the surface tags. Furthermore, in section (4.5), it is discussed how to use similar design concepts to determine the impact of different kinds of variations[2] of the considered rubber belts on the tag characteristics [3].

4.2. Representation of a belt with an electrical model

For developing the electrical model of a belt, it is required to know two electrical parameter values, i.e., the relative permittivity (ϵ_{r}) and the tangent loss ($\tan\delta$) of different constituting materials (such as different rubber layers and fiber cords), and their respective geometrical dimensions. It can be seen from figure 4.2 that the thickness of some layers of the rubber belt is quite small (up to few fractions of a millimeter), and some belt layers consist of fiber cords. These cords are placed at various layers inside the considered rubber belt structure. Therefore, it is hard to determine the electrical properties of such kinds of rubber belt structures directly with any characterization method. However, the electrical modeling process can be simplified by adopting the procedure mentioned in the following section [2].

Steps to follow to construct an electric model of a belt

To construct the model the required information is obtained using the following procedure [2].
First, the electrical parameters of the different rubber layers are determined in-

[2]e.g. different shapes, thicknesses and different electrical parameters

dividually based on the developed electrical characterization setup[3] (details were presented in the previous chapter) [1]. The determined electrical parameters of the three different rubber sheets are given in table 4.1. However, it is neither possible

Table 4.1.: *Electrical parameters of the different rubber sheets*

	Cog sheet		top sheet		cushion sheet	
	ϵ_r	tanδ	ϵ_r	tanδ	ϵ_r	tanδ
Minimum	12.1	0.33	8.5	0.16	6.4	0.18
Average	13.8	0.36	9.9	0.18	7.2	0.21
Maximum	14.9	0.39	10.4	0.2	7.6	0.23

to measure the electrical parameters of fiber cords with the developed setup nor to obtain unique information from literature. Only a general range of ϵ_r is mentioned in [69]. For the construction of the belt, the following electrical parameter values are assumed: $\epsilon_r = 3.5$ and tan$\delta = 0.002$.
Then, the required geometrical dimensions of all the rubber layers and fiber cords are obtained by measurements.
Once all the required information is gathered, the electrical model is constructed using a bottom-up approach, as shown in figure 4.4 [2]. To start the preliminary

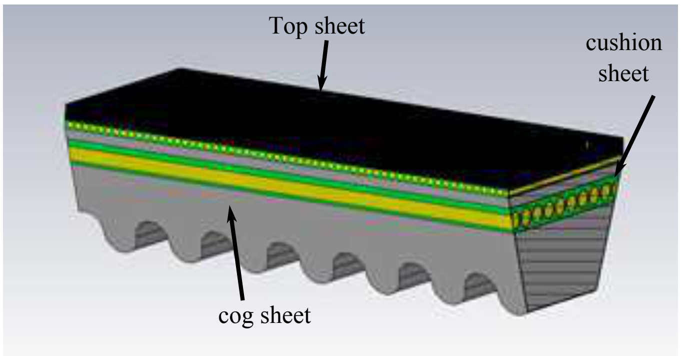

Figure 4.4.: *Electrical model of the considered rubber belt*

investigation and to understand the tag design process, only a small portion on one side of the belt is considered to design the surface tag antennas. This simplification

[3] In this case, the changes are sensed via the VNA at the interface of the open-ended probe and the MUT. The de-embedding of the probe fixture is carried out using the auto port extension option. Then these changes are compared with the equivalent model to extract the electrical parameters. In the virtual equivalent model, the waveguide port is shifted towards the MUT and probe interface using shift reference plan option. The equivalent measurement models are utilized to evaluate electrical parameters. Therefore this shift of the measurement plane does not have much influence on the determined results.

has some impact on the tags performance. However, if the full model of the belt would have been considered for simulation then a lot of time would have been required to conduct the preliminary investigations. Therefore, this simplification is made. If a more precise tag design is required then the whole model needs to be included.

Variation in the electrical versus the physical model of the belt

The electrical model may contain few variations compared to a real rubber belt due to following reasons [2].

- Due to the fabrication process, the thickness of each rubber layer in the real belt may vary by few 100 μm. However, typical thicknesses of each rubber layer are considered in the model.
- Electrical parameters of the different rubber layers are determined in the form of individual sheets which are fabricated in the lab. Therefore electrical properties of the real rubber belt layer may contain some variations compared to those of the modeled rubber sheets.
- Average electrical parameter values of each rubber sheet are considered in the model. However, during measurements it is observed that the electrical parameters of individual rubber sheets contain variations approximately up to 10 to 12 percent compared to the average value.

Based on measurements, it is hard to individually distinguish the effect of these variations on the tag characteristic parameters. However, the simulation model is used to determine the impact of such kind of variations. Further details about that procedure are mentioned in section 4.5.

4.3. Surface UHF RFID tag design process

As already discussed in chapter 2, when an UHF tag is attached to the surface or embedded in an object, the complex impedance value of the tag antenna alters, which in turn results in a mismatch between the IC and the tag antenna's complex impedance values. Due to this mismatch, the detection read range of an UHF RFID tag is reduced. This mismatch can be reduced either by changing the tag IC parameters by redesigning or by changing the tag antenna parameters. Since the designing cost of a new tag IC huge, mostly tag antennas are designed with the required impedance value for a specific tag IC [2, 27]. In this chapter, the designed antenna complex impedance values are matched with the Monza 4 tag IC fabricated by Impinj. The considered tag IC, when connected in the shunted connection, has a complex impedance value $Z_{\text{chip}} = 5.5 - j74\ \Omega$ and a minimum read sensitivity P_{th} (i.e. minimum power required by a tag to be detected by a reader) value of -16.9

dBm at a frequency of 868 MHz [37]. When connected in the open connection, it has a complex impedance value $Z_{\text{chip}} = 13 - j155\ \Omega$ and a minimum read sensitivity P_{th} value of -17.3 dBm at a frequency of 868 MHz [37].
In the following section, a design process for obtaining tag antennas with the desired impedance values is discussed in detail [2]. However, using a similar concept, the optimized tag antenna could be designed for any other tag IC.

4.3.1. Basic of designed tag antenna

There are different kinds of antenna designs [30] which can be selected to obtain a high performance UHF RFID tag. An antenna design with inductive coupled loop is selected, because it offers various advantages. One major benefit is that it is relatively easy to get the desired complex impedance (explained later in detail in this section). Besides, it provides a wider impedance bandwidth compared to other antenna designs such as T match antenna designs [31].
The fabricated prototype tag antennas based on the inductive coupled loop principle to achieve the impedance matching are shown in figure 4.5. The antenna

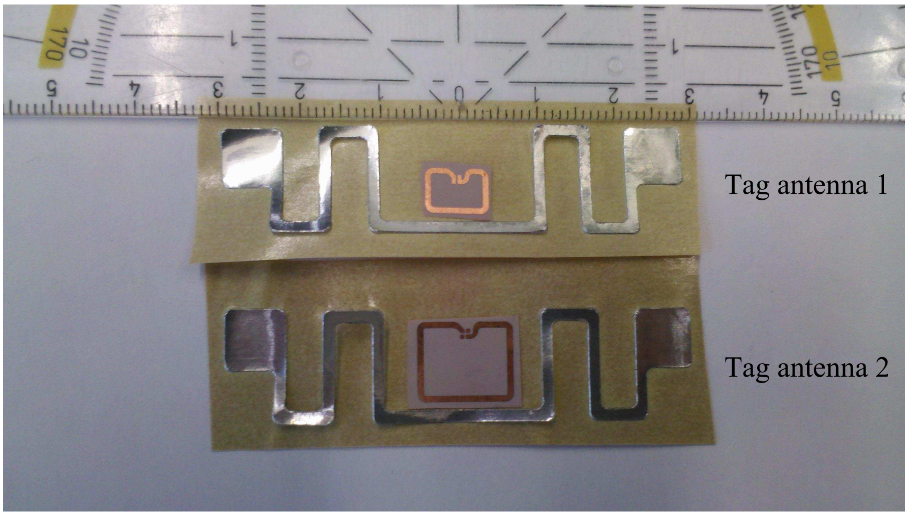

Figure 4.5.: *Prototypes of the designed tag antennas*

design consists of two antennas, an external dipole antenna and an inner loop antenna:

The external dipole antenna is used to enhance the gain of the overall tag antenna. It can easily be matched to the dielectric environment and shows a real input impedance value only at resonance frequency. This real part is inductively coupled from the external antenna to the inner loop antenna, and the desired real part of the impedance value of the tag antenna is obtained by controlling the distance between these antennas [2].

The inner loop antenna is primarily responsible for the imaginary part of the overall antenna impedance value. Furthermore, due to its inductive character, this structure is hardly influenced by the electrical parameters of the environment. So it is possible to design this small part of the structure once for a given Tag IC, and later on a change of the external dipole antenna design is needed only for use in different dielectric environments [2].

Evaluation of the tag antenna dimensions and mechanism to obtained the desired impedance value

For surface tagging applications, due to the higher flexibility of the rubber belt, the overall length of the dipole antennas at UHF frequency need to be shrunk to approximately 60 mm. Therefore the external antennas are wrapped in a meander form and in arbitrary shapes to reduce their overall size, so that the devices can be properly fixed or attached on the belts. As the overall $\frac{\lambda}{2}$ dimensions of the external tag antenna depend on the belt's electrical parameters, shape and size, it is quite complex to determine its dimensions with analytic expressions. Therefore, first the overall $\frac{\lambda}{2}$ dimensions of the external tag antennas are obtained with the help of parametrized simulations of the model (as shown in figure 4.6) for both tags. For the desired surface tags, the external antenna with same dimensions is used

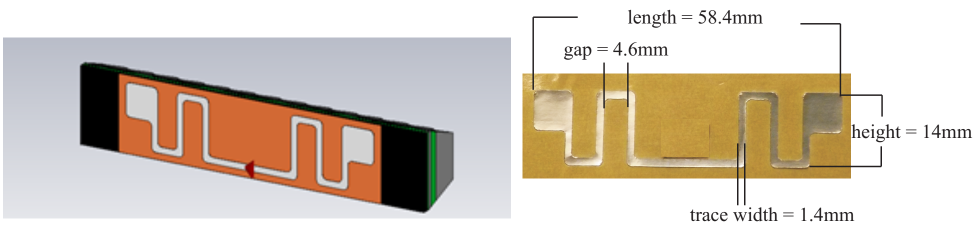

(a) Determination of the external antenna dimensions using the model (b) Dimensions of the external tag antennas

Figure 4.6.: *Dimensions of the external antenna and the simulation model used to determine it*

because it is designed for the same material environments. The dimensions of the external antenna used for both tags are depicted in figure 4.6(b).

Afterwards dimensions of the inner loop antennas and the desired complex impedance values are obtained using the following procedure. The impedance control mechanism of the inductive coupled feed loop antenna can be described using the simplified antenna layout as shown in figure 4.7(a). If the simplified layout is modeled using the transformer circuit, as shown in figure 4.7(b), then the approximated expressions (i.e. to evaluate the inner antenna dimension and desired impedance value) can be obtained as follows [2, 70, 71].

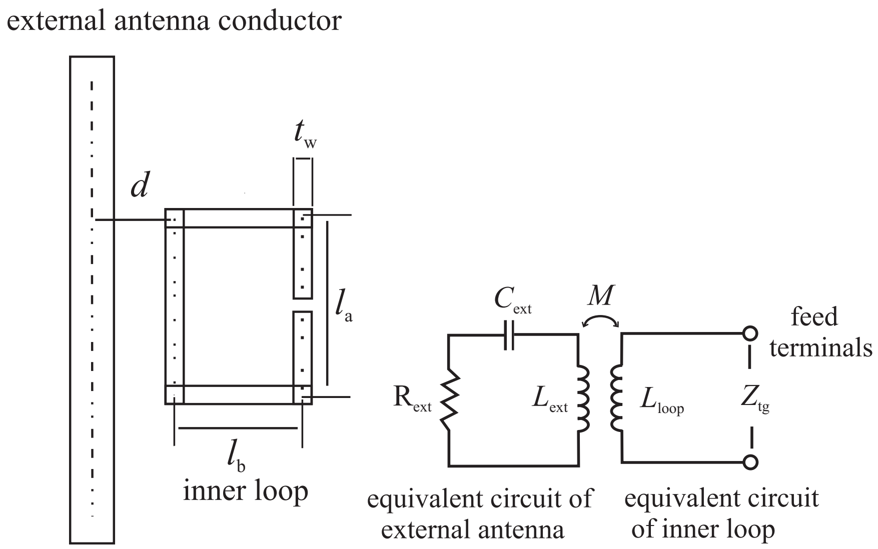

(a) Layout of the inductive coupled loop feed antenna (b) Circuit schematic of inductive coupled loop feed antenna

Figure 4.7.: *Layout and circuit schematic of inductive coupled loop feed antenna*

At resonance frequency, the input impedance of the external antenna (shown in figure 4.7 as serial circuit L_{ext}, C_{ext} and R_{ext}) is simplified to the real resistance R_{ext}. On the other side the resistive part of the inner loop can be neglected[4], so that its imaginary part of impedance is mainly defined by the inductance L_{loop}, and the real part is contributed via the mutual coupling factor (M). The total complex impedance value of the combined tag antenna seen from the feed terminal can be determined as follow [2, 70].

$$Z_{\text{tg}} = R_{\text{tg}} + jX_{\text{tg}} = \frac{(2\pi f M)^2}{Z_{\text{ext}}} + Z_{\text{loop}} \tag{4.1}$$

The value of the imaginary part of the tag antenna impedance can be calculated

$$Z_{\text{loop}} = jX_{\text{tg}} = 2\pi f M L_{\text{loop}} \tag{4.2}$$

The value of the inductance of a single loop (L_{loop}) inner antenna in air can be calculated by [70]

$$L_{\text{loop}} = \frac{\mu_0}{\pi}\left[l_{\text{b}}\ln\left(\frac{2l_{\text{a}}l_{\text{b}}}{\frac{t_{\text{w}}}{2}(l_{\text{b}}+l_{\text{c}})}\right) + l_{\text{a}}\ln\left(\frac{2l_{\text{a}}l_{\text{b}}}{\frac{t_{\text{w}}}{2}(l_{\text{b}}+l_{\text{c}})}\right)\right] + 2\frac{\mu_0}{\pi}\left(\frac{t_{\text{w}}}{2} + l_{\text{c}} - (l_{\text{b}}+l_{\text{c}})\right)$$

[4]as it has quite small resistance values

$$(4.3)$$

where $l_c = \sqrt{l_a^2 + l_b^2}$, units of l_a, l_b, and t_w are in m, unit of l_{Loop} is H, and $\mu_0 = 4\pi 10^{-7}$ H/m.
Using (4.3) the approximated dimensions, the X_{tg} value can be calculated as the inductance is hardly influenced by various material relative permittivity values.

Using (4.3) approximated information about the designed inner antenna's dimensions, the desired X_{tg} values are obtained. Then the final dimensions of the inner antenna and impedance values are calculated using the 3D model. As it is required to achieve a different imaginary impedance value for both prototype tags, the two loops are designed with different dimensions. To acquire the desired imaginary value matched to the shunted connection impedance of the tag IC, the following dimensions of the inner loop antenna are selected; $l_a = 7.62$ mm, $l_b = 5.62$ mm and $t_w = 0.75$ mm. Its calculated imaginary value using (4.3) and (4.2) is $X_{tg} = 62\ \Omega$ whereas the simulated imaginary part value is $X_{tg} = j74.8\ \Omega$. To obtain the desired imaginary value matched to the open connection impedance of the tag IC, the following dimensions of the inner loop antenna are selected; $l_a = 11.62$ mm, $l_b = 9.62$ mm and $t_w = 0.75$ mm. Its calculated imaginary value using (4.3) and (4.2) is $X_{tg} = 121\ \Omega$ whereas the simulated imaginary part value is $X_{tg} = j167.7\ \Omega$.

When an external antenna is at resonance, the value of R_{tg} can be calculated as

$$R_{tg} = \frac{(2\pi f M)^2}{R_{ext}} \tag{4.4}$$

The value of R_{ext} for resonance dimension can be obtained with the help of a simulation model by exciting only the external antenna at its center and observing the corresponding value [70]. The value of Mutual inductance (M) can be evaluated by

$$M = \frac{\mu_0 l_a}{2\pi} \ln\left(d + \frac{l_b}{d}\right) \tag{4.5}$$

The value of M is a function of distance d as illustrated in figure 4.7(a) for the selected shape having l_a and l_b dimensions. Hence by controlling the value of d, the real part of the impedance value of the tag antenna can be controlled [2].

In the case of the designed tag antennas, the impedance R_{ext} of the external tag antennas at resonance frequency has a value of 33.4 Ω. Therefore, to get the desired real part of the impedance value matched to shunted connection impedance of the tag IC i.e. 5.5 Ω, the distance $d = 1.675$ mm is set between the two antennas: it is calculated using (4.4) and (4.5). To obtain the desired imaginary value matched to the open connection impedance of the tag IC i.e. 13 Ω, the distance $d = 2.557$ mm need to be set between the two antennas. However, due to the higher losses with the increase in d, the gain of the antenna also gets affected a bit, too. Therefore, a compromise needs to be made between the matching coefficient and the overall gain of the tag antenna. Furthermore, their is not much space available to move away the inner antenna from the external antenna, and then attaching the tag properly to the belt. Due to this in the final design, distance $d = 2.075$ mm is maintained between the two antennas; it is approximated using (4.4) and (4.5).

4.3.2. Designed surface UHF RFID tags

Based on the above mentioned process, a couple of tags are fabricated for the surface tagging applications as shown in figure 4.8. The tag design marked as 1, uses the

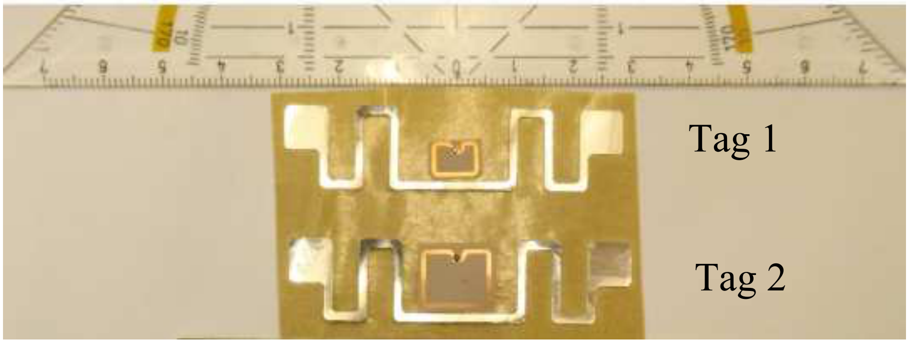

Figure 4.8.: *Surface UHF RFID tags designed for the belt*

tag IC connected in shunted connection, whereas, in the tag design marked as 2, the tag IC is connected in open connection. Now on, these designs will be referred as tag 1 and tag 2 in order to differentiation between the two designs.

4.4. Performance analysis of the designed surface tags

One of the most important way to analyze an UHF RFID tag design is to measure its performance in terms of the maximum read range. Just for recap (already discussed in chapter 2), it is the distance over which a RFID tag attached to an object can be detected in free space by an RFID reader if maximum allowed power is transmitted.

4.4.1. Estimating the theoretical read range of the surface tags

Principally, to estimate the maximum theoretical read range via (2.21), information about two parameters of a tag antenna at 868 MHz are needed. Those parameters are the maximum Gain (G_{tg}) and the impedance (Z_{tg}) to calculate the value of

τ. In this thesis, the information on both parameters is obtained via numerical simulation of the tag antenna [2, 3].
To simplify the presentation of results of the two tags, first simulated results of tag 1 are discussed and presented. Later on, using the same process, the read range of tag 2 is evaluated and will be presented.

Gain of the tag antenna

In 3D, the gain pattern of the designed tag antenna 1 is shown in figure 4.9. In polar

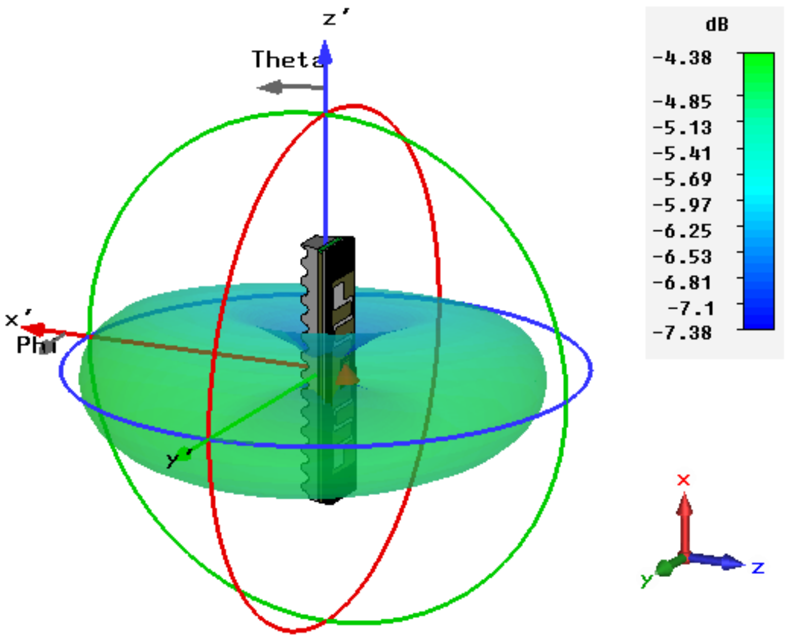

Figure 4.9.: *Gain pattern of the simulated tag antenna 1 in 3D*

plot, the gain pattern across the tag antenna (in H plane) is shown in figure 4.10. It can be seen that the gain pattern of the designed tag antenna is slightly asymmetrical. This is caused mainly due to the asymmetric nature of the tag antenna. This effect has negligible impact on the implementations on the inventory management application i.e. to detect several tagged belts packed in a box. For such applications orientation issue is not of great importance. However, the tag orientation is of great importance while detecting the tag during operation. In this case it should be analyzed more carefully. From these radiation patterns, it can be observed that the tag antenna has a maximum gain value of -4.38 dB which corresponds to the linear value of $G_{\text{tg}} = 0.37 = (10^{-4.38\frac{\text{dB}}{10}})$. The gain degradation of the simulated antenna is quite high compared to the linear dipole antenna having the resonance dimension around $\frac{\lambda}{2}$ in air. The designed antenna has approximately 6 dB more loss compared to the linear dipole antenna. This is mainly contributed by losses

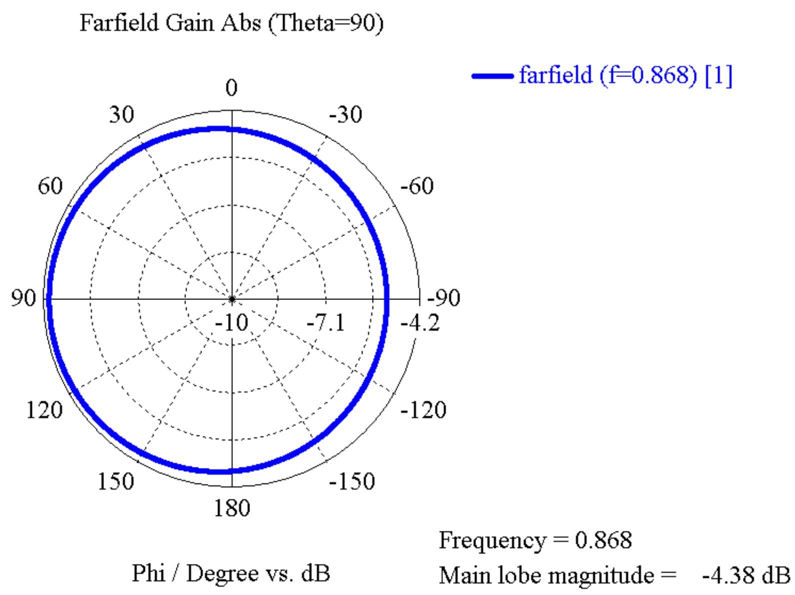

Figure 4.10.: *Gain pattern of the simulated tag antenna 1 in H plane*

due to the rubber sheets and by a reduction in radiation resistance of the antenna due to shrinking its length.

Impedance of the tag antenna

For tag 1, the simulated complex impedance is shown in figure 4.11. At 868 MHz frequency, the tag antenna has an impedance value of $Z_{\mathrm{tg}} = 5.8 + \jmath 74.8\ \Omega$. Based on simulation results, the calculated value of the power transmission coefficient (τ) obtained using (2.1) is 0.99 and $\sqrt{\tau} = 0.99$. Furthermore, it can be observed

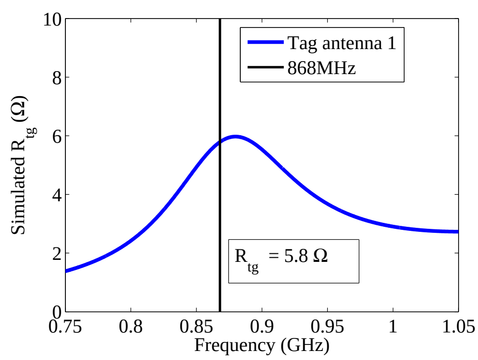

(a) R_{tg} value of the tag antenna 1

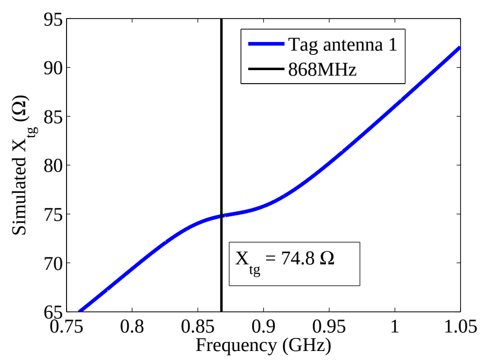

(b) X_{tg} value of the tag antenna 1

Figure 4.11.: *Simulated impedance of the surface tag antenna 1*

from figure 4.11 that the complex impedance values do not vary much around the desired operating frequency. This effect is caused mainly by the losses induced by the considered rubber belt. The overall benefit of this effect is that even if the simulated tag antenna impedance show a little offset in terms of frequency, the performance of the designed tag will stay close to the predicted one.

Once the required parameters i.e. the gain and the complex impedance value of the designed tag antenna are gathered, the read range of tag 1 is calculated using (2.21). The calculated theoretical read range (R_{sim}) of the tag 1 is 6.6 m.

Similarly, tag 2 antenna is simulated, the required parameters are determined and then the read range is calculated. The simulated gain in 3D is depicted in figure 4.12 and in polar plot, the gain pattern across the tag antenna 2 (in H

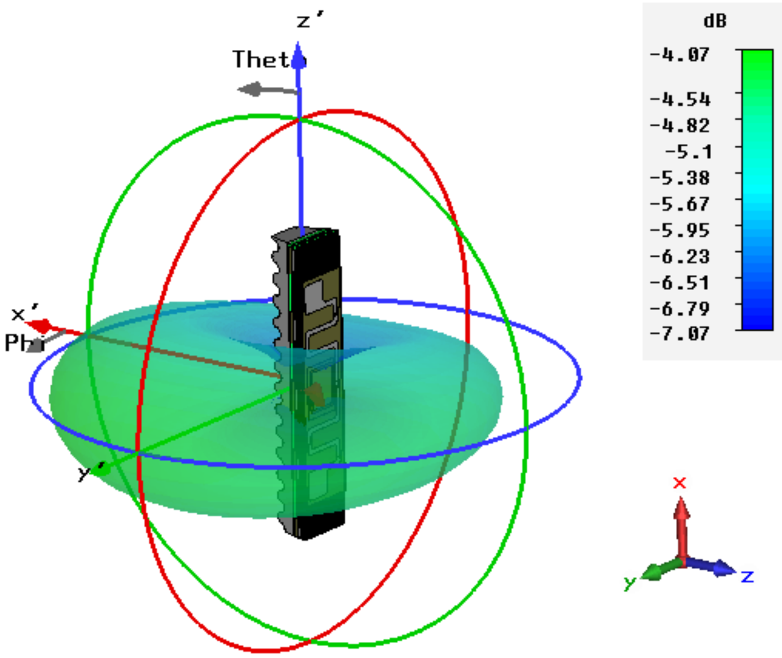

Figure 4.12.: *Gain pattern of the simulated tag antenna 2 in 3D*

plane) is shown in figure 4.13. Whereas, the simulated impedance is depicted in figure 4.14. From gain pattern of figure 4.12, it can be observed that the tag antenna has a maximum gain value of -4.07 dB which corresponds to the linear value of $G_{\text{tg}} = 0.39 = (10^{-4.07\frac{\text{dB}}{10}})$. At 868 MHz frequency, the tag antenna 2 has $Z_{\text{tg}} = 24.8 + j167.7\ \Omega$. Based on simulation results, the calculated value of the power transmission coefficient (τ) obtained using (2.1) is 0.75 and $\sqrt{\tau} = 0.87$.

Next the tag 2 maximum theoretical read range (R_{sim}) is evaluated using (2.21). The calculated maximum read range of the tag 2 is 6.4 m.

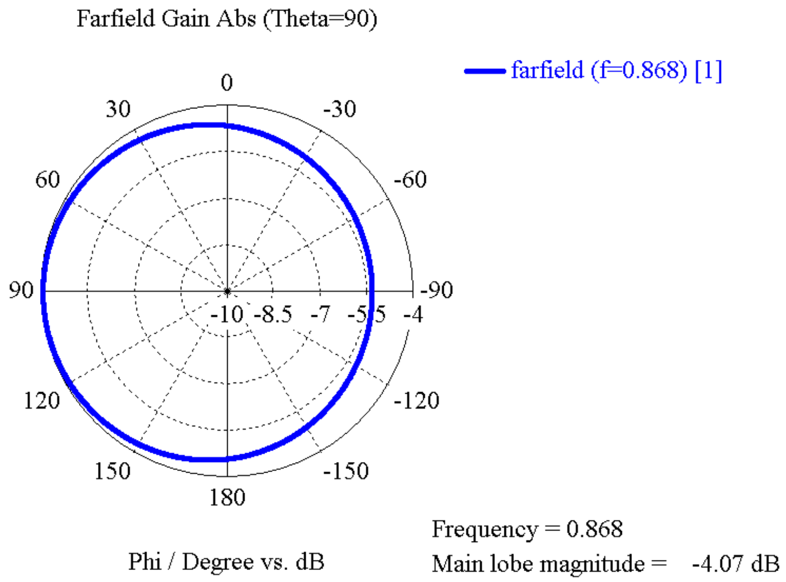

Figure 4.13.: *Gain pattern of the simulated tag antenna 2 in H plane*

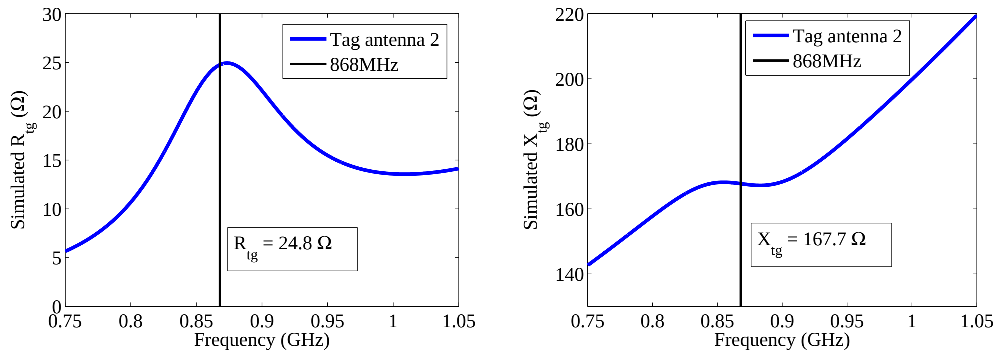

(a) R_{tg} value of the tag antenna 2

(b) X_{tg} value of the tag antenna 2

Figure 4.14.: *Simulated impedance of the tag antenna 2*

The difference between the two tags read range is caused due to the difference in the τ, the G_{tg} and the P_{th} value. Read range of tag 2 is less compared to tag 1 due to the smaller power transmission factor value.

4.4.2. Read range estimations of the surface prototype tags via anechoic chamber

As discussed in chapter 2, principally, to estimate the read range of the prototype tags via anechoic chamber, only one parameter, i.e. the $P_{\min}$ value, needs to be

determined. Once that value is determined then the maximum read range of each designed tag can be estimated using (2.22). The results of both designed tags will be presented one after the other.
Before presenting the results, the detail how to interpret the plot obtained via performing the test and how to make the read range estimation process easier is discussed below.

For performing the measurement to determine P_{min} value, a 500 mW RFID reader from the RF-embedded GmbH is used. The amount of transmitted power from the reader can be controlled automatically by the application software provided by the manufacturer, over a wide UHF frequency range by setting different attenuator values. A typical plot displayed after performing the test is shown in figure 4.15. In figure 4.15 the y-axis indicates the attenuation factor number and corresponds

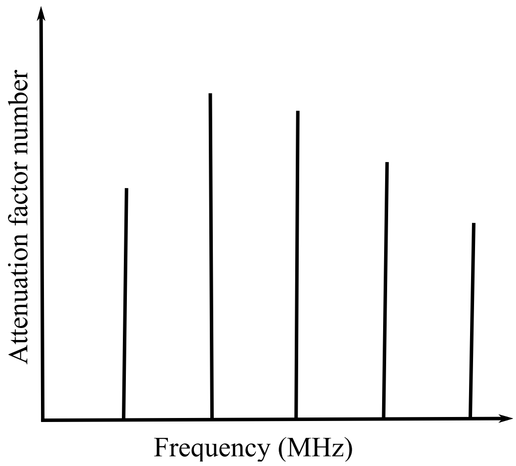

Figure 4.15.: *A typical plot displayed after performing measurement test*

to a certain power that is transmitted from the reader to get the response from the tagged object, whereas the x- axis indicates the frequency at which that power is transmitted.
The prior information about the transmitted power corresponding to various attenuation factor numbers is not provided by the manufacturer. Therefore, the amount of the transmitted power corresponding to the various attenuated factor numbers at desired frequency points is measured in the lab using the power meter. As the read range of the designed tags is estimated for the European ISM frequency, i.e. 868 MHz, for that frequency point, a prior relationship between the transmitted power versus the attenuation factor numbers is determined and tabulated in table 4.2. The P_{min} value required to estimated the read range is equal to the power corresponding to the attenuation factor number given in the table.

Table 4.2.: *Transmitted power (in mWatt) corresponding to various attenuation factor number after 10 dB attenuation (for the 500 mWatt RF embedded reader module)*

attenuation factor numbers	transmitted power	attenuation factor numbers	transmitted power
19	3.4	10	16.6
18	4.0	09	20.0
17	4.8	08	23.6
16	5.8	07	27.9
15	6.9	06	32.1
14	8.3	05	36.3
13	10.1	04	40.1
12	12.0	03	45.0
11	14.1	02	49.1
10	16.6	01	50.2

Estimation of the read range of the prototype tags via anechoic chamber

To measure the read range of the fabricated tags, the experimental setup used to perform the tests in the anechoic chamber has the following parameters: d_{rt} = 80 cm, G_{rd} = 8 dBi and L_{loss} = 0.45 dB. The information of these parameters is also required to estimate the read range using (2.22).
Once the measurement setup is set, the belt is tagged with both tags one by one. These are placed in front of the reader to determine the P_{min} values. The obtained results for both tags are presented one by one as follows.
The result of the performed test to detect the presence of tag 1 is shown in figure 4.16. It can be seen, using table 4.2 and figure 4.16, that the tag's presence is detected by the RFID reader at a transmitted power of P_{min} = 14.1 mWatt on a frequency of 868 MHz. Based on measured P_{min}, the maximum read range of the designed tag 1 is calculated using (2.22). The calculated measured read range (R_{meas}) of tag 1 is around 5.15 m.

Similarly, the read range of tag 2 is measured. Figure 4.17 shows the result of the measurement performed in the anechoic chamber to detect the presence of tag 2. It can be seen, using table 4.2 and figure 4.17, that the tag presence is detected by the RFID reader at the transmitted power of P_{min} = 6.9 mWatt on a frequency of 868 MHz. Based on measured P_{min}, the maximum read range of the designed tag 2 is calculated using (2.22). The calculated measured read range is around 7.4 m.

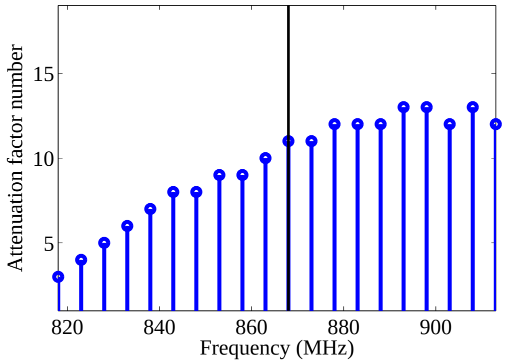

Figure 4.16.: *The attenuation factor number at which tag 1 is detected by the reader at various frequencies*

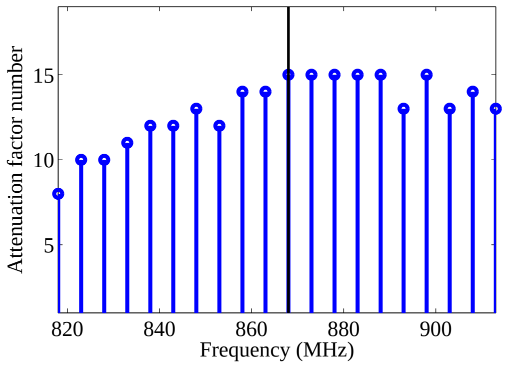

Figure 4.17.: *The minimum power at which tag 2 is detected by the reader at various frequencies*

4.4.3. Checking the model by comparison of the read range for the tags

One way to determine the model accuracy is to design a tag antenna based on the model, then measure the fabricated tag antenna impedance and compare the simulated and the measured impedance value with each other [39]. Using a similar concept, it is tried to determine the accuracy of the model. But in case of the belt model, it is quite challenging to verify this with quite good accuracy and reliability. Especially, due to mechanical issues such as holding a differential probe over the device used test, making a proper contact with the designed antenna, and difficulties in performing calibration. Due to the mentioned issues it was not possible to get reliable results. However, some results are obtained and are presented in the appendix, section A.1. This measured results show similar tendency and give some idea about the suitability of the model. Due to time limit, this procedure can not be optimized.

However, as explained in chapter 2, using an indirect way although less accurate, it may be possible to determine the usefulness and approximately validate the model. Using that procedure, the simulated (i.e. theoretical range) and the actual measured read range of the designed tags are compared with each other citekan13. The theoretical read range of the simulated tags and the actual measured read range of the fabricated tags are tabulated in table 4.3. It can been seen from

Table 4.3.: *Comparison between the simulated and measured read range of the designed tags*

Tag number	Theoretical read range	Measured read range	Relative error
tag 1	6.6 m	5.1 m	23 (%)
tag 2	6.4 m	7.4 m	16 (%)

table 4.3 that 16% relative error in the estimated tag performance is observed. This is quite a good result keeping in mind the electrical parameter variations (approximately upto 12%) of the belt, various tolerances at different design stages such as measurement tolerances in various components used in the anechoic chamber setup in estimating the read range, quantization of the transmitted power value, accuracy of the tag chip information provided by the manufacturer, placement of the inner loop antenna to the external antenna, the impedance change due to the manual chip bonding with the tag antennas e.t.c. [4].

The results show a good correlation. Especially the designed tag 2 shows the suitability of the developed model in designing the high performance tags for such complex structures. Based on the results, it can be concluded that a high performance tag for such complex structure can be obtained by the established design process [2].

4.4.4. Variation in the read range due to various tolerances

As can be seen from the results the difference in the read range of tag 1 is bigger than for tag 2. The difference in the read range might be caused due to various error contributing sources. One of the main sources can be the impedance value change due to the chip bonding with the tag antennas by hand. Furthermore, as the impedance values are small especially for tag 1, its transmission coefficient factor is more sensitive compared to tag 2. The impact of these variations on the impedance value and hence the transmission coefficient are unknown. However, the possible impact of these variations on the transmission coefficient may be observed with (2.1), if the effect of these changes are incorporated in terms of varying the impedance value. Figure 4.18 and figure 4.19 show the impact of variations in the antenna impedance values on τ and $\sqrt{\tau}$ of the designed tags. It can be seen from figure 4.18 and figure 4.19 that tag 2 is quite insensitive to the changes in the impedance values in comparison to tag 1. Depending on the availability of space on the belt and on the required read performance both tag designs can be used.

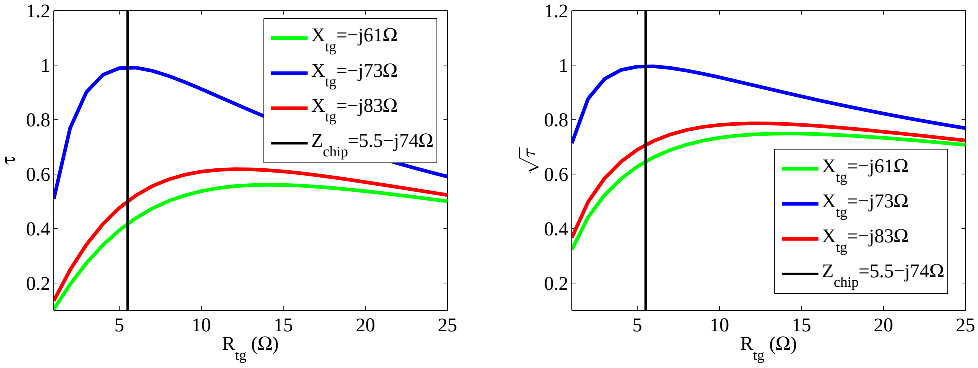

(a) Variation in τ of the tag 1 due to changing the impedance values

(b) Variation in $\sqrt{\tau}$ of tag 1 due to varying the impedance values

Figure 4.18.: *Variation in the impedance and its impact on the transmission coefficient considering tag 1*

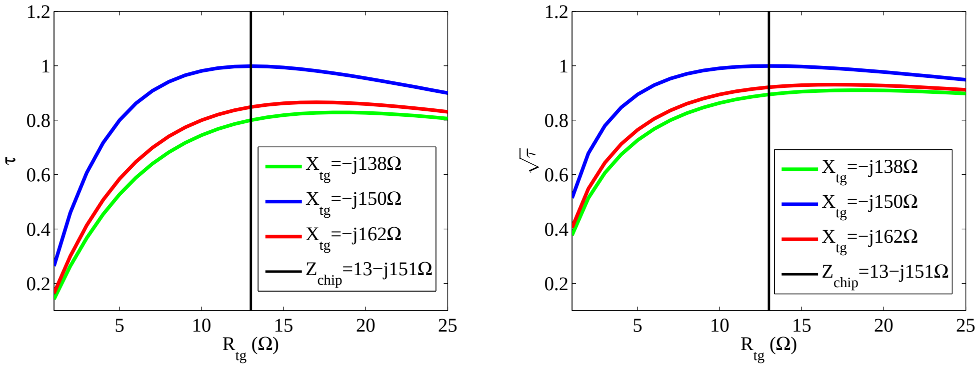

(a) Variation in τ due to changes in the impedance values in the tag antenna 2

(b) Variation in $\sqrt{\tau}$ due to difference in the impedance values in the tag antenna 2

Figure 4.19.: *Variation in the impedance and its impact on the transmission coefficient considering tag 2*

4.5. Investigation of the impact of different parameter variations of the belts

From table 4.1 it can be observed that there are some variations in the electrical parameters of different rubber sheets. The impact of these variations are hard to measure but using the simulation model it is possible to quantify the impact of those changes on the designed tag. Furthermore, due to diverse belt applications, the considered physical belt is fabricated in different shapes and width and with different chemical recipes. To carry out the effective feasibility, it is important to determine the impact of these few mentioned variations on the designed tag. One way to determined the impact of the variations is to use the developed strategy and then to analyze the impact of those variations on a tag characteristic [4]. Results of those investigations will be discussed in this section.

4.5.1. Impact of the electric parameter variations on the tag characteristics

As shown in table 4.1, the different rubber sheets used in the belt have some variations in their electrical parameters. By changing the sheet's electric parameter values in the belt, the impact of these variations on the tag antenna impedance and consequently the overall performance of the tag are evaluated. Figure 4.20 shows the impact of those variations on the overall impedance value. Figure 4.21 shows

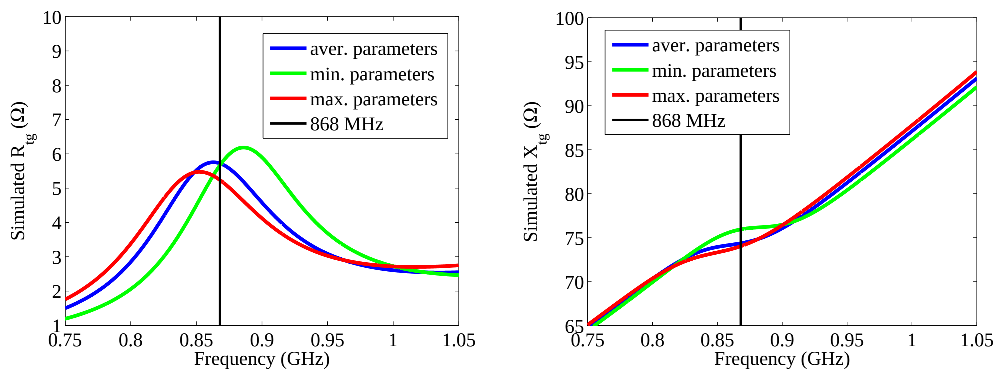

(a) Impact on the R_{tg} of the simulated impedance (b) Impact on the X_{tg} of the simulated impedance

Figure 4.20.: *Electric parameter variations (present in different rubber sheet) impact on the antenna simulated impedance*

the impact on the gain of the designed antenna.
From these results it can be observed that the impact on the impedance and gain is rather small. The resonance of the tag antenna shifts by a few tens of MHz and the gain by a fraction of dB. The impact of these variations (determined using (2.21)) on the performance of the tag is not much. Hence, even if the belt has some electrical parameter variations, the designed tag will still be detected as it has similar performances [4].

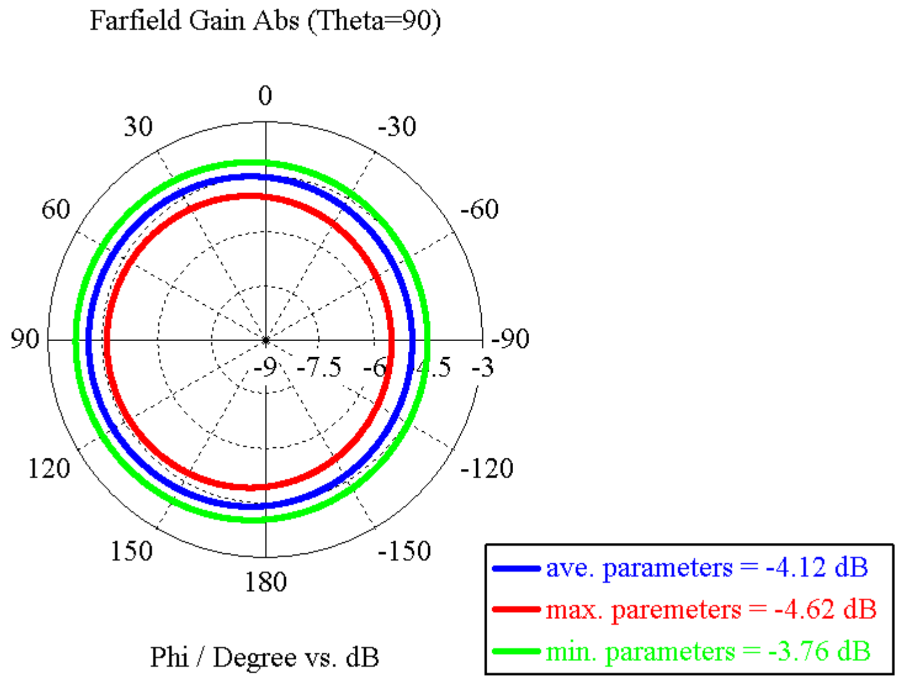

Figure 4.21.: *Impact of the electrical parameter variations on the antenna gain*

4.5.2. Impact of thickness variations on the tag characteristics

Due to fabrication process, the thickness of different rubber layers of the fabricated belt can vary by a few 100's of μm. The impact of these variations, present in various layers of the belt, on the antenna impedance, the gain and the read range can also be determined using simulations of the belt model by changing the respective sheet's thickness. Figure 4.22 shows the impact of those variations on the overall impedance value and figure 4.23 shows the impact on the gain.
It can be seen from these results that these variations in the antenna parameters is quite negligible. Hence, the influence of these variation on the performance of the tag can be ignored, too.

4.5.3. Impact of changes in the shape of the rubber belt on the tag characteristics

Due to numerous rubber belt applications, a rubber belt of the same fabrication recipe can have various shapes. Consequently, it is quite important to know, if the designed tag also works with similar performance on other rubber belts or not. The most common shape change is that the belt is fabricated in a rectangular shape instead of the V shape (shape of the considered belt model). As the electrical pa-

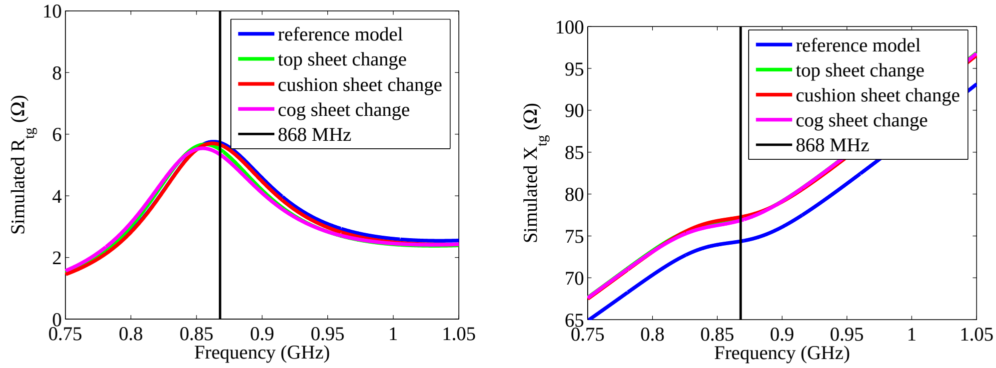

(a) Impact of thickness change on the R_{tg} of the simulated impedance (b) Impact of thickness change on the X_{tg} of the simulated impedance

Figure 4.22.: *Impact of thickness variations on the impedance of the tag antenna*

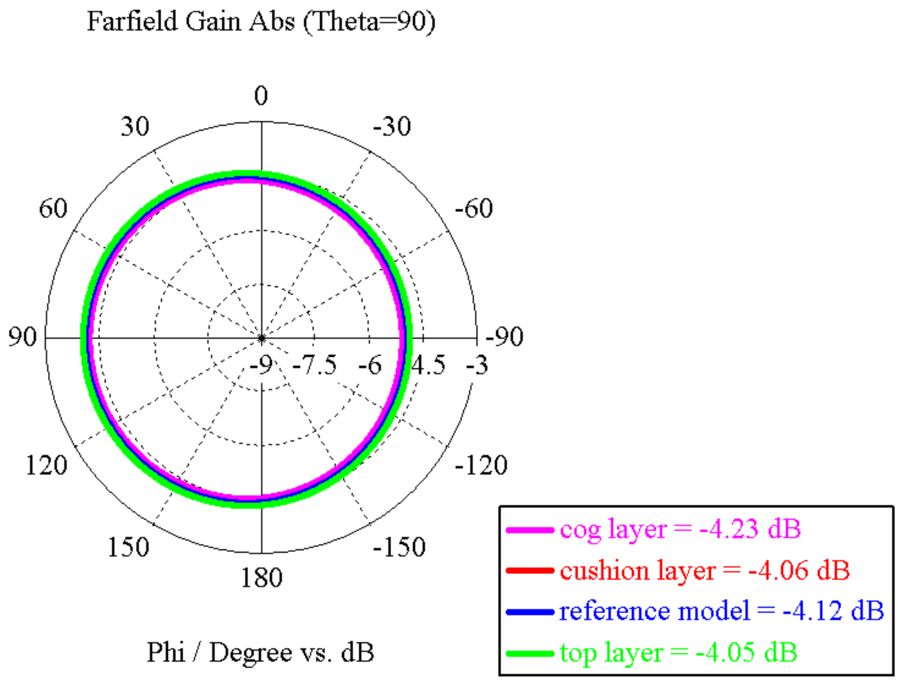

Figure 4.23.: *The influence of thickness changes of different rubber sheets on the antenna gain*

rameters are the same, only the shape is different from the originally considered belt. Thus, it is easy to investigate the impact of such a common shape variation on the tag antenna with the help of simulation, just modifying its geometry, changing it into a rectangular shape. The modified electrical model is depicted in figure 4.24, the corresponding simulated impedance values are displayed in figure 4.25. Figure 4.26

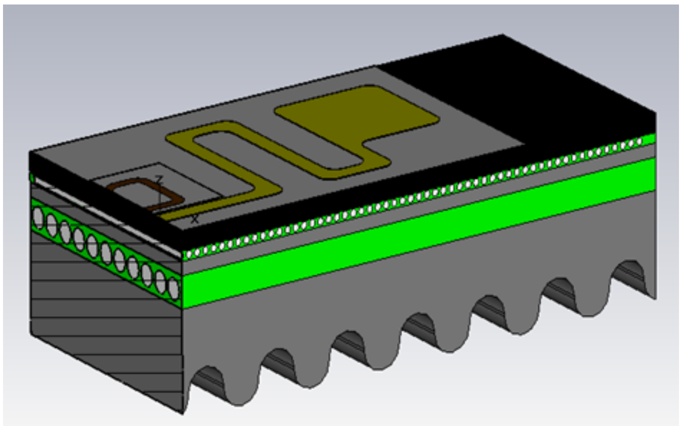

Figure 4.24.: *Modified belt in rectangle shape instead of V shape*

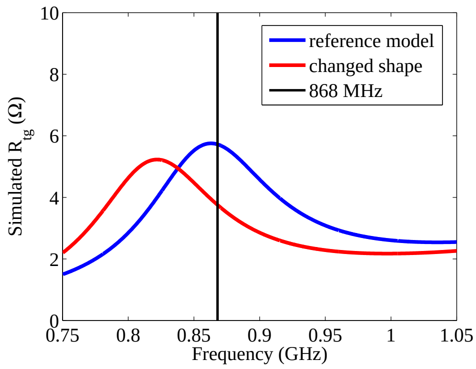

(a) Impact on the R_{tg} of the simulated impedance

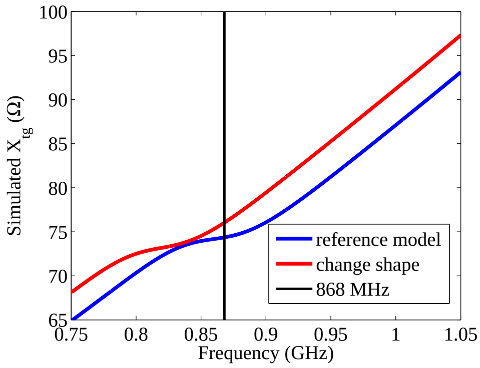

(b) Impact on the X_{tg} of the simulated impedance

Figure 4.25.: *The impact of shape change on the simulated impedance of the tag antenna*

depicts the gain of the antenna for corresponding changes. In figure 4.25 it can be seen that the geometry change shifts the resonance frequency, it is detunned by approximately 40 MHz. The reason for this effect is that the effective relative permittivity value of the belt is higher compared to the V shape belt. The higher relative permittivity reduces the resonance dimensions of the dipole tag antenna. Therefore when a tag antenna designed for the V shape belt is attached to a rectangular shaped belt, the resonance dimensions of the tag antenna appears to be bigger than $\frac{\lambda}{2}$ for such kind of the belt. Due to this, the impedance at 868 MHz frequency drops, as shown in figure 4.25. For that reason the resonant antenna structures i.e. the external antenna dimension needs to be reduced for such a shape. However, its impact on the transmission coefficient is not big. This can be determined based on

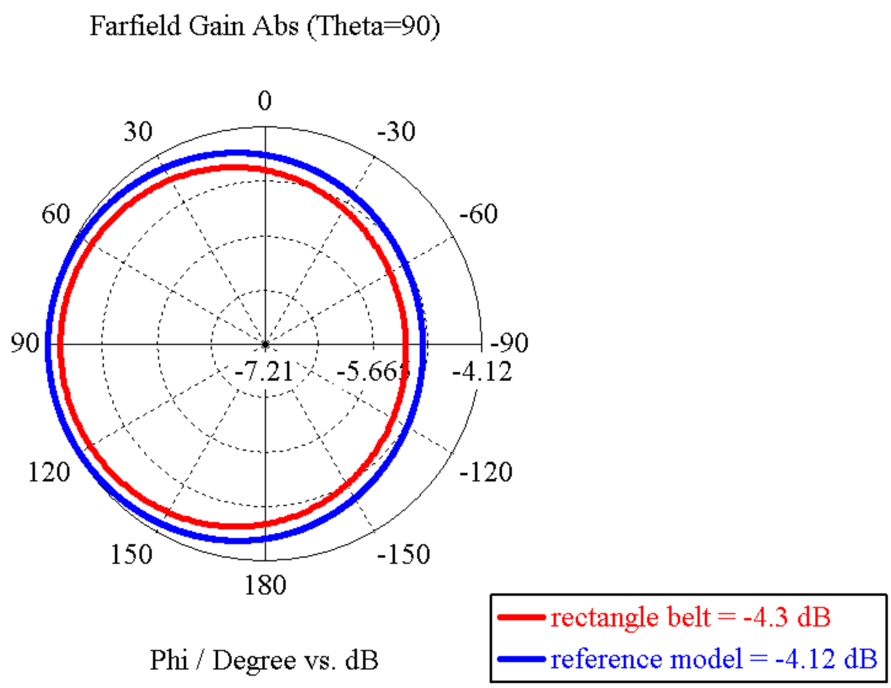

Figure 4.26.: *The impact of shape change on the simulated antenna gain*

(2.1) [4].
Similarly, from figure 4.26 it can be observed that the impact of a geometry change on the gain is not much. The possible reason is that as the tag is attached on the surface it is not impacted by the belt shape change. If the designed tag is used for such a belt, then based on (2.21), it is observed that the reduction in read range is not much. Thus, the tag design can be used to tag belts with various shapes having similar fabrication recipe without compromising too much on the performance. Nevertheless, if optimized design is required then only the external antenna dimensions need to be fitted [4].

4.5.4. Impact of electrical parameter changes (caused by different chemical recipes) on the tag characteristics

Based on different application requirements, belts of the same shape can be fabricated with different recipes. As the electrical parameter values of various rubber sheets depend on the fabrication recipe, it is interesting to predict the performance of the tag for such kind of rubber belts. Suppose the changes in electrical parameters are 25 % or 50 % compared to the considered optimized belt electrical parameter values. Then, the effect of these changes on the belt can be predicted by changing these electrical parameter values in the belt model [4]. Figure 4.27 shows the simulated impedance for the mentioned changes in electrical parameters. Figure 4.28

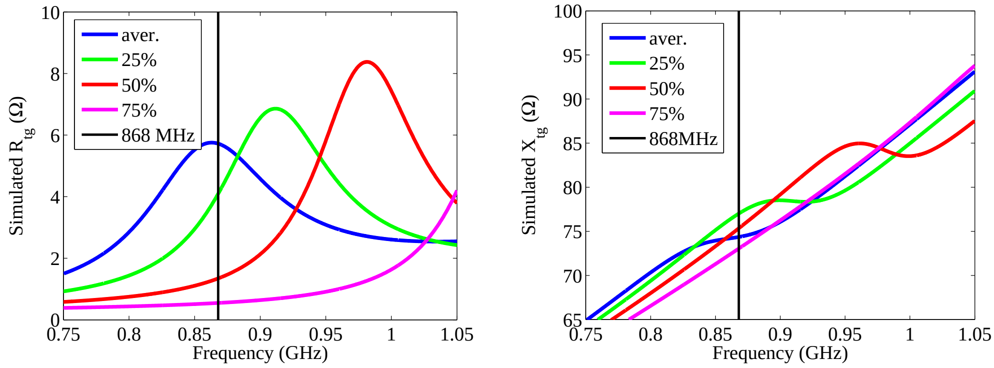

(a) Impact on the R_{tg} of the simulated impedance (b) Impact on the X_{tg} of the simulated impedance

Figure 4.27.: *Impact of variations in the electric parameters due to recipe change*

shows the gain of the antenna for corresponding changes. Using (2.21), it is ob-

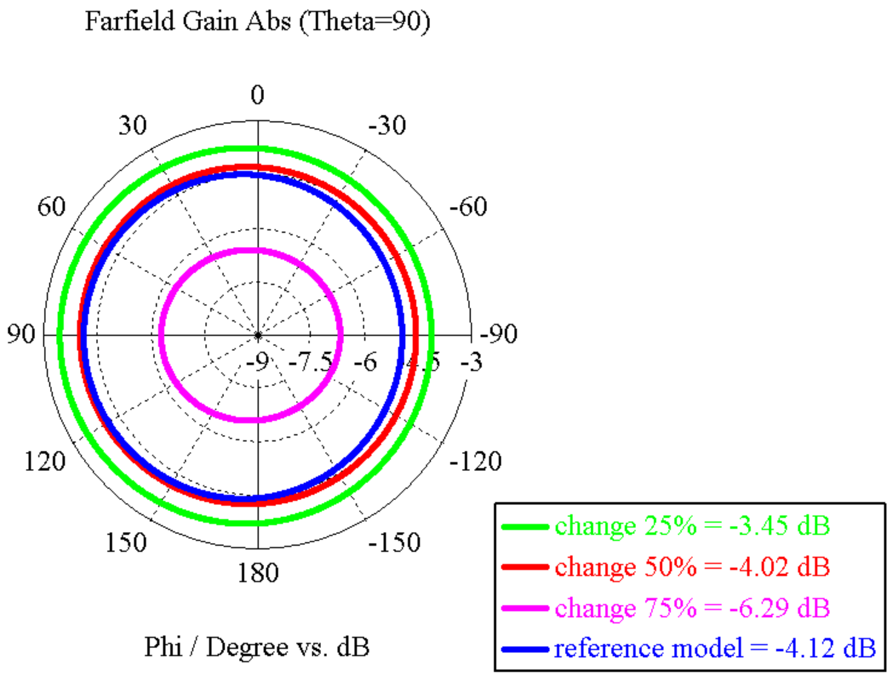

Figure 4.28.: *Gain of the antenna if the electrical parameters change by various percentages due to different fabrication recipes*

served that the considered tag can be used with similar performance up to 25% changes in electrical parameter values. When changes in electrical parameters are more than half compared to the considered belt then the performance deteriorates to a great extent. For such cases, higher performance antenna with good matching can be designed just modifying the external antenna dimension and the distance between the inner and the external antenna [4].

4.6. Bulk reading test to investigate logistic application

To check the suitability of the designed tags for logistic applications in real belts, a bulk reading test is carried out. Basically in bulk reading testing, a packed box filled with a given number of tagged objects passes a standard reader gate. At the reader gate, a reader module detects unique assigned IDs of tags attached to the products via reader antenna. If all IDs are detected and counted exactly the success rate is 100 %. In this case bulk testing is successful.
For carrying out this test, the typical experimental setup consists of a gate, 1 reader patch antennas, a 1 W reader module and the application software. This setup is shown in figure 4.29.

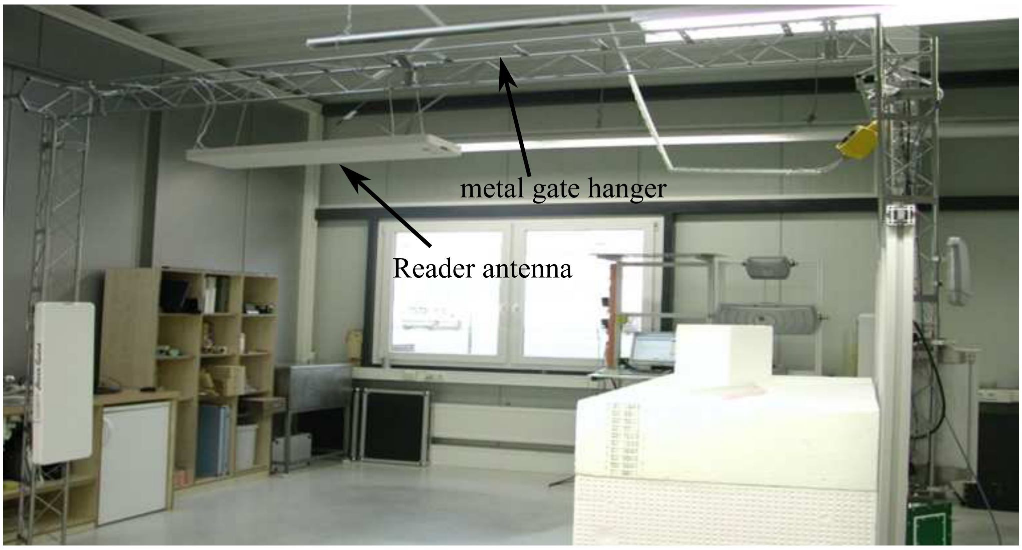

Figure 4.29.: *A typical detection gate for counting tagged objects*

Before performing the test, a typical number of tagged objects in the box needs to be mentioned in the application software (in this case 17 is mentioned). After that in the box 17 tagged belts are packed. Before packing them into the box, unique IDs were assigned to the 17 tags via the application software. The attached tags are shown in figure 4.30. Then this box passes the gate (as shown in figure 4.31). Afterward, at the screen of the application software, as shown in figure 4.32, it can be seen that the detection/read success rate is 100% i.e. all 17 tagged belts are identified and counted by the reader module. This means the performed bulk test

Figure 4.30.: *Tagged belts*

Figure 4.31.: *Tagged belts packed into a box*

is successful.
By carrying out this test, it is shown that the designed RFID tags can be used for logistic applications and can improve the counting mechanism of such complex and heterogeneous structures.

4.7. Summary and outlook of the chapter

In this chapter, a design process established to obtain an optimized (in terms of the transmission coefficient) UHF tag for rubber transmission belts, is presented. The summary of the design process is depicted in figure 4.33.

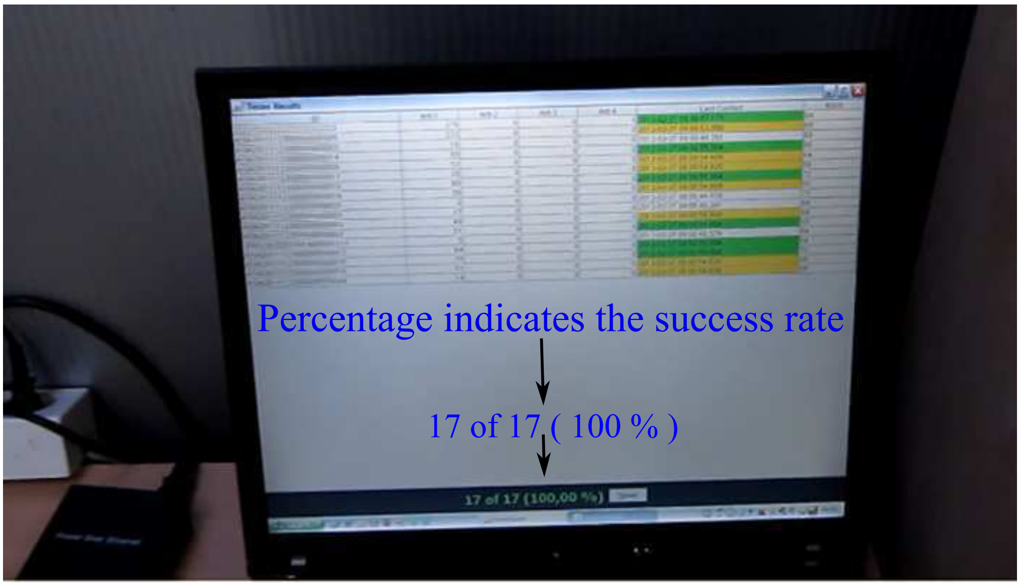

Figure 4.32.: *Results of the performed bulk test*

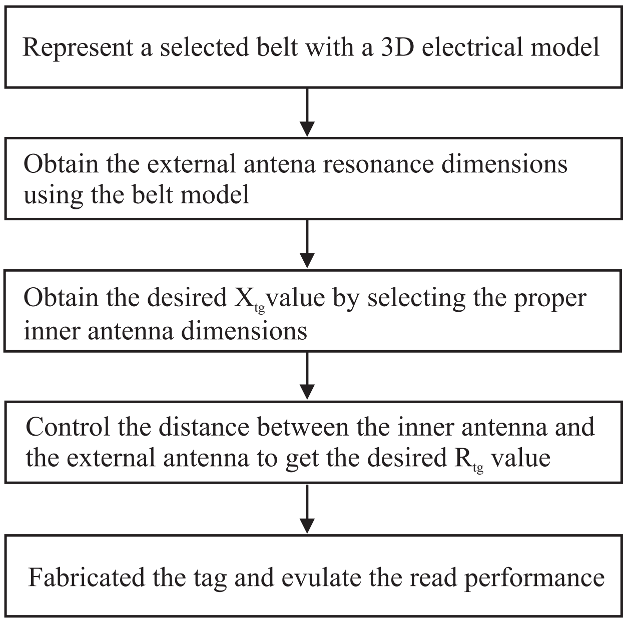

Figure 4.33.: *Summary of main steps to design a surface tag for a rubber belt*

Furthermore, the performance of the designed UHF RFID tags in terms of read range are evaluated and results are presented. The results in table 4.3 show that up to 16% relative error in the measured read range of a tag matches to the theoretical read range. In addition, the impact of different variations of the belt's structure on the tag antenna are investigated with the help of simulations and the results are presented. From these results it is observed that, if the designed tag is attached to another belt having a similar fabrication recipe and different shape, then the performance of the tag does not vary much. This is caused due to the fact that the considered rubber belts have higher losses which exhibits wider impedance bandwidth phenomena, which in turn keep the transmission coefficient quite similar for various changes and shapes. This phenomena makes the design insensitive to this variation. Hence, for such cases, a certain performance of the designed tag can be granted.

Furthermore, from the results, it is observed that only a few different tag antenna designs are required to cover a wide range of different rubber belts. Only external antennas of the designed tags need to be modified as the imaginary part remains quite constant for different electrical parameter values. Hence in a quite fast time all kinds of rubber belts can be covered with high performance tags using the established process.

By adopting this presented process established for the rubber belts, a high performance and a good matched RFID tag for various kind of rubber products can be achieved. Furthermore using the 3D electric model of the belt, the major information required to analyze the performance of a tag can be gathered quickly. Additionally, quite fast feasibility of various UHF RFID tags (e.g. sensor enabled RFID tags) for different application can be carried out, too [2].

CHAPTER 5

Embedded tag design process for the rubber belt

To establish an optimized design and an analysis process of UHF RFID tags for the rubber belts, as a first step, a design and analysis process for the surface UHF RFID tag is presented in chapter 4. Using the gathered know-how of the surface tag design, in this chapter, major problems are tackled to obtain a high performance embedded RFID tag design. Few of the typical problems investigated in this chapter are: design and analysis of an embedded tag antenna for various applications, determination of a suitable antenna structure and fabrication technique to get the embeddable tag antenna, its chemical (adhesion compatibility) and mechanical impact on the belt structure, and life cycle tests of the embedded tag in the physical belt under various harsh conditions [3].

5.1. Determination of a suitable antenna structure and fabrication technique

Broadly, two forms of tag antennas are used in tagging applications i.e. planar and wire based antenna structures. These are fabricated in various shapes with different structuring techniques, such as etching, printing, plotting and stitching e.t.c. [17–21, 72]. Out of these, a suitable technique which has negligible chemical[1] and mechanical[2] impact on the belt structure, during the embedding process and throughout its full life cycle usage needs to be determined. In addition, the cost

[1] adhesion problem between antenna material and rubber layers due to incompatible bonding
[2] crack in the belt structure due to various dimensions of an embedded tag antenna

of a tag depends on the adopted fabrication process. Therefore, to obtain a cheap embedded tag, it is also important to determine, which antenna structure and fabrication technique is feasible for the considered belts.
To check these facts, based on a few of the available fabrication techniques, various dipole type tag antennas[3] were structured onto the individual raw CR material rubber layer and then covered with a rubber layer of the same material. After that, those various sample rubber layers were vulcanized at a temperature of 180 °C in the lab, under similar manufacturing conditions as used for the standard rubber belt. Before discussing the outcome of the vulcanization results, a brief description about those fabrication techniques and the structured antennas is presented below [3].

The tag antenna structured by printing technique

Using printing technique, an antenna in a desired shape is structured by printing a conductive material on a substrate or on an object. Then the printed material is hardened onto the substrate by blow-drying [17]. A prototype of a tag antenna structured onto the rubber sheet using this technique is shown in figure 5.1. The

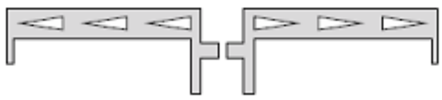

Figure 5.1.: *Antenna structured with pasting technique [17]*

printed antenna is made out of silver paste and has the approximate dimension of 100 mm by 10 mm. This antenna was manufactured at the department of the Fraunhofer ENAS, Chemnitz, Germany [17]. The main advantage of the antenna obtained by using this technique is that no chemical residues are created. Due to this the handling and the structuring cost of the antenna are less compared to the etching technique. Additionally, the overall thickness of the antenna is quite small. The tag antennas are suitable for tagging various books in the library, tagging wind screens of cars e.t.c. [17].

The tag antenna structured using the plotter and etching technique

A prototype of a tag antenna structured via the plotter and the etching technique is shown in figure 5.2. The external antenna is structured via a plotter machine by cutting the aluminium foil. The thickness of the aluminium is 35 μm on top

[3]There are different kinds of tag antenna designs, such as dipole or patch type, which can be selected to design the embedded UHF RFID tag [13, 30, 73]. Dipole type tag antennas are structured into the rubber sheets because of relative less amount of external materials required to structure them.

of a paper substrate of 65 μm. The inner antenna[4] is structured via an etching process on the polypropylene substrate. The details about a typical etching process on flexible substrates can be found in [18]. The external antenna dimension is 90

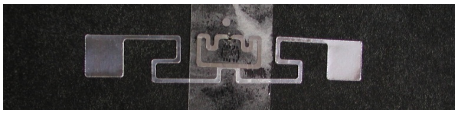

Figure 5.2.: *Antenna structured with the plotted and etching technique*

mm by 15 mm whereas the inner antenna is 15 mm by 5 mm. The main advantage of the antenna obtained by using this combined techniques is that the tag antenna, especially the external antenna can be structured quite fast. This feature is quite beneficial to get the high performance tags in quick time for various materials (a typical application is discussed in the previous chapter). The tag antennas are utilized in various objects tagging applications, for instance wood cases, plastic cases, key chains e.t.c..
In addition, if no visible impact of the inner antenna on the rubber sheet is observed then the stand alone etching technique can also be considered to construct the embedded tag antenna. These tag antennas structured with the etching technique are widely applied in various type of object tagging such as clothes, boots, boxes, parcels, books e.t.c..

The tag antenna structured using stitching and etching technique

A typical tag antenna prototype[5] structured at large scale using a combination of the stitching and the etching technique is shown in figure 5.3. However, at the time of performing the test, the tag antenna structure depicted in figure 5.4 is used. In this prototype the external antenna is structured in arbitrary shape by hand. Later on large scale, by attaching a thread to a wire and then using stitching

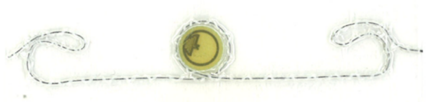

Figure 5.3.: *Typical tag design with combination of stitching and etching*

technique, the external antenna for the embedded tag in the desired shape and dimensions can be obtained like the one shown in figure 5.3. In the considered tag antenna, the external antenna is made of a steel wire, it has a diameter of 200

[4]for performing the test, this was provided by our partner, tagItron GmbH, Salzkotten, Germany
[5]http://www.tagitron.com/

Figure 5.4.: *Antenna structured with combination of stitching and etching(tested)*

μm. It is approximately 70 mm long and 6 mm wide. The inner loop antenna[6] is structured on a FR-4 substrate with the etching technique [18]. The loop has a diameter of 5 mm and is covered with similar material from the top. Hence the inner antenna is fully enclosed in a FR-4 material body. The advantage of this tag antenna combination is that it is mechanically strong and may survive in harsh conditions such as high flexibility and high temperature. The tags fabricated using this combination are mostly used in tracking washing textile used in various fields.

Now the impact of these tested antenna structures after vulcanization with the rubber sheets is discussed [3].

The sheets obtained after vulcanization are shown in figure 5.5, figure 5.6 and figure 5.7. From figure 5.5 and figure 5.6 it can be observed that some bubbles

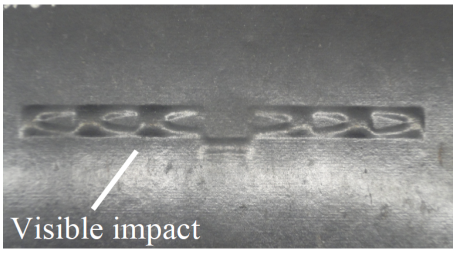

Figure 5.5.: *Impact of the antenna structured by printing technique on the rubber sheet*

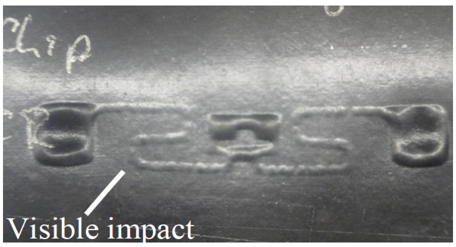

Figure 5.6.: *Impact of the antenna structured by plotting and etching technique on the rubber sheet*

[6] for performing the test, this was provided by our partner this is provided by our partner, tagItron GmbH, Salzkotten, Germany

are created around the embedded antennas. The bigger bubbles are created around

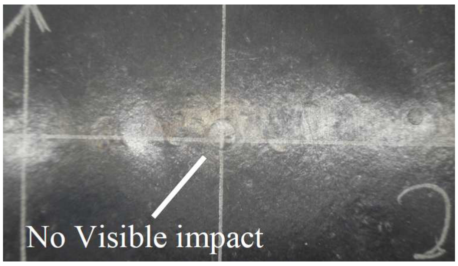

Figure 5.7.: *Impact of the antenna structured by the etching and the stitching technique on the rubber sheet*

the area where more metal or substrate materials are used, and smaller bubbles are created where less materials are used. This may be caused due to the different melting points of the materials or unknown chemical reactions which might occur inside the rubber sheet during the vulcanization process. At such high vulcanization temperature i.e. 180 °C, these materials inside the sheet may have changed their matter form i.e. from the solid form to the viscous form partially or fully inside the rubber sheet, and may also get mixed with rubber material. After the vulcanization process, when the device is cooled down, then these materials might have changed their state back to the solid form. During this process, the materials may have not chemically bonded well with each other. The exact reason of the bubble creation is not known exactly up to now. It could be either caused by the antenna materials or due to limits (e.g. it can not handle such materials which are suitable to get an embeddable antenna) of the fabrication techniques. Due to high investigation cost and time limit this aspect is not investigated further. In future, more detailed investigations could be carried out in this direction to determine the more accurate causes of this effects.
However, from figure 5.7, it can be seen that no visible bubbles are created by the embedded antenna between the rubber sheets. The amount of material used in the antenna structure is less compared to the other two tag designs, and probably it did not melt or interact chemically inside the rubber sheet during vulcanization. Due to this reasons, no bubbles are raised in the sheet after the vulcanization process.
Therefore, based on these results, it is found that the antenna structure using a combination of the stitching and the etching technique is suitable for the embedded antenna, because no visual impact on the adhesion between the rubber sheets has been observed [3]. This antenna structure is selected for the embedded antenna.

5.2. The embedded UHF RFID tag design process

As described in chapter 2, when an UHF RFID tag is attached onto a surface or embedded into an object, the complex impedance value of the tag antenna alters which in turn results in a mismatch between the tag IC and the tag antenna's complex impedance values. Due to this mismatch, the detection read range of an UHF RFID tag is reduced[7]. One cost effective way to improve this mismatch is to design a tag antenna matched to the considered tag IC [2, 27].
In this chapter, the designed embedded tag antenna complex impedance value is matched with the Monza 4 tag IC. The considered tag IC has a typical complex impedance value $Z_{\text{chip}} = 13 - j151\ \Omega$ at 868 MHz frequency [37].

Design of the embedded tag antenna

Based on previous results, a dipole type tag antenna based on the inductive coupled loop principle is selected for the embedded tag. The prototype of the designed tag antenna is shown in figure 5.8 [3]. The tag antenna basically consists of the two

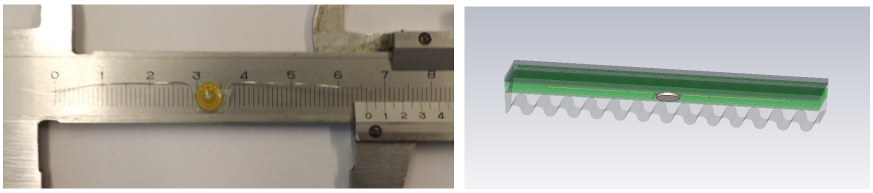

(a) A prototype of the embedded UHF RFID tag (b) Model to simulate the embedded tag antenna

Figure 5.8.: *Designed embedded tag antenna for the belt*

antennas, i.e. an inner and an external antenna. The function of these antennas and impedance mechanism is similar to the tag antennas presented in the previous chapter. In the following section, a brief summary of the designed tag antenna and its dimensions are presented.

External antenna: The basic purpose of an external antenna is to enhance the overall gain of a tag antenna. In the tag antenna it is the main contributor of the overall real part of the complex impedance value. It can be matched to any dielectric environment, and it only shows a real part at resonance. The amount of transformed impedance to the inner antenna and hence the real part of the tag antenna depends on many factors. A few of them are shape of a loop, trace width,

[7] A typical impact on the air optimized tag characteristics is shown in appendix A.2

distance between the two antennas e.t.c. [30]. For the considered complex belt structure, the information regarding the real part of the impedance value and the over all $\frac{\lambda}{2}$ dimensions of the external wire antenna are obtained using parametrized EM simulations of the electrical model. The external antenna is wire based, it is 66 mm long and 5.5 mm wide. It major dimensions are depicted in figure 5.9(a) [3].

Inner antenna: The function of the inner antenna is to counter balance a capacitive part of a tag chip. In the tag antenna, it adds the overall imaginary part of the complex impedance. For keeping the width of the tag small (to avoid any kind of mechanical damage to the belt), the inner antenna is made of double loops, because it is very hard to achieve a high imaginary part with a single loop with approximately 5 mm diameter. Its major dimensions are shown in figure 5.9(b). In

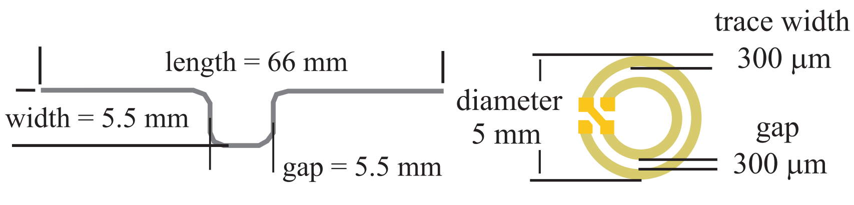

(a) External antenna (b) Inner antenna

Figure 5.9.: *Dimensions of the embedded tag antenna*

the inner antenna[8], the outer loop has a 5 mm diameter and the inner loop has a 4.4 mm diameter. The trace width is 300 μm for each loop. These two loops are separated from each other by 300 μm. The inner antenna embedded in the belt is encapsulated with FR-4 material and has a diameter approximately of 5.3 mm and has an overall thickness of 0.7 mm [3].

5.3. Mechanical testing of the embedded tag

A couple of the prototype tags are embedded inside a couple of physical rubber belts for performing the mechanical tests. Due to fabrication costs, it was not possible to select the same belts for mechanical tests and performance analysis. Therefore, different belts are selected. However, this does not affect the objectives of this section i.e. to investigate and determine how the embedded RFID tag would behave in the belt during various stages in the full life cycle of a physical belt. The size of the tagged belts used for performing this test has smaller dimensions than the tagged belts intended for the performance analysis (as discussed in section 5.5). Both types of belts are shown in figure 5.10 [3].

[8]This double loop antenna is designed by Impinj for our partner tagItron GmbH, Salzkotten, Germany

Figure 5.10.: *Considered rubber belts for investigation purpose*

5.3.1. Tag placement inside a physical belt

The approximated location of an embedded tag inside the rubber belt is marked in figure 5.11. At the indicated position, a minimum force is exerted onto the tag

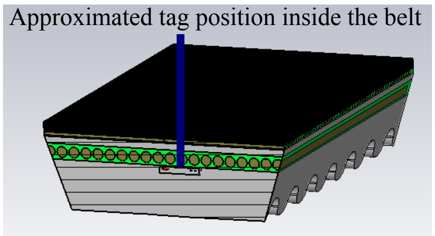

Figure 5.11.: *Approximated position of tag inside the belt*

during the real application of the belt. The placement of the tag on the rubber sheet during the fabrication cycle is shown in figure 5.12(a). The tagged belt obtained

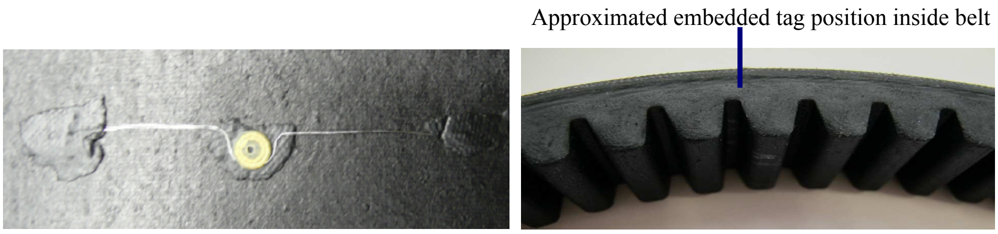

(a) Tag placed on the sheet

(b) The fabricated belt

Figure 5.12.: *Tag placement during manufacturing and in the fabricated belt*

after following all standard manufacturing steps is shown in figure 5.12(b). After visual inspection of the location and moving the belt in different directions by hand, it is observed that the rubber belt structure is not impacted by the embedded tag. In fact, it is impossible to realize that the belt contains any embedded UHF RFID tag in it [3].

5.3.2. Mechanical test to check damages

After a tagged belt is fabricated, the next challenge is to check whether the embedded tag will survive without damaging the belt, in standard belt application for its full life cycle. Typical moving speed of such rubber belts ranges from 20 m/sec to 80 m/sec. To find this fact, generally two separate tests of the belts with different time durations need to be performed in the quality control testing lab [3].
First a short duration test is carried out. The duration of this test is around 20 minutes. Usually, by performing such a short duration test, any mechanical effect of the tag on the belt can be observed either visually or in terms of wear and tear signs in the belt structure. If no signs of damages are observed after this short duration test then in the next stage a long duration test is performed. The duration of such type of test is several hours. By executing this test, it is possible to determine that if the tag survived inside the belt in its full life cycle without influencing the original usage of the belt or not.
To find out the damages to the tag or to the belt these tests are conducted one after another and results are shown in figure 5.13. After carrying out both tests, no

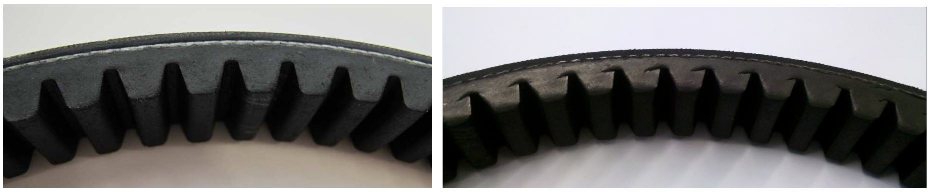

(a) Belt after the short duration test (b) Belt after the long duration test

Figure 5.13.: *Life cycle test of the tag in a physical belt*

visible unexpected mechanical problems on the belt have been observed. Furthermore, the tag is still detectable after these tests. Therefore, based on these results, it can be concluded that if such tag is embedded in similar flexible rubber belts, then it is possible to track and identify the belts in it full life cycle without any damages [3]. Furthermore, it may be possible to use such a tag antenna structure for sensor-enabled RFID tag applications.

5.4. High speed test to detect a belt during operation

A preliminary high speed detection test of the embedded tag is conducted to determine that a tagged belt can be detected at upto a speed of 3000rpm. Details of the performed test and results are discussed in the following section.
Figure 5.14 shows the layout of the experimental setup that is used to detect the

tag embedded in the belt during high speed operation. Normally this setup is used in the quality lab to check the quality of the fabricated belts. In this setup only air is present in the belt ambient. But in the real application scenarios usually a lot of complex material structures surround the belt. Hence this setup for detecting the tag is not optimum. Nonetheless, to obtain the initial feeling the detection of UHF RFID tags at high speed this test is done using this setup. By carrying out

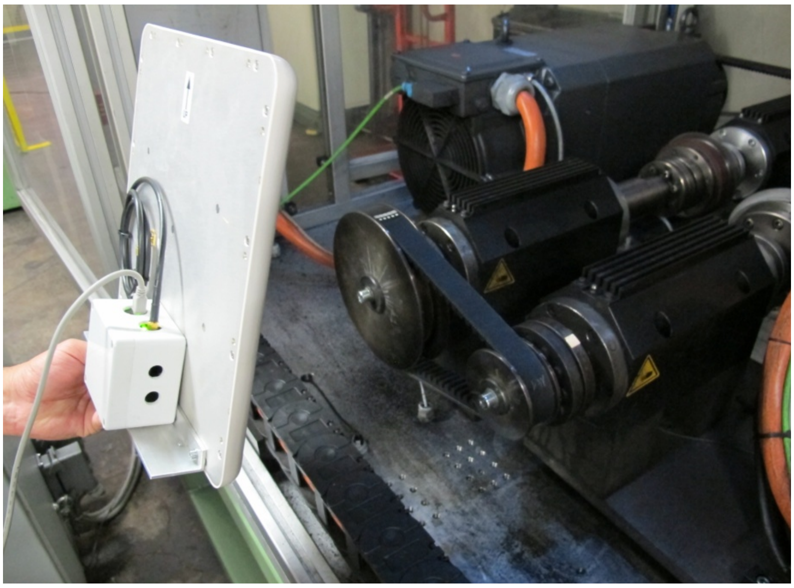

Figure 5.14.: *Detection of the belt during high speed operation*

this test, it is found that the designed tags can be detected by the reader system up to a belt revolution speed of 3000 rpm. However, the read count of the moving tagged belt is not much compared to the still tagged belt. Nonetheless, this is a quite encouraging result and gives the idea that it is possible to detect the belt at such high speed.
After this high speed test it is found that a rubber belt authentication and the data transfer may be done during high speed operation of the belt. Though, for the real belt application this test has to be optimized.

5.5. Performance analysis of the embedded RFID tags

The performance analysis of the embedded tag is carried out in a similar way as discussed in chapter 4. Results of this analysis are presented in this section [3].

5.5.1. Estimating the theoretical read range of the embedded tag based on the simulation

Principally to estimate the maximum read range via (2.21), information about two parameters of the tag antenna are required. Those parameters are the Gain (G_{tg}) and the impedance (Z_{tg}) value at 868 MHz to calculate the value of τ. The information about both factors is obtained via a simulation of the tag embedded inside the belt model [3].

Gain of the tag antenna

The gain pattern of the tag antenna in 3D is shown in figure 5.15. It can be observed that the simulated tag antenna has a maximum gain value of $G_{\text{tg}} = -7.5$ dB. The gain degradation of the simulated antenna is high compared to a standard dipole tag antenna. It is mainly caused due to the high tanδ values (i.e. ranges between 0.18 to 0.36) of the rubber sheets used in the belt [3].

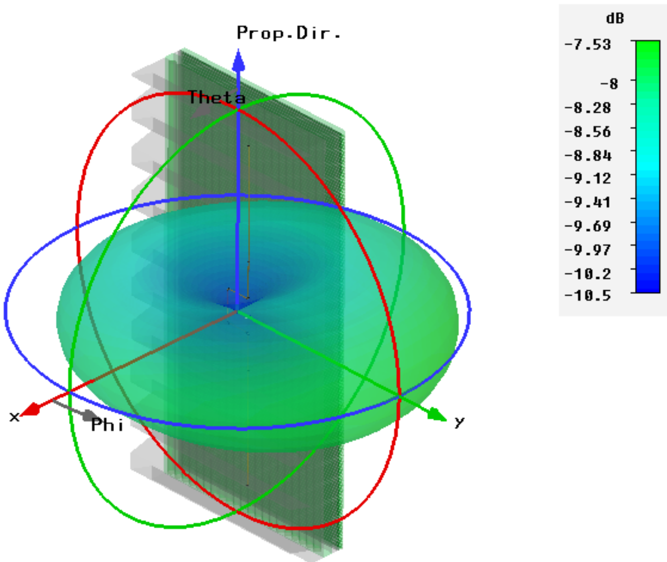

Figure 5.15.: *Simulated gain of the embedded tag antenna*

Impedance of the embedded tag antenna

The simulated complex impedance of the designed tag antenna is shown in figure 5.16. At 868 MHz, the tag antenna has the impedance value of $Z_{\text{tg}} = 8.5 + j157.2\ \Omega$. Hence, the value of τ obtained using (2.1) is 0.89 and $\sqrt{\tau}$ factor is 0.93.
In addition, it can be observed from figure 5.16 that the simulated complex impedance value has a wider impedance bandwidth compared to a tag antenna

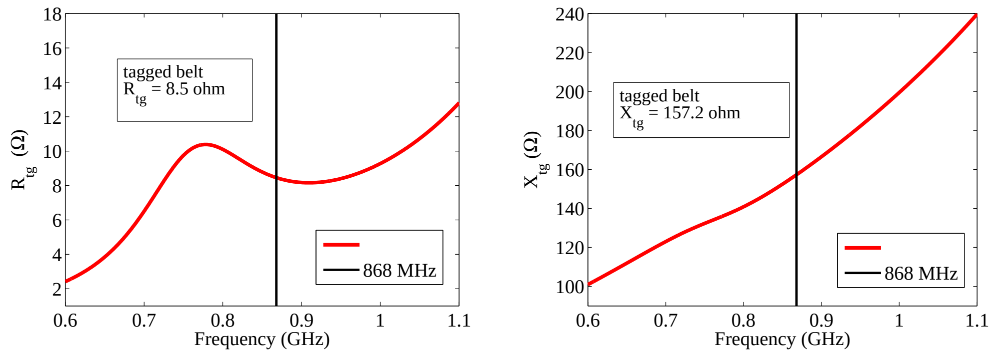

(a) Real part of impedance

(b) Imaginary part of impedance

Figure 5.16.: *Simulated impedance of the embedded tag antenna*

designed for low loss materials. Due to this phenomena, a small variation occurs in $\sqrt{\tau}$ factor. The overall benefit of this effect is that a tagged belt can have an approximately similar $\sqrt{\tau}$ factor value in a similar layer stack with similar chemical belt recipes having various width and sizes.

Once the required parameter values i.e. the gain and the complex impedance value are obtained, the maximum theoretical read range of the simulated tag is calculated using (2.21). The calculate read range is 4.6 m [3].

5.5.2. Estimating the read range of the embedded tag based on anechoic chamber

As explained in chapter 2, to estimate the read range of the prototype tag, only one parameter $P_{\min}$ needs to be determined. To find this value in an anechoic chamber a tagged object is placed at a fixed distance in front of a reader antenna. Then the power is stepped up gradually at the desired frequency from the reader with variable power until the tag presence is detected. The minimum power at which the tag is detected by the reader corresponds to $P_{\min}$.

To find $P_{\min}$ the tagged belt is placed in an anechoic chamber at a distance (d_{rt}) of 120 cm in front of the read antenna having a gain of 8 dBi. The tagged belt has been detected by the reader at the transmitted power $P_{\min}$ of 40 mWatt [3].

Once all parameters are known, the maximum read range of the prototype tag is calculated using (2.22). The calculate read range is 4.2 m [3].

Comparison of the read ranges

The maximum theoretical read range based on simulation results is 4.6 m whereas the read range based on measurements is 4.2 m [3]. These results show a good correlation. Despite of -9.7 dB difference[9] between the gain of that embedded antenna to the dipole antenna in air, the achieved read range is quite good. This read range is quite beneficial to build a power efficient UHF RFID system for the inventory management of the rubber belts. Furthermore, using the presented design process, the high performance tag or a sensor enabled tag for any kind of rubber belts or other rubber products can be designed.

5.5.3. Variation in the tag performance

From the simulated results of figure 5.16 it can be observed that the designed antenna resonance is not at the desired European ISM band. The reason is that the belt in which the tag is embedded in has a bigger width than the reference belt (originally planned to embed the tag). The difference between both belts is shown in figure 5.17. Due to higher testing costs and time limits, the external antenna

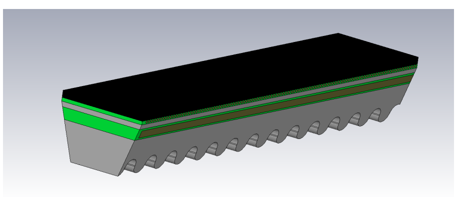

(a) Reference belt model

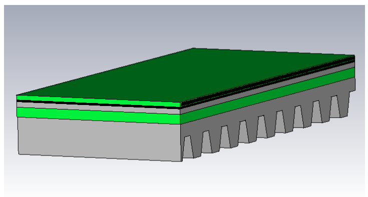

(b) tagged belt width 39 mm

Figure 5.17.: *Difference in tagged belt and reference belt structure*

dimension of the embedded tag could not be re-optimized. However, using the mentioned design procedure, the difference in performance of the designed tag is determined for both belts. The difference between the simulated impedance for both belts is shown in figure 5.18, whereas variations in parameters of the embedded tag are summarized in table 5.1 [3].

The results in the table show that the designed tag antenna has a similar τ factor is caused mainly due to wider impedance bandwidth phenomena in such high loss object. However, the gain of the tag antenna has a difference of -1.7 dB and is caused due to the thicker belt size compared to the reference belt. Overall impact of the belt changes on the designed tag performance is that its read range is reduced by approximately 20 %. By re-optimizing the external antenna dimension the performance of the tag can be increased [3].

[9] mainly caused due to high electrical parameters of the rubber belt

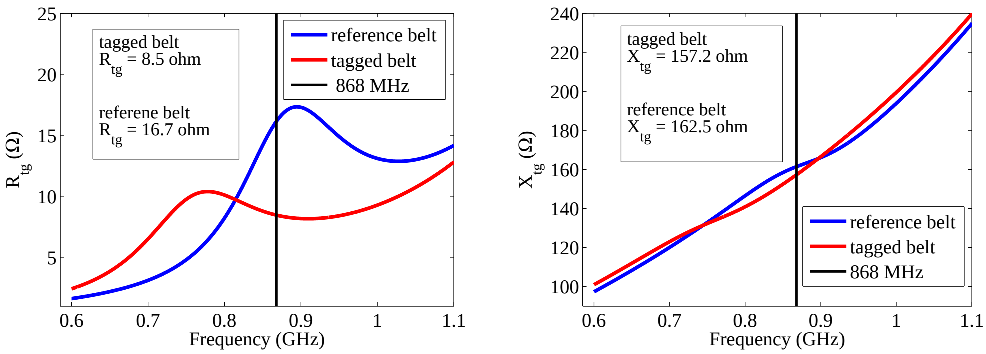

(a) Real part of impedance

(b) Imaginary part of impedance

Figure 5.18.: *Simulated impedance of the antenna in reference and tagged belt*

Table 5.1.: *Summary of different parameters of the tag*

	Reference belt	Tagged belt
Width of belt	14 mm	39 mm
antenna impedance	$16.7 - j162.5\ \Omega$	$8.5 - j157.2\ \Omega$
τ	0.85	0.88
$\sqrt{\tau}$	0.92	0.93
Gain	-5.8 dB	-7.5 dB
R_{sim}	5.5 m	4.6 m
R_{meas}	$N - A$	4.2 m

5.6. Summary of the chapter

A design process to get the optimized (in terms of the matching coefficient) embedded UHF RFID tags for rubber transmission belts, based on a 3D simulation approach is presented. The usefulness of this approach is evaluated by a comparison of the theoretical read range and the measured read range of the fabricated prototype tag. In addition, adhesion problems of different kinds of antenna structuring techniques on the considered belt are investigated. From these investigations it is found that the antenna fabricated using a combination of stitching and etching is suitable for the embedded tag because no visible adhesion problems are observed. Furthermore, to investigate and determine how the embedded RFID tag will behave throughout the belt full life cycle, a mechanical test has been carried out. From the test results it is observed that the embedded tag passes the test, too, and is still operational after a full life cycle of the belt. Furthermore, it is shown that the tagged belt having such high electrical parameter values still can be detected up to

a distance of 4.2 m by the embedded tag, having the overall dimensions of 66 mm by 5.5 mm only [3].
Using the established process, quite easily and effectively preliminary investigation for the considered complex structures can be carried out to check the feasibility of various RFID applications. In addition, numerous types of efficient and high performance tag antennas for item level tagging and for sensor-enabled RFID tags[10] can be designed [3].

[10]to sense different parameter changes of the belt e.g. elongation of the belt due to continuous operation, aging of the belt etc

CHAPTER 6

Summary and conclusions

The major focus of this thesis is to investigate the RFID technology usage in complex heterogeneous structures such as rubber transmission belts. This technology can be utilized to improve in the belt counting mechanisms, the supply management of the rubber belts and to transmit or to sense the changes in physical parameters of the rubber belts. However, various issues (such as unknown electrical parameters of rubber materials, high flexibility, bending and vulcanization temperature) of the considered rubber belts pose a great challenge to adopt the existing UHF tag antenna design strategies for obtaining an efficient embedded RFID tag. These mentioned problems are studied in this thesis, and an optimized design and analysis process is established to get an efficient tag antenna for such rubber structures.

In this regard, first an electrical characterization setup is developed to determine the electrical parameter values of different rubber materials. This setup is based on the open-ended coaxial probe method. Using it, electrical parameters are determined in two steps. In step one, an open-ended coaxial connector is placed on the material under test (MUT) and then changes in the complex reflection coefficients caused due to the MUT are measured using a vector network analyzer. Afterwards for extracting the electrical parameter values, these measured reflection coefficients are compared with the simulated reflection coefficient, obtained from the equivalent 3D measurement model. The major benefit of building a setup with the open-ended probe method is that with a single fixture and simple implementation process the required electrical parameters can be determined quickly. Then by utilizing this setup the electrical properties of two important materials (i.e. EPDM and CR) used in the considered rubber belts are evaluated.

From the evaluated electrical parameter values it is noticed that due to mixing of different chemical compounds, electrical parameters of the same material sheet can vary up to 15 percent. In addition, the accuracy and the reliability of the electrical characterization setup are examined and results are discussed in this thesis.

Afterward, a design and analysis process is presented to obtain an optimized (in terms of matching coefficient) surface UHF RFID antenna using a 3D model of the belt. With the established process, two different surface UHF RFID tags are designed. Then the performance of these tags is analyzed in terms of read range. From the outcome it is observed that the read range of the fabricated tags shows a good agreement with the simulated one. In addition, the impact of different parameter variations of the belt on the tag characteristics are inspected. From the obtained results it is perceived that, if the tag is attached to another belt having a similar fabrication recipe but a different shape, the performance of the tag does not vary much. This is mainly caused due to the high losses of the different rubber materials used in the considered rubber belts. Due to these high losses, a wider impedance bandwidth phenomena in the tag antenna is observed. This keeps the transmission coefficient of the antenna quite similar for both shapes of the belt. Due to this, the tag performance is quite insensitive and can be used with approximately similar read range performance. Furthermore, from these probing experience, it is recognized that only a few different tag antennas are required to cover a wide range of different rubber belts. Only the dimension of the external dipole structure and its distance to the inner loop in the designed antenna need to be modified. Hence with the designed tag antenna, all the range of belts can be covered quickly with high performance tags. Furthermore, to determine the viability of the designed tags in the exact automatic counting of several belts a counting test is carried out. It is noticed that the tagged belts can be counted accurately.

Later on, based on the 3D model of a rubber belt, a design process of the embedded tag for the rubber transmission belt is presented. Using the established process, an embedded UHF RFID tag is designed and then a prototype tag is fabricated. After that the performance of this tag in terms of read range is analyzed. From the results, it is found that the fabricated tag shows a good coherence with the simulated one. In addition, adhesion problems of different kind of tag antenna structures and fabrication techniques to the considered belt material are examined. After inspecting the results it is observed that the antenna structure fabricated using a combination of the stitching and etching is suitable for the embedded tag. Additionally, a life cycle test of the tagged belt is performed to check the damages caused to the belt structure or to the functioning of the tag. From this test, it is observed that the embedded tag in the belt survives and is still functional without damaging the belt structure after its whole application life. From the investigations it is shown that several benefits of RFID technology (such as individual item labeling, inventory management and tracking e.t.c.) can be achieved with efficient tags in the considered rubber transmission belts.

APPENDIX A

Appendix

A.1. Comparison of the electrical and physical belt model

As explained in subsection 4.4.3, one way to check the accuracy of the electrical model of the belt with the real physical belt is to compare the simulated and measured impedance curves of a tag antenna with others [39]. Generally a differential probe is preferred over a single-ended coaxial probe in measuring the tag antenna impedance due to accuracy [74]. In this thesis, initially, using the single-ended probe, it is tried to determine the accuracy of the model. However, during measurement experiments it is observed that it is quite challenging to verify this with quite good accuracy and reliability. Especially, due to mechanical issues such as holding a semi rigid coaxial probe over the model, making a proper contact with the designed antenna and difficulties in performing calibration. Due to the mentioned issues it was not possible to get reliable results. Nonetheless, some results are obtained and are presented as follows.

To show the model comparison, first a tag antenna with the required impedance value is designed using the electrical model by parametrized simulations. The simulated impedance of the designed antenna is shown in figure A.1. Then, the impedance of the prototype antenna attached to the belt is measured by the single ended semi-rigid coaxial probe after carrying out the calibration procedure (open, short and load). Results are shown in figure A.2.

It can be seen from both figure A.1 and figure A.2 that the simulated and the

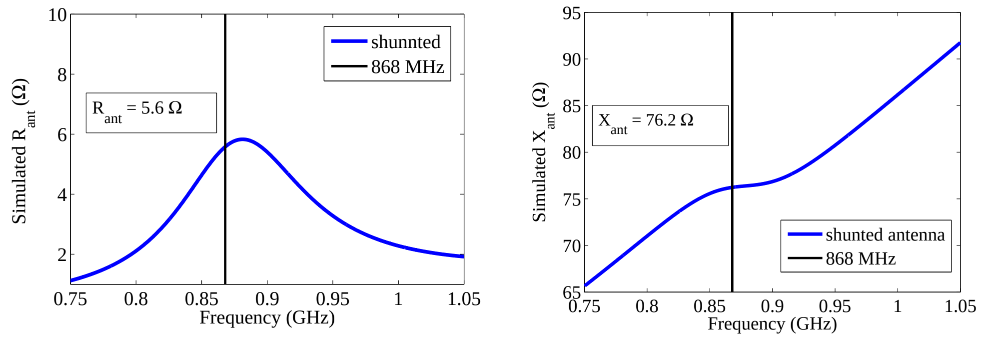

(a) Real part of the simulated impedance (b) Imaginary part of the simulated impedance

Figure A.1.: *Simulated impedance of a tag antenna attached to the model*

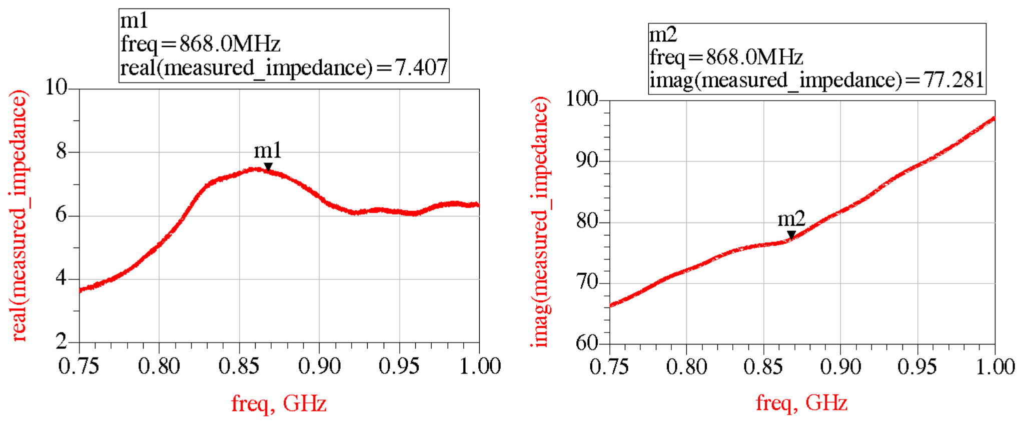

(a) Real part of the measured impedance (b) Imaginary part of the measured impedance

Figure A.2.: *Measured impedance of a tag antenna attached to the model (unit in Ω)*

measured impedance curves show quite similar tendencies. Therefore, based on these results, it can be observed that the belt is modeled quite well. Hence, the developed rubber model may be used further on to design and analyze the UHF RFID tags for the rubber belt.

A.2. Impact of the belt on the tag characteristics

As described in chapter 2, when an UHF tag is attached onto a surface or embedded into an object, its characteristic parameters are changed. Few of those important parameters are impedance, gain, read range e.t.c.. To get a typical idea by which amount a tag characteristic changes due to rubber belt, first an air optimized surface tag is designed, using the process mentioned in chapter 4. Then it is attached to the rubber belt 3D electric model and then changes in the tag characteristics are analyzed using the simulation [4]. The simulated gain and the impedance results are shown in figure A.3 and figure A.4.

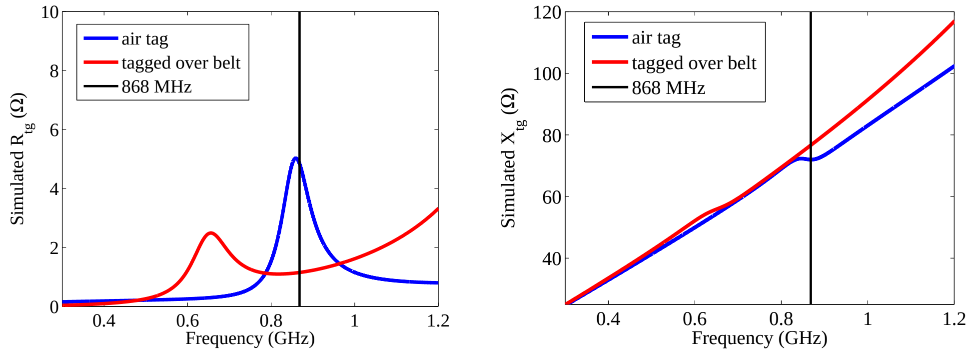

(a) Impact on the $R_{\rm tg}$

(b) Impact on the $X_{\rm tg}$

Figure A.3.: *Detuning of the impedance of an optimized air tag when placed on a rubber belt*

Figure A.3 shows the simulated impedance of a tag antenna in air and on the rubber belt. Whereas, figure A.4 shows the simulated gain of a tag antenna when it is in air and attached on the surface of the belt.

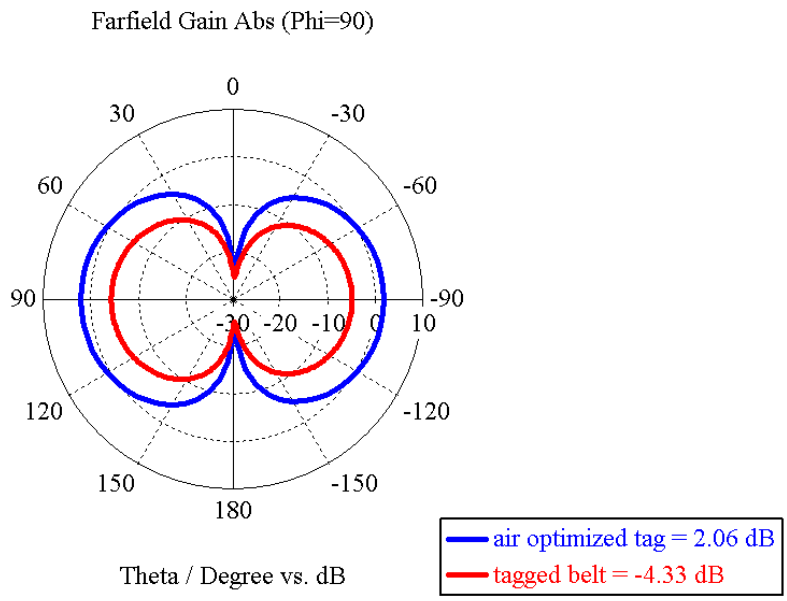

Figure A.4.: *Impact on the gain when an air optimized tag is placed on the rubber belt*

A typical impact of the belt onto the air optimized tag characteristics are summarized in table A.1 [4].

Table A.1.: *Impact of the belt onto the air optimized tag characteristics*

	air tag	Tagged on belt
Z_{tg}	$4.8 - j72\ \Omega$	$1.15 - j76.6\ \Omega$
τ	0.96	0.49
G_{tg}	2.1 dB	-4.3 dB
R_{sim}	13.7 m	4.7 m

It can be seen from figure A.3 that the frequency of the tag antenna is detuned by 350 MHz from the resonance frequency, i.e. 868 MHz. Subsequently, the antenna impedance changes and results in a mismatch between the tag antenna and the tag IC. Typically this mismatch impacts the τ value and changes it from 0.96 to 0.49, calculated using 2.1. Additionally, the gain of a tag antenna is reduced from 2.1 dB to -4.3 dB, which means approximately 6.4 dB power decrease due to material losses in the rubber sheets and detunning of the antenna dimensions. In terms of the read range estimated using (2.21), the typical degradation of the air optimized tag is from 13.7 m to 4.7 m [4].

List of Figures

1.1. Block diagram of a typical RFID system 2

2.1. Common frequency bands in which RFID systems operate 8
2.2. Passive UHF back scattering RFID system 9
2.3. 96 bits EPC data structure 11
2.4. Typical commercials UHF RFID tags 12
2.5. A UHF tag circuit schematic 12
2.6. Linear dipole antenna and its typical orientation in spherical coordinate system 14
2.7. Two port transmission line 14
2.8. A simple form of linear dipole structure on the two port transmission line 15
2.9. Changes in radiation pattern due to different bended lengths 15
2.10. 3D far field Radiation pattern of a resonant dipole wire antenna . . 16
2.11. Radiation pattern of a resonant dipole wire antenna in E and H plane 17
2.12. Comparison of a typical isotropic vs dipole antenna radiation pattern 18
2.13. Antenna circuit schematic 19
2.14. Dependance of the impedance value versus frequency of a linear dipole antenna 20
2.15. Power dissipated by different component of a antenna 20
2.16. A passive UHF RFID system schematic redraw 22
2.17. The layout of the setup used to measure read range of a tag 25

3.1. A parallel plate dielectric resonator 31
3.2. Measurement setup to measure changes in the applied signal 32
3.3. Picture of the complete measurement system built up in the lab utilized to detect the changes in terms of the reflection coefficient . . . 34

3.4. An open-ended coaxial probe 35
3.5. Spring fixture and its contact to a rubber sheet 35
3.6. An equivalent model of the measurement setup to extract electrical parameters from the measured reflection coefficient 37
3.7. Relationship between thickness of a sample and corresponding simulated reflection coefficient values 38
3.8. 3D numerical EM model of measurement setup 39
3.9. Concept of extraction of electric parameters from the measured point 41
3.10. Look-up data showing the relationship between the simulated reflection coefficient and the electrical parameters 42
3.11. S_{11}^{meas} values measured at various positions on the CR sheet 44
3.12. Measured complex S_{11} in complex form of CR rubber sheet at 868 MHz at different positions 45
3.13. One to one relationship between the measured S_{11}^{meas} and determined electrical parameters 46
3.14. Placement of measured S_{11}^{meas} in the simulated parameter space of the look-up table 46
3.15. Measured complex S_{11} at various positions on the EPDM 48
3.16. EPDM measured S_{11}^{meas} values at 868 MHz at different positions . . 48
3.17. Comparison of measured and simulated curves to show effectiveness of the numerical code (red color curve shows the simulated curve and the cyan color shows the measured curve) 49
3.18. Prototype of fabricated parallel plate dielectric resonator 51
3.19. Resonance modes excited in the fabricated parallel plate dielectric resonator 51
3.20. Summary of the steps to find the electrical parameters of an unknown rubber material 52

4.1. Different configurations of rubber transmission belts 56
4.2. Physical layout of the chosen rubber belt 56
4.3. Various rubber belts having a similar layer stack up 57
4.4. Electrical model of the considered rubber belt 58
4.5. Prototypes of the designed tag antennas 60
4.6. Dimensions of the external antenna and the simulation model used to determine it 61
4.7. Layout and circuit schematic of inductive coupled loop feed antenna 62
4.8. Surface UHF RFID tags designed for the belt 64
4.9. Gain pattern of the simulated tag antenna 1 in 3D 65
4.10. Gain pattern of the simulated tag antenna 1 in H plane 66
4.11. Simulated impedance of the surface tag antenna 1 66
4.12. Gain pattern of the simulated tag antenna 2 in 3D 67
4.13. Gain pattern of the simulated tag antenna 2 in H plane 68
4.14. Simulated impedance of the tag antenna 2 68

4.15. A typical plot displayed after performing measurement test 69
4.16. The attenuation factor number at which tag 1 is detected by the reader at various frequencies 71
4.17. The minimum power at which tag 2 is detected by the reader at various frequencies 71
4.18. Variation in the impedance and its impact on the transmission coefficient considering tag 1 73
4.19. Variation in the impedance and its impact on the transmission coefficient considering tag 2 73
4.20. Electric parameter variations (present in different rubber sheet) impact on the antenna simulated impedance 74
4.21. Impact of the electrical parameter variations on the antenna gain . 75
4.22. Impact of thickness variations on the impedance of the tag antenna 76
4.23. The influence of thickness changes of different rubber sheets on the antenna gain 76
4.24. Modified belt in rectangle shape instead of V shape 77
4.25. The impact of shape change on the simulated impedance of the tag antenna 77
4.26. The impact of shape change on the simulated antenna gain 78
4.27. Impact of variations in the electric parameters due to recipe change 79
4.28. Gain of the antenna if the electrical parameters change by various percentages due to different fabrication recipes 79
4.29. A typical detection gate for counting tagged objects 80
4.30. Tagged belts 81
4.31. Tagged belts packed into a box 81
4.32. Results of the performed bulk test 82
4.33. Summary of main steps to design a surface tag for a rubber belt . . 82

5.1. Antenna structured with pasting technique [17] 86
5.2. Antenna structured with the plotted and etching technique 87
5.3. Typical tag design with combination of stitching and etching 87
5.4. Antenna structured with combination of stitching and etching(tested) 88
5.5. Impact of the antenna structured by printing technique on the rubber sheet 88
5.6. Impact of the antenna structured by plotting and etching technique on the rubber sheet 88
5.7. Impact of the antenna structured by the etching and the stitching technique on the rubber sheet 89
5.8. Designed embedded tag antenna for the belt 90
5.9. Dimensions of the embedded tag antenna 91
5.10. Considered rubber belts for investigation purpose 92
5.11. Approximated position of tag inside the belt 92
5.12. Tag placement during manufacturing and in the fabricated belt . . 92

5.13. Life cycle test of the tag in a physical belt 93
5.14. Detection of the belt during high speed operation 94
5.15. Simulated gain of the embedded tag antenna 95
5.16. Simulated impedance of the embedded tag antenna 96
5.17. Difference in tagged belt and reference belt structure 97
5.18. Simulated impedance of the antenna in reference and tagged belt . 98

A.1. Simulated impedance of a tag antenna attached to the model 106
A.2. Measured impedance of a tag antenna attached to the model (unit in Ω) 106
A.3. Detuning of the impedance of an optimized air tag when placed on a rubber belt 107
A.4. Impact on the gain when an air optimized tag is placed on the rubber belt 107

List of Tables

2.1. UHF RFID band allocation in different countries around the world . 10

3.1. Electrical parameters of the CR rubber sheet 45
3.2. Electrical parameters of rubber and not rubbed CR rubber sheet . . 47
3.3. Electrical parameters of the EPDM rubber sheet 48
3.4. Reproducibility test results 50
3.5. Comparison between the measurement results of two characterization methods 52

4.1. Electrical parameters of the different rubber sheets 58
4.2. Transmitted power (in mWatt) corresponding to various attenuation factor number after 10 dB attenuation (for the 500 mWatt RF embedded reader module) 70
4.3. Comparison between the simulated and measured read range of the designed tags 72

5.1. Summary of different parameters of the tag 98

A.1. Impact of the belt onto the air optimized tag characteristics 108

References

[1] Kanwar, K. ; Fischer, C. ; Geneiss, V. ; Mager, T. ; Ballhausen, U. ; Hedayat, C. ; Hilleringmann, U.: Electrical characterization of rubber mixture sheets based on a coaxial probe method in combination with 3D electromagnetic simulation model. In: *RFID-Technologies and Applications (RFID-TA), 2012 IEEE International Conference on*, 2012, S. 182–187

[2] Kanwar, K. ; Geneib, V. ; Mager, T. ; Scheele, S. ; Ballhausen, U. ; Hedayat, C. ; Hilleringmann, U.: Design and analysis of UHF RFID tag for a rubber transmission belt based on 3D electrical model. In: *Software, Telecommunications and Computer Networks (SoftCOM), 2013 21st International Conference on*, 2013, S. 1–5

[3] Kanwar, K. ; Mager, T. ; Hilleringmann, U. ; Geneiss, V. ; Hedayat, C.: Embedded UHF RFID tag design process for rubber transmission belt using 3D model. In: *RFID Technology and Applications Conference (RFID-TA), 2014 IEEE*, 2014, S. 97–102

[4] K., Kanwar ; T., Mager ; V., Geneis ; C., Hedayat ; T., Gessner ; U., Hilleringmann: Performance investigation of UHF RFID tags designed for air and rubber belts - impact of electrical parameters and the shape of the belts (accepted and will be published soon). In: *Smart Systems Integration conference (SSI 2015)*, 2015, S. 8

[5] Finkenzeller, Klaus: *RFID Handbook: Fundamentals and Applications in Contactless Smart Cards, Radio Frequency Identification and Near Field Communication*. Wiley, 2010

[6] Dobkin, Daniel M.: *The RF in RFID Passive UHF RFID in Practice*. Elsevier Inc, 2008

[7] Nicolay, T. ; Treib, A. ; Blum, A.: RF identification in the use of belt rip detection [mining product belt haulage]. In: *Sensors, 2004. Proceedings of IEEE, vol. 1*, 2004, S. 333–336

[8] Yang, Li ; Rida, A. ; Li, Jiexin ; Tentzeris, M.M.: Antenna Advancement Techniques and Integration of RFID Electronics on Organic Substrates for UHF RFID Applications in Automotive Sensing and Vehicle Security. In: *Vehicular Technology Conference, 2007. VTC-2007 Fall. 2007 IEEE 66th*, 2007, S. 2040–2041

[9] He, Shanhong ; Xie, Jidong: A Novel Compact Printed Antenna Used in TPMS or Other Complex and Variable Environments. In: *Antennas and Propagation, IEEE Transactions on* 56 (2008), Jan, Nr. 1, S. 24–30

[10] Lehpamer, Harvey: *RFID Design Principles.* Artech House, 2008

[11] Optibelt: *Optibelt GmbH, Höxter, Germany, accessed on 01.07.2014.* `http://optibelt.de`

[12] Grosinger, Jasmin: *Backscatter radio frequency systems and devices for Novel Wireless Sensor applications*, Vienna University of Technology, Diss., 2012

[13] Basat, S.: Design and development of a miniaturized embedded UHF RFID tag for automotive tire applications. In: *Electronic Components and Technology Conference, 2005. Proceedings. 55th, Vol. 1*, 2005, S. 867–870

[14] Inc., GAO R.: *860 to 950MHz RFID Tire Tag (116042), accessed on 30.01.2015.* `http://www.gaorfid.com/RFID-PDF/860%20to%20950MHz%20RFID%20Tire%20Tag.pdf`

[15] Inc., GAO R.: *860 to 950MHz RFID Tire Tag (116043), accessed on 30.01.2015.* `http://www.gaorfid.com/RFID-PDF/860%20to%20950MHz%20Gen%202%20RFID%20Tire%20Tag.pdf`

[16] Tagitron, GmbH ; Salkotten, Germany: *TagItron introduces an innovative elastic rubber tag for integration in or applications on a rubber production, accessed on 30.01.2015.* http://www.tagitron.com/news-press/73-tagitron-introduces-an-innovative-elastic-rubber-tag-for-integration-in-or-applications-on-a-rubber-production.html,

[17] Zichner, Ralf: *Hochfrequenz-Kommunikation gedruckter Antennen in herausfordernden dielektrischen oder metallischen Umgebungen*, TU-Chemnitz, Diss., 2013

[18] Catarinucci, L. ; Colella, R. ; Tarricone, L.: Smart prototyping techniques for UHF RFID tags: electromagnetic characterization and comparison with traditional approaches. In: *Progress In Electromagnetics Research* 132 (2012), S. 91–111

[19] Bjorninen, T. ; Virkki, J. ; Virtanen, J. ; Sydanheimo, L. ; Ukkonen, L. ; Tentzeris, M.M.: Inkjet-printing and performance evaluation of UHF RFID tag antennas on renewable materials with porous surfaces. In: *Antennas and Propagation (EuCAP), 2013 7th European Conference on*, 2013, S. 1721–1725

[20] Koski, E. ; Koski, K. ; Bjorninen, T. ; Babar, A.A. ; Sydanheimo, L. ; Ukkonen, L. ; Rahmat-Samii, Y.: Fabrication of embroidered UHF RFID tags. In: *Antennas and Propagation Society International Symposium (APSURSI), 2012 IEEE*, 2012. – ISSN 1522–3965, S. 1–2

[21] Kim, Yeonho ; Lee, Kyounghwan ; Kim, Yongju ; Chung, You C.: Wearable UHF RFID tag antenna design using flexible electro-thread and textile. In: *Antennas and Propagation Society International Symposium, 2007 IEEE*, 2007, S. 5487–5490

[22] Grosinger, J. ; Mayer, L.W. ; Mecklenbrauker, C.F. ; Scholtz, A.L.: Determining the Dielectric Properties of a Car Tire for an Advanced Tire Monitoring System. In: *Vehicular Technology Conference Fall (VTC 2009-Fall), 2009 IEEE 70th*, 2009, S. 1–5

[23] Bolic, M. ; Simplot Ryl, D. ; Stojmenovic, I.: *RFID Systems: Research Trends and Challenges*. Wiley, September 2010. – 576 S.

[24] EPCglobe, InC.: *EPC^{TM} Radio-Frequency Identity Protocols Generation-2 UHF RFID , accessed on 11.02.2015*. `http://www.gs1.org/sites/default/files/docs/epc/uhfc1g2_2_0_0_standard_20131101.pdf`

[25] Ashon, Syed ; Ilyas, Mohammad ; Ashon, Syed (Hrsg.) ; Ilyas, Mohammad (Hrsg.): *RFID handbook application, Technology, Security, and Privacy*. CRC Press, 2008. – 712 S.

[26] Zhonghao, Hu: *Solutions for Hard to tag Objects in UHF RFID systems*, Northwestern Polytechnical University, China, Diss., 2006

[27] Rao, K. V S. ; Nikitin, P.V. ; Lam, S.F.: Antenna design for UHF RFID tags: a review and a practical application. In: *Antennas and Propagation, IEEE Transactions on* 53 (2005), Dec, Nr. 12, S. 3870–3876

[28] Ukkonen, L. ; Sydanheimo, L.: Impedance matching considerations for passive UHF RFID tags. In: *Microwave Conference, 2009. APMC 2009. Asia Pacific*, 2009, S. 2367–2370

[29] Ghiotto, A ; Vuong, T.-P. ; Wu, K.: Chip and antenna impedance measurement for the design of passive UHF RFID tag. In: *Microwave Conference (EuMC), 2010 European*, 2010, S. 1086–1089

[30] Marrocco, G.: The art of UHF RFID antenna design: impedance-matching and size-reduction techniques. In: *Antennas and Propagation Magazine, IEEE* 50 (2008), Feb, Nr. 1, S. 66–79

[31] Grosinger, J.: Antennas and Wave Propagation in Novel Wireless Sensing Applications Based on Passive UHF RFID. In: *Elektrotechnik und Informationstechnik, Springer-Verlag* Volume 128, Issue 11-12 (2011), S. 408–414

[32] Babar, AA ; Bjorninen, T. ; Bhagavati, V. A. ; Sydanheimo, L. ; Kallio, P. ; Ukkonen, L.: Small and Flexible Metal Mountable Passive UHF RFID Tag on High-Dielectric Polymer-Ceramic Composite Substrate. In: *Antennas and Wireless Propagation Letters, IEEE* 11 (2012), S. 1319–1322

[33] Medeiros, C.R. ; Costa, J.R. ; Fernandes, C.A: Passive UHF RFID Tag for Airport Suitcase Tracking and Identification. In: *Antennas and Wireless Propagation Letters, IEEE* 10 (2011), S. 123–126

[34] Warren L. Stutzman, Gary A. T.: *Antenna Theory and Design.* 2nd. Edition. Wiley, 1998

[35] Balanis, Constantine A.: *Antenna Theory: Analysis and Design.* Wiley, 1997

[36] Wolff, Edward A.: *Antenna Analysis.* Artech House, 1988

[37] Impinj: *Monza® 4 Tag Chip Datasheet, Rev 5.1, accessed on 07.02.2015.* https://support.impinj.com/hc/en-us/articles/202756908-Monza-4-RFID-Tag-Chip-Datasheet

[38] NXP: *SL3S1204, UCODE 7, accessed on 05.27.2014.* http://www.nxp.com/documents/data_sheet/SL3S1204.pdf

[39] Grosinger, J. ; Lasser, G. ; Mecklenbrauker, C.F. ; Scholtz, AL.: Gain and efficiency measurement of antennas for an advanced Tire monitoring system. In: *Antennas and Propagation Society International Symposium (APSURSI), 2010 IEEE*, 2010, S. 1–4

[40] Sung-Lin, Chen ; Ken-Huang, Lin: Characterization of RFID Strap Using Single-Ended Probe. In: *Instrumentation and Measurement, IEEE Transactions on* 58 (2009), Oct, Nr. 10, S. 3619–3626

[41] Nikitin, P.V. ; Rao, K. V S.: Performance limitations of passive UHF RFID systems. In: *Antennas and Propagation Society International Symposium 2006, IEEE*, 2006, S. 1011–1014

[42] Nikitin, P.V. ; Rao, K. V S.: Antennas and Propagation in UHF RFID Systems. In: *RFID, 2008 IEEE International Conference on*, 2008, S. 277–288

[43] Strauss, W. ; Kraus, S. ; Hartmann, M. ; Grabowski, C. ; Bernhard, J.: Read range measurements of UHF RFID transponders in mobile anechoic chamber. In: *RFID, 2009 IEEE International Conference on*, 2009, S. 48–55

[44] Deleruyelle, T. ; Pannier, P. ; Alarcon, J. ; Egels, M. ; Bergeret, E.: RFID tag antennas with stable impedance to mounted material. In: *Microwave Conference (EuMC), 2010 European*, 2010, S. 1090–1093

[45] Toivonen, M. ; Bjorninen, T. ; Sydanheimo, L. ; Ukkonen, L. ; Rahmat-Samii, Y.: Impact of Moisture and Washing on the Performance of Embroidered UHF RFID Tags. In: *Antennas and Wireless Propagation Letters, IEEE* 12 (2013), S. 1590–1593. http://dx.doi.org/10.1109/LAWP.2013.2293334. – DOI 10.1109/LAWP.2013.2293334. – ISSN 1536–1225

[46] Ciesielski, Andrew: *An Introduction to rubber technology.* iSmithers Rapra Publishing, 1999. – 188 S.

[47] Bhowmick, Anil K. ; Bhowmick, Anil K. (Hrsg.): *Handbook of Elastomers, Second Edition.* Marcel Dekker Inc, 2000

[48] Bhowmick, Anil K. ; Bhowmick, Anil K. (Hrsg.): *Rubber Products Manufacturing Technology.* Marcel Dekker Inc, 1994

[49] Morgenthaler, Frederic R.: *The Power and Beauty of Electromagnetic Fields.* Wiley, 2011

[50] Orfanidis, Sophocles J.: *Electromagnetic Waves and Antennas, accessed on 03.04.2014.* http://www.ece.rutgers.edu/~orfanidi/ewa/. Version: 2008

[51] Collin, Robert E.: *Foundations for Microwave Engineering.* 2nd. Wiley, 2001

[52] Chen, L. F. ; Varadan, V. K.: *Microwave Electronics: Measurement and Materials Characterization.* Wiley, 2004

[53] Ege Engin, A: Extraction of Dielectric Constant and Loss Tangent Using New Rapid Plane Solver and Analytical Debye Modeling for Printed Circuit Boards. In: *Microwave Theory and Techniques, IEEE Transactions on* 58 (2010), Jan, Nr. 1, S. 211–219

[54] Shevgaonkar, R. K.: *"Electromagnetic Waves".* McGraw Hill Education India, 2006

[55] Someda, Carlo G.: *Electromagnetic Waves.* Chapman and Hall, 1998

[56] Radim ZAJICEK, Jan V. Ladislav OPPL O. Ladislav OPPL: Broadband Measurement of Complex Permittivity using Reflection Method and Coaxial Probes. In: *RADIOENGINEERING* VOL.17, NO. 1 (APRIL 2008), S. 14–19

[57] Wagner, N.: Robust low cost open eneded coaxial probe for diaelectric spectroscopy in laboratory and in situ appplication. In: *Innovative Feuchtemessung in Forschung und Praxis,Proceedings CMM Conference 2011*. Karlsruhe, 2011, S. 11

[58] Misra, Devendra ; Chabbra, M. ; Epstein, Benjamin R. ; Microtznik, M. ; Foster, K.R.: Noninvasive electrical characterization of materials at microwave frequencies using an open-ended coaxial line: test of an improved calibration technique. In: *Microwave Theory and Techniques, IEEE Transactions on* 38 (1990), Jan, Nr. 1, S. 8–14

[59] Decreton, Marc C. ; Gardiol, F.E.: Simple Nondestructive Method for the Measurement of Complex Permittivity. In: *Instrumentation and Measurement, IEEE Transactions on* 23 (1974), Dec, Nr. 4, S. 434–438

[60] Berube, D. ; Ghannouchi, F.M. ; Savard, P.: A comparative study of four open-ended coaxial probe models for permittivity measurements of lossy dielectric/biological materials at microwave frequencies. In: *Microwave Theory and Techniques, IEEE Transactions on* 44 (1996), Oct, Nr. 10, S. 1928–1934

[61] Akdagli, Ali: *Behaviour of Electromagnetic Waves in Different Media and Structures*. InTech, 2011

[62] HUBER ; SUHNER: *Type 23 SMA 50 01 111 N, accessed on 10.07.2014*. http://www.hubersuhner.com/ProdDet/2413084

[63] Dunsmore, Joel P.: *Handbook of Microwave Component Measurements: with Advanced VNA Techniques*. Wiley, 2012

[64] Agilent Technologies, Inc.: *Agilent AN 1287-3 Applying Error Correction to Network Analyzer Measurements*. http://cp.literature.agilent.com/litweb/pdf/5965-7709E.pdf. Version: accessed on 05.31.2014

[65] Tarantola, Albert: *Inverse Problem Theory and Methods for Model Parameter Estimation*. Society for Industrial and Applied Mathematics, 2005

[66] Stuchly, M.A. ; Athey, T.W. ; Samaras, George M. ; Taylor, G.E.: Measurement of Radio Frequency Permittivity of Biological Tissues with an Open-Ended Coaxial Line: Part II - Experimental Results. In: *Microwave Theory and Techniques, IEEE Transactions on* 30 (1982), Jan, Nr. 1, S. 87–92. http://dx.doi.org/10.1109/TMTT.1982.1131022. – DOI 10.1109/TMTT.1982.1131022. – ISSN 0018–9480

[67] MATLAB: *TriScatteredInterp, accessed march 26, 2012,*. www.mathworks.de/help/techdoc/ref/triscatteredinterpclass.html

[68] Seewattanapon, Somporn ; Akkaraekthalin, Prayoot: A Broadband Complex Permittivity Probe Using Stepped Coaxial Line. In: *Journal of Electromagnetic Analysis and Applications* 3 (August 2011), 312-318. http://dx.doi.org/doi:10.4236/jemaa.2011.38050. – DOI doi:10.4236/jemaa.2011.38050

[69] *Dielectric Constants of Common Materials, accessed on 28.09.2014*. http://www.kabusa.com/Dilectric-Constants.pdf,

[70] Zhang, Ning ; Li, Xiuping: RFID tag antenna design and its EM simulation based measurement method. In: *Communication Technology (ICCT), 2010 12th IEEE International Conference on*, 2010, S. 644–647

[71] Son, H.-W ; Pyo, C.-S: Design of RFID tag antennas using an inductively coupled feed. In: *Electronics Letters* 41 (2005), Sept, Nr. 18, S. 994–996

[72] Catarinucci, L. ; Colella, R. ; Tarricone, L.: Prototyping flexible UHF RFID tags through rapid and effective unconventional techniques: Validation on label-type sensor-tag. In: *RFID-Technologies and Applications (RFID-TA), 2012 IEEE International Conference on*, 2012, S. 176–181

[73] Ukkonen, L.: Operability of Folded Microstrip Patch-Type Tag Antenna in the UHF RFID Bands Within 865-928 MHz. In: *Antennas and Wireless Propagation Letters, IEEE* 5 (2006), Dec, Nr. 1, S. 414–417. – ISSN 1536–1225

[74] Kuo, S.K. ; Chen, S.L. ; C.T., Lin: An accurate method for impedance measurement of RFID tag antenna. In: *Progress In Electromagnetics Research* 83 (2008), 93-106. http://dx.doi.org/doi:10.2528/PIER08042104. – DOI doi:10.2528/PIER08042104

List of Publications

1. Kanwar, K. ; Fischer, C. ; Geneiss, V. ; Mager, T. ; Ballhausen, U. ; Hedayat, C. ; Hilleringmann, U.: Electrical characterization of rubber mixture sheets based on a coaxial probe method in combination with 3D electromagnetic simulation model. In: RFID-Technologies and Applications (RFID-TA), 2012 IEEE International Conference on, 2012, S. 182-187

2. Kanwar, K. ; Geneib, V. ; Mager, T. ; Scheele, S. ; Ballhausen, U. ; Hedayat, C. ; Hilleringmann, U.: Design and analysis of UHF RFID tag for a rubber transmission belt based on 3D electrical model. In: Software, Telecommunications and Computer Networks (SoftCOM), 2013 21st International Con- ference on, 2013, S. 1-5

3. Kanwar, K. ; Mager, T. ; Hilleringmann, U. ; Geneiss, V. ; Hedayat, C.: Embedded UHF RFID tag design process for rubber transmission belt using 3D model. In: RFID Technology and Applications Conference (RFID-TA), 2014 IEEE, 2014, S. 97-102

4. K., Kanwar ; T., Mager ; V., Geneis ; C., Hedayat ; T., Gessner ; U., Hilleringmann: Performance investigation of UHF RFID tags designed for air and rubber belts - impact of electrical parameters and the shape of the belts (accepted and will be published soon). In: Smart System Integration Conference (SSI 2015), 2015, S. 8